Table of contents

Abbreviations

°C	degree Celsius
aa	amino acid(s)
AID	auxin-inducible degron
APC/C	anaphase promoting complex/cyclosome
APS	ammonium persulphate
ATM	ataxia telangiectasia, mutated
ATP	adenosine-5'-triphosphate
ATR	ATM-Rad3 related
ATRIP	ATR-interacting protein
BER	base excision repair
BLAST	basic local alignment search tool
Bp	base pair(s)
BRCA1	breast cancer associated gene 1
BRCA2	breast cancer associated gene 2
BSA	bovine serum albumin
CAK	cyclin activating kinases
CDK	cyclin-dependent kinase
CDK5RAP2	cyclin-dependent kinase 5 regulatory associated protein 2
cDNA	complementary DNA
Chk	checkpoint kinase
CKI	cyclin-dependent kinase inhibitor
C-NAP1	centrosomal NEK2-associated protein 1
C-terminus	carboxy terminus
DAPI	4', 6-diamidino-2-phenylindole
DAV	distal appendage vesicle
DDR	DNA damage response
DMSO	dimethyl-sulfoxide
DNA-PK	DNA-dependent protein kinase
DNA-PKcs	DNA-PK catalytic subunit
dNTP	deoxyribonucleotide-5'-triphosphate
DSB	double-strand break
dsDNA	double-stranded DNA
E. coli	*Escherichia coli*
E2F	adenovirus E2 promoter binding factor
EDTA	ethylenediaminetetraacetic acid
EGTA	ethylene glycol tetraacetic acid
FACS	fluorescence-activated cell sorting
FANCD2	Fanconi anaemia, complementation group D2
FBS	foetal bovine serum
Fig	figure
FITC	fluorescein isothiocyanate
FLAG	epitope tag
G	gravitational force
GFP	green fluorescent protein
GTP	guanosine-5'-triphosphate
γ-TURC	γ-tubulin ring complex
γ-TUSC	γ-tubulin small complex
GFP	green fluorescent protein

h	hour or human
HR	homologous recombination
hTert-RPE1	human telomerase reverse transcriptase- retinal pigment epithelial
IF	immunofluorescence microscopy
IR	ionizing radiation
IRIF	IR-induced foci
kb	kilobase pair(s)
kDa	kilodaltons
LB	Luria-Bertani medium
µ	micro
m	milli, metre, or mouse
M	mega or molar (mol/l)
MCC	mitotic checkpoint complex
MCPH	microcephalin
Mg^{2+}	magnesium ion
MillQ	'ultrapure' water
min	minute(s)
MMR	mismatch repair
MOPD II	microcephalic osteodysplastic primordial dwarfism type II
MRE11	meiotic recombination 11
MRN	MRE11-RAD50-NBS1 complex
mRNA	messenger RNA
MT	microtubules
MTOC	microtubule-organising centre
NBS1	Nijmegen breakage syndrome 1
NEK/NRK	NIMA-related kinase
NER	nucleotide excision repair
NHEJ	non-homologous end joining
NIMA	never-in-mitosis A
N-terminus	amino terminus (N-terminal: aminoterminal)
NuMA	nuclear mitotic apparatus
NuRD	nucleosome remodelling deacetylase
ORC	origin recognition complex
Parp	poly(ADP-Ribose) polymerase 1
PBS	phosphate buffered saline
PCM	pericentriolar material
PCNT	pericentrin
PCR	polymerase chain reaction
Pen/Strep	penicillin/streptomycin
PFA	paraformaldehyde
PIKK	phosphoinositide 3-kinase related protein kinase
Plk	polo-like kinase
PP2A	protein phosphatase 2A
Rb	retinoblastoma
RNA	ribonucleic acid
RNAi	RNA interference
RPA	replication protein A
rpm	revolutions per minute
RT	room temperature

SAC	spindle assembly checkpoint
SAP	shrimp alkaline phosphatese
SCC	sister chromatid cohesion protein
SDS	sodium dodecyl sulphate
SDS-PAGE	SDS polyacrylamide gel electrophoresis
SEM	standard error of the mean
Ser/Thr	serine/threonine
siRNA	short interfering RNA
SMC	structural maintenance of chromosomes
ssDNA	single-stranded DNA
TAE	tris acetate EDTA
TEMED	N,N,N‘,N‘-tetramethylethylenediamine
Tris	tris(hydroxymethyl)aminomethane
U	unit
V	volt
v/v	volume per volume
WT	wild-type
XP	xeroderma pigmentosum

Acknowledgements

Firstly I would like to thank Ciaran Morrison for his supervision and support throughout my PhD. The optimism and encouragement he provided made the lab a very enjoyable place to learn. His teachings extended beyond the world of science, nearly as far as the Astroturf on Mondays. Nearly.

Next I'd like to thanks all the members of the lab past and present for providing such superb place to work in. In particular I'd like to thank: Tiago for helping me at the beginning of my PhD with remarkable patience. My initial year would have been much more difficult if it was not for him; Anne-Marie for her generosity of time and reagents, and for her sporting prowess on the tag rugby field; Lisa for showing me the power of argument, turns out being right is irrelevant; Shiva for the numerous PocketTanks battles, he is a worthy silver medallist; Yetunde for her singing, it definitely helped keep me awake on those late nights and Sandra for her peace-keeping exploits. Others including Ebtissal, Pauline, Lorreta, Sinead and Suzy all helped create a good atmosphere and it was great to work with them.

I would also like to thank my family for all their support especially my parents and grandmother for supporting me throughout my education.

Thanks to all my friends who were more than keen to disrupt any potential progress with nights out that always led to weekends out.

Finally thanks to Triona for her support through the last year and especially in the last couple of months when I was wasting away. All the sandwiches and dinners kept me alive.

This thesis is dedicated to the memory of my grandfather

Abstract

Components of the centrosome have been reported to have a role in the DNA Damage Response (DDR) pathway. Cep164, a protein localised to the distal appendages of centrioles, is theorised to play a part in the DDR. As with the centrosomal protein Centrin2, Cep164 has been linked to Nucleotide Excision Repair (NER), the mechanism used to repair DNA lesions induced by UV light. This link has been established through a study which reported that Cep164 interacts with the NER repair factor XPA and that Cep164 depletion results in hampered survival after UV-induced DNA damage.

To further elucidate the centrosomal and DNA repair roles of Cep164, we targeted its gene locus in both chicken and human model systems. Our targeting strategy in chicken DT40 cells was designed to attach both an Auxin Inducible Degron (AID) and a GFP tag to the Cep164 protein. This allowed us to track and deplete the protein in a controlled manner. In the human RPE-1 cell-line, we conducted a gene disruption of *CEP164* using CRISPR/Cas9. We verified the successful gene targeting in both cell lines through a combination of Western and/or Southern analysis. Using immunofluorescence microscopy we confirmed the localisation of the Cep164 protein to the centrosome and also described a novel monoclonal antibody to human Cep164.

This is the first study examining a Cep164 knockout cell line. Our results indicate that Cep164 is essential for ciliogenesis. Through transmission electron microscopy analysis of the human knockout we confirm that Cep164 is necessary for the binding of distal appendage vesicles to the mother centriole. However, in contrast to published data, we have shown Cep164 to be dispensable for the DNA damage response. We show exclusive localisation of Cep164 to the centrosome after DNA damage and through clonogenic survival assays, have found no sensitivity to IR or UV radiation when Cep164 is absent.

Chapter 1. Introduction

1.1. The centrosome

The first depiction of the centrosome dates back to 1876 when Édouard Van Beneden published work on Dicyemida, a cephalopod kidney parasite (Van Beneden, 1876). Although Van Beneden's report was not focused on the centrosome (which he termed the polar corpuscle), it is clearly represented in his drawings as a small circle at the poles of the mitotic spindle. 10 years on from this initial description, seminal research was published independently by both Van Beneden and a German biologist, Theodor Boveri. Working on the nematode *Ascaris megalocephala*, they studied mitosis in fertilised eggs and came to the same conclusion; the centrosome was a permanent cell organelle that organised cell division and, by self-replication, was passed from mother to daughter cells (Van Beneden & Neyt, 1887; Boveri, 1887).

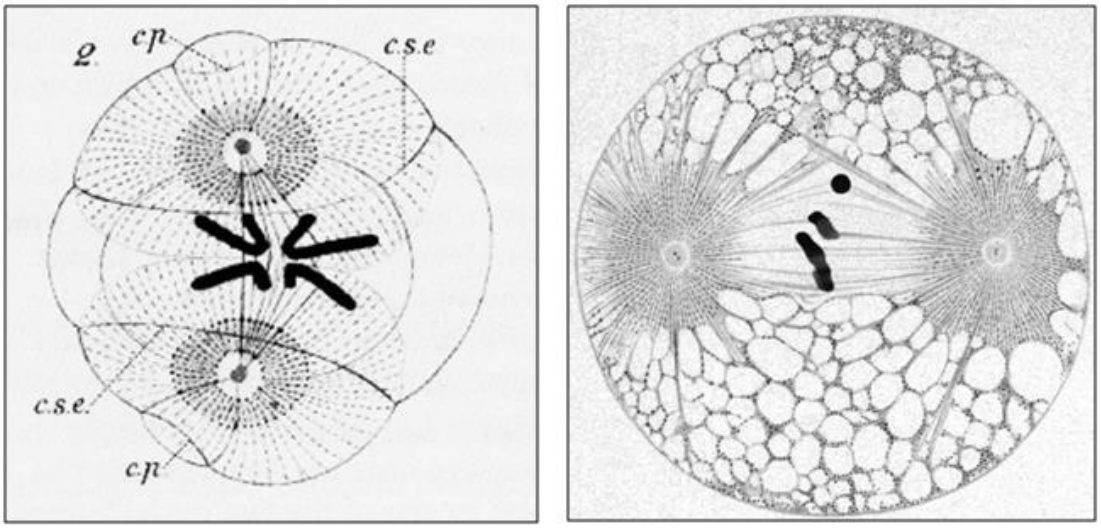

Figure 1.1 Van Beneden's (left) and Boveri's (right) drawings of the first cleavage division in the egg of the nematode *Ascaris megalocephala.* Van Beneden and Boveri clearly depict the centrosome with microtubules emanating from it and connecting to the chromosomes. On close inspection, two centrioles are also visible in Boveri's drawing. Drawings originally taken from (Van Beneden and Neyt, 1887) and (Boveri, 1900).

Due to the limitations of light microscopy, little was known about the structure of the centrosome at this stage. However, by choosing to study the relatively large egg cells of *Ascaris* and sea urchins, Boveri could discern a small dark granule at the centre of the centrosome, naming it a centriole (Boveri, 1895). A

couple of years later, he described the cyclical nature of these centrioles and how they appeared to double and separate during the cell cycle (Boveri, 1900). While the field of centrosome biology has expanded rapidly in the subsequent century, it is important to acknowledge these beginnings, as the work of Van Benden and Boveri laid the foundations for further investigation.

1.2. Centrosome structure

1.2.1. General structure

Being a small organelle of $<1\mu m^3$, the complexity of the centrosome was not fully appreciated until it was viewed under the electron microscope. This revealed a remarkable structure; two barrel-shaped centrioles within an electron-dense protein lattice, the pericentriolar material (Figure 1.2) and (Sorokin, 1962). The centrioles are composed of nine cylindrically-arranged triplet microtubules. Each triplet is composed of A, B and C microtubules, named in relation to their location (Figure 1.2) and (Anderson, 1972). Of the two centrioles, one is at least a cell cycle older and is referred to as the mature or 'mother' centriole. It is from the proximal end of the mother centriole that the new 'daughter' is produced. The mother and daughter centrioles are distinguished by the presence or absence of appendages, as these are features attained upon maturation (Paintrand et al., 1992).

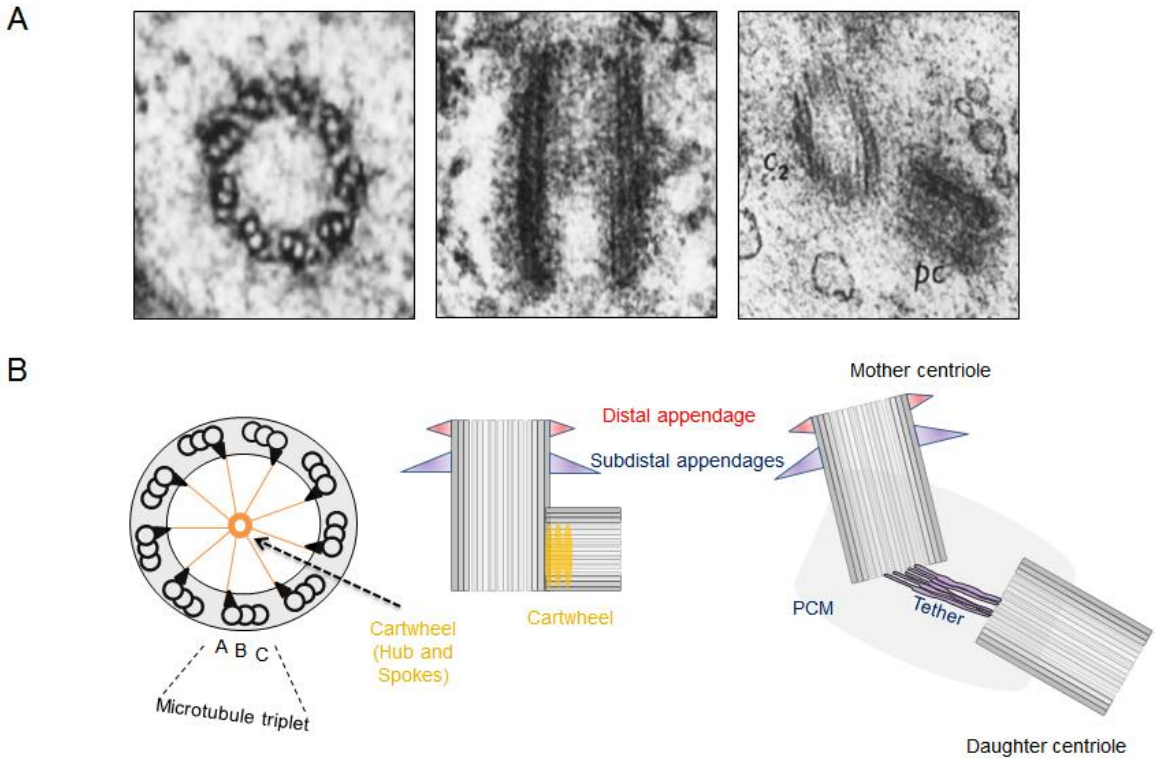

Figure 1.2 The composition and structure of the centrosome.
A. Original electron microscopy images of the centrioles from Sorokin, 1962. The triplets of microtubules are clearly visible as is the barrel-shape of the centrioles. B. Schematic with more detail than is observable in the EM images. Each centriole is composed of nine microtubule triplets connected to the centre of the lumen via the cartwheel (orange). Each of these triplets is composed of α- and β-tubulin-containing protofilaments A, B and C. The mother centriole is distinguishable from the daughter by the presence of appendages, represented in purple and red. The centrioles are membrane-less but are surrounded by a protein matrix, the pericentriolar material (PCM).

The centrosome is now described as the main microtubule organising centre (MTOC) of the animal cell. The events for which it is responsible include: arranging a bipolar spindle during mitosis, maintaining the astral microtubule network during interphase, and nucleating cilia or flagella at the plasma membrane. Aside from these functions involving microtubule organisation, the centrosome has also been implicated in broader activities, such as cell cycle control and cell signalling (Doxsey et al., 2005; Nigg and Stearns, 2011).

1.2.2. Inside the centriole

Within the microtubule frame of the centriole is a ~130nm wide lumen, composed of a defined cartwheel structure surrounded by "undefined luminal density" (Gibbons and Grimstone, 1960). As depicted in Figure 1.2, the cartwheel is composed of a central hub and spokes which link it to the microtubule triplet. In human cells the cartwheel defines the proximal end of the centriole and acts as a scaffold for procentriole assembly. After the formation of the centriole, the cartwheel disappears as a result of the tight regulation of Sas6. Indeed, increased levels of Sas6 promote formation of more than one procentriole per centriole (Strnad et al., 2007).

The cartwheel was original described in the highly ciliated, unicellular organisms, *Paramecium* and *Tetrahymena* (Allen, 1969; Dippell, 1968). The hub can be viewed under electron microscopy as a 20-25nm wide structure and has been shown to be composed of Sas6 dimers organised in a ninefold symmetric arrangement (Kitagawa et al., 2011; van Breugel et al., 2011). The globular head of the Sas6 dimers form the hub while a coiled-coil tail domain initiates the spoke. Several other proteins appear to be important in extending these spokes and thus completing the cartwheel, including Cep135 (Kleylein-Sohn et al., 2007). Expression of Bld10p/Cep135-deletion mutants in *Chlamydomonas* causes the formation of centrioles with altered numbers of centriolar microtubules due to reduced cartwheel diameters (Hiraki et al., 2007). Besides Sas6 and Cep135, several other proteins are localised to the cartwheel and essential for the assembly of centrioles (Hirono, 2014). STIL (Sas5) and CPAP (Sas4) are two well-studied examples that form a complex to promote cartwheel assembly (Stevens et al., 2010). In human cells, the depletion of STIL blocks centriole duplication, while its overexpression results in the generation of extra centrosomes (Arquint et al., 2012). CPAP is known to regulate microtubule nucleation through its interaction with γ-tubulin. Depletion of CPAP prevents centriole duplication, while its overexpression results in overly-long centrioles (Hung et al., 2000; Kohlmaier et al., 2009). Interestingly, both STIL and CPAP can cause microcephaly if mutated (Cottee et al., 2013).

Mature centrosomes consist of two centrioles, which need to be duplicated exactly once per cell cycle. The assembly of cartwheels initiates new centriole formation (Strnad and Gonczy, 2008). Therefore, in order to maintain proper centriole number, this process must be tightly regulated. The amount of Sas6 present

in the cell has been shown to be crucial in this regard. In human cells at the end of G1, Sas6 accumulates until anaphase when it is degraded by the proteasome. This ensures the proper number of centrioles is produced per cell cycle. If Sas6 levels are increased through the expression of a non-degradable form of the protein, excess procentrioles are formed on the mother (Strnad et al., 2007). The degradation of Sas6 is mediated through ubiquitination by the SCF-FBXW5 E3 ligase. However, the activity of this complex is in turn negatively regulated by what turns out to be the master regulator of centriole assembly, Plk4 (Puklowski et al., 2011). Plk4 becomes active at the G1/S transition and acts to inhibit the degradation of Sas6, thereby promoting cartwheel assembly. At the end of mitosis, when the new centriole is fully formed, the Sas6 protein levels are lowered to prevent improper centriole assembly.

While the understanding of the cartwheel has become more refined, little is known about the remainder of the lumen. Centrin and Poc5 are known to localise to the lumen but their exact function there remains to be uncovered (Azimzadeh et al., 2009; Paoletti et al., 1996).

1.2.3. Centriole composition

The nine triplet repeat, which constitutes the microtubule frame, is the most recognisable feature of the centrioles. Variations of this structure, while rare, do exist. *Drosophila* and *Caenorhabditis elegans* embryos display a doublet and singlet repeat, respectively, while the spermatogonia of *Acerentomon microrhinus* have a large centriole composed of 14-doublet microtubules (Gonczy, 2012). The functional significance of these variations, if any, is unknown.

The dimensions of the mature microtubule scaffold in human are a cylinder of diameter ~250nm and length ~500nm. The microtubules that compose the triplet are named A, B and C in relation to their position. Each microtubule consists of 13 α- and β-tubulin-containing protofilaments (Li et al., 2012). Tubulin polymerizes from end to end, with the β-subunits of one tubulin dimer contacting the α-subunits of the next dimer. Therefore, in a protofilament, one end will have the α-subunits exposed while the other end will have the β-subunits exposed. These ends are designated the (−) and (+) ends, respectively. The protofilaments bundle parallel to one another with the same polarity, so, in a microtubule, there is one end, the (+) end, with only β-subunits exposed, while the other end, the (−) end, has only α-

subunits exposed. While microtubule elongation can occur at both the (+) and (-) ends, it is 3 times quicker at the (+) end (Walker et al., 1988).

In vitro assembly of microtubules can be induced when sufficient concentrations of pure α/β-tubulin heterodimer are incubated with Mg^{2+} and GTP (Fellous et al., 1977). However, this spontaneous assembly rarely occurs in vivo but requires a nucleating factor as necessary to initiate polymerization. The best-characterised microtubule nucleating factors are protein complexes that contain highly conserved γ-tubulin. γ-tubulin is a homologue of α-tubulin and β-tubulin and has been found at all MTOCs, centrosomal or otherwise (Kollman et al., 2011). γ-tubulin was first discovered in *Aspergillus nidulans* and was subsequently purified from *Xenopus laevis* eggs (Oakley and Oakley, 1989; Zheng et al., 1995). Analysis of the purified γ-tubulin revealed that it is part of a larger complex with at least six other proteins: GCP, GCP3, GCP4, GCP5, GCP6 and NEDD1. Electron microscopy of the complex revealed a ring structure of ~25nm diameter (Oegema et al., 1999). It was termed the γ-tubulin ring complex or γ-TuRC.

The γ-TuRCs act to cap the minus ends of microtubules, increasing their stability by impeding depolymerisation. Experiments using biotinylated tubulin highlighted this stability, as the triplet microtubules do show significant exchange with the cytoplasmic protein pool (Kochanski and Borisy, 1990). At the microtubule triplets, nucleation begins with the A-microtubule at the spokes of the cartwheel. This is followed by bidirectional growth of B- and C- microtubules from the wall of the neighbouring microtubule. This suggests that the γ-TuRC, while indispensable for A- microtubule formation, is not directly required for B- and C- microtubule nucleation (Guichard et al., 2010). When these microtubules fully extend, the centriole matures and acquires appendages.

1.2.4. The appendages

There are two juxtaposed but distinct sets of appendages present on the mature centriole (Figure 1.2), located distally and sub-distally. Both sets of appendages are composed of multiple proteins. Using the distal appendages to attach to the plasma membrane, the mother centriole has the ability to nucleate a cilium or flagellum. Centrioles that lack distal appendages cannot form cilia (Ishikawa et al., 2005).

Components of the distal appendages include: Cep83, Cep89, Cep164, FBF1 and SCLT1. An siRNA analysis of these proteins has revealed a hierarchy in their recruitment. CEP83 recruits both SCLT1 and CEP89 to centrioles. Subsequent recruitment of FBF1 and CEP164 is independent of CEP89 but mediated by SCLT1 (Tanos et al., 2013). FBF1, Cep89 and Cep164 are all required for ciliogenesis (Schmidt et al., 2012; Sillibourne et al., 2013; Wei et al., 2013). In fact, due to the epistatic relationship of these proteins with Cep83 and SCLT1, all these distal appendage components are required for efficient ciliogenesis (Figure 1.3).

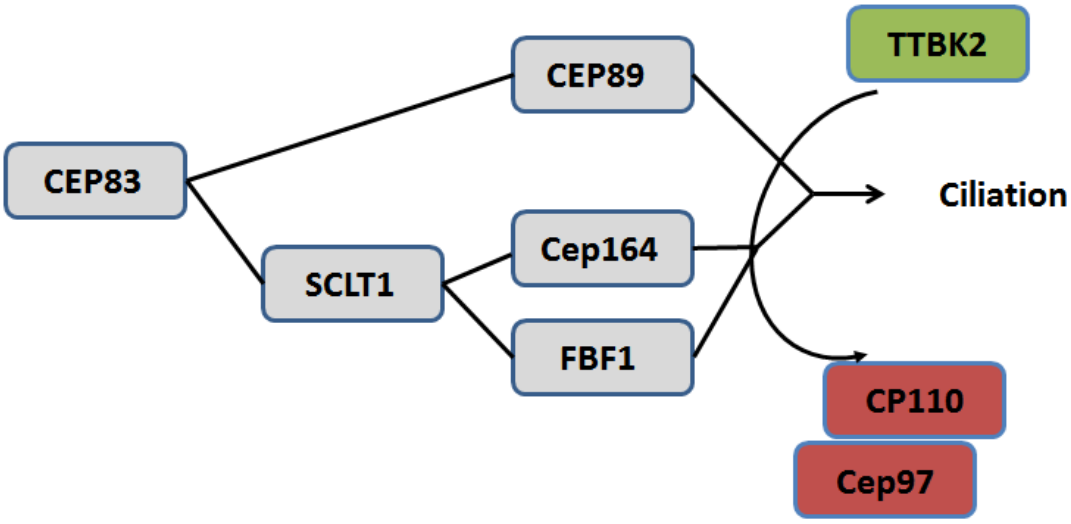

Figure 1.3 Distal appendage components and their hierarchy in assembly.
This schematic illustrates the known proteins involved in the assembly of functional distal appendages (grey). If any one of the components is missing ciliogenesis is impaired (adapted from Tanos et al, 2013). Cep164 has been shown to recruit TTBK2, which is necessary for the removal of CP110 and Cep97, thus allowing ciliation (Oda et al., 2014).

Proximal to the distal appendages are the subdistal appendages, which have been implicated in microtubule anchoring and nucleation (De Brabander et al., 1982; Piel et al., 2000). CC2D2A and Odf2 are reported to be essential for subdistal appendage assembly, with Ninein organising and anchoring microtubules at these appendages (Ishikawa et al., 2005; Mogensen et al., 2000; Veleri et al., 2014). OFD1, a protein known to be essential in early development of the brain, has also been shown to localise to the distal appendages and is necessary for their proper assembly. In addition, OFD1 also regulates the length of the centrioles, providing a link between centriole length and distal structure (Singla et al., 2010). As the distal appendages become the transition fibres during ciliogenesis, the subdistal

appendages form the basal foot. Distal appendages are increasingly recognised for their role in ciliogenesis, with knockdown/knockout of the associated proteins being linked to reduced ciliation capacity.

1.2.5. The PCM

Surrounding the centrioles is a protein network known as the pericentriolar material (PCM) (Bobinnec et al., 1998). Identified as harbouring γ–tubulin ring complexes (γ–TuRCs), the PCM is responsible for the nucleation of microtubules (Moritz et al., 2000). The role of the PCM in the formation of daughter centrioles was also demonstrated by the overexpression of pericentrin (PCNT) in S-phase arrested cells, which lead to the formation of multiple daughter centrioles (Loncarek et al., 2008). Originally described by electron microscopy as a densely stained amorphous mass, the PCM is now being recognised as having a more definitive structure (Fu and Glover, 2012; Lawo et al., 2012; Mennella et al., 2014; Robbins et al., 1968; Sonnen et al., 2012). However, while organised it is still dynamic, expanding and contracting in response to cellular cues. As the cell progresses towards mitosis the PCM expands, a process known as centrosome maturation (Palazzo et al., 2000). This expansion is the result of an accumulation of proteins such as pericentrin, AKAP450 and CDK5RAP2, which are notably largely composed of coiled-coil domains (Woodruff et al., 2015; Yue et al., 2008). These proteins play an important role in maintaining centrosome number, as when they are disrupted through DNA damage, centrosome amplification can ensue (Antonczak et al., 2015). However, the exact role the PCM proteins play in centrosome amplification after DNA damage is still unknown.

1.3. The cell cycle

1.3.1. Introduction

Every cell is born from a pre-existing cell through a process known as cell division. This division process is the culmination of a series of molecular events that occur as the cell goes through the cell cycle. The cell cycle is described as a progression of three phases: interphase, mitosis and cytokinesis (Hochegger et al., 2008). Interphase is the longest phase of the cell cycle and can be broken up again into G1, S and G2. During interphase the cell grows as it prepares for cell division, duplicating its DNA and much of its contents. During mitosis, the cell orchestrates the accurate segregation of the duplicate chromosomes. And finally during cytokinesis the cells separate to become two distinct daughter cells (Hochegger et al., 2008).

1.3.2. Regulation of cell cycle

The cell cycle is a tightly regulated process dependent on a family of proteins, cyclin-dependent kinases (Cdk). The activity of these serine threonine kinases oscillates through the cell cycle in response to alterations in the binding of regulatory cyclin subunits as well as Cdk-activating kinase activity. Specific Cdks regulate specific cell cycle phases: Cdk4 and Cdk6 regulate G1, Cdk2 controls G1/S and Cdk1 is responsible for M. The cyclins which bind the Cdks can also be separated by the phases in which they operate with cyclin D1-3 and cyclin E in G1/S, cyclin A1-2 in S and cyclin B1 and B2 in M. The oscillating expression of cyclins determines their binding and activation of their respective Cdk partners. This triggers precise and specific cell cycle transitions via phosphorylation of a range of substrates (Malumbres and Barbacid, 2009). Contributing to the precise control of Cdks are the regulatory Cdk-inhibitory kinases (CKIs) which act to phosphorylate Cdks, inhibiting them. An additional component of cell cycle progression is the anaphase-promoting complex or cyclosome (APC/C). The acts to induce the degradation of key regulatory substrates, thus promoting M-phase (Peters, 2006). In addition to the cyclin-Cdks and the APC/C, there are a number of other proteins which contribute to cell cycle progression. As previously mentioned some of these also act to ensure the cell and centrosome cycles are co-ordinated.

1.4. The centrosome cycle

1.4.1. Introduction

Centrosome duplication is the process whereby the interphase centrosome doubles before entry into mitosis. If this process is perturbed and more than two centrosomes are present at the onset of mitosis, there is a much greater risk of a multipolar spindle (Holland and Cleveland, 2009). If only one centrosome is present the cell is likely to form a monopolar spindle. Spindle abnormalities often results in abnormal chromosome segregation, which can lead to genomic instability and tumourigenesis. To prevent this from happening, the centrosome duplication cycle is tightly regulated and co-ordinated with the cell cycle (Hinchcliffe et al., 1999; Lacey et al., 1999). In addition, the cell often clusters any extra centrosomes to maintain a bipolar spindle. While this can prevent mitotic catastrophe, the chances of chromosome mis-segragation are greatly increased (Holland and Cleveland, 2009).

A key experiment that demonstrated the control on duplication was conducted in the late 1950's in sea urchin eggs. It was found that when mitosis is artificially prolonged in a zygote, the two spindle poles could split to yield four functional poles (Figure 1.4). However, these four poles will not split further, regardless of how long the cell is kept in mitosis. During the next cell cycle each of the four daughter cells inherited one spindle pole (Figure 1.4.f). This was able to form a bipolar spindle suggesting the inherited pole had functionally duplicated which then allowed it to split (Figure 1.4.g). The conclusions drawn from this were that each spindle pole normally contained two linked mitotic centres or centrioles (Mazia et al., 1960). These are normally kept as pairs but could be induced to split under experimental circumstances. This splitting revealed that centrioles can act as spindle poles. From these data three distinct events in the centrosome cycle were hypothesised: splitting, separation and duplication. This work laid the foundations for further research in this highly regulated process.

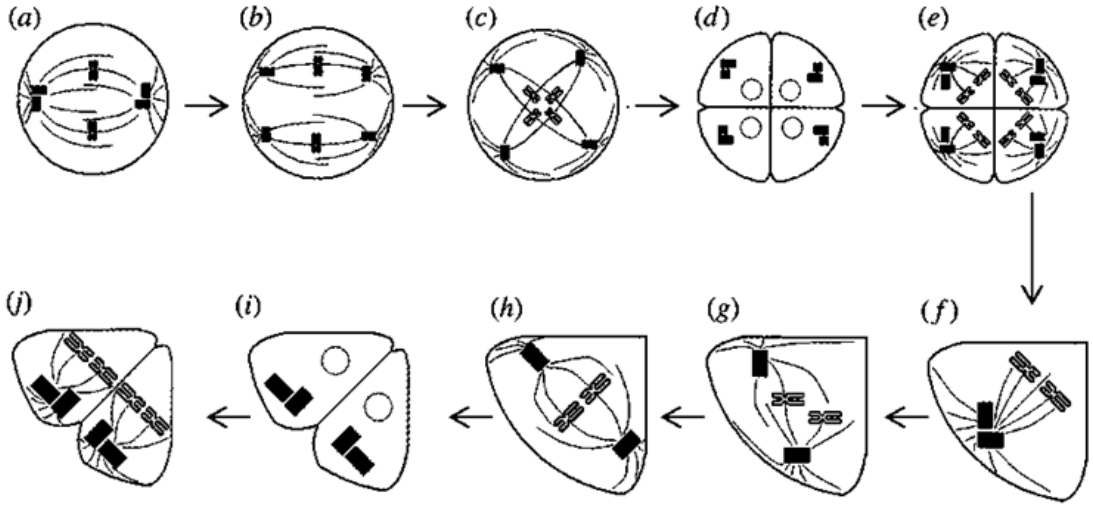

Figure 1.4 Schematic representing centrosome cycle observations after prolonged mitosis in sea urchin eggs.
When mitosis is prolonged the centriolar pairs split without duplication (a,b). This results in a tetrapolar spindle that splits the cell in four (c-e). Each of the daughter cells contains a centriole which duplicates to form a bipolar spindle (f-h). This results in cell division based on the components of one centrosome rather than two. Figure adapted from (Sluder, 2014)

We now know that the first centrosome cycle of an animal begins upon fertilisation. During this process the centrioles from the sperm and the proteins for the egg combine to form a centrosome. This centrosome duplicates and initiates the first mitosis of embryogenesis (Nigg and Stearns, 2011). Centrosome duplication shares many similarities with DNA replication; they are both duplicated in a semi-conservative manner, once per cell cycle during S phase. However while DNA is replicated through copying a template strand, centriole duplication is a process where the new centriole assembles at a specific location on a pre-existing centriole (Delattre and Gonczy, 2004; Vorobjev and Chentsov Yu, 1982). In proliferating cells, the centrosome cycle has five distinct events that occur once during the cell cycle. These are centriole disengagement, procentriole biogenesis, procentriole elongation, centrosome maturation and centrosome separation (Figure 1.5). In non-cycling quiescent cells (G0), the centrosome can become a basal body at the plasma membrane and nucleate a cilium (Nigg, 2007; Nigg and Stearns, 2011; Tsou and Stearns, 2006).

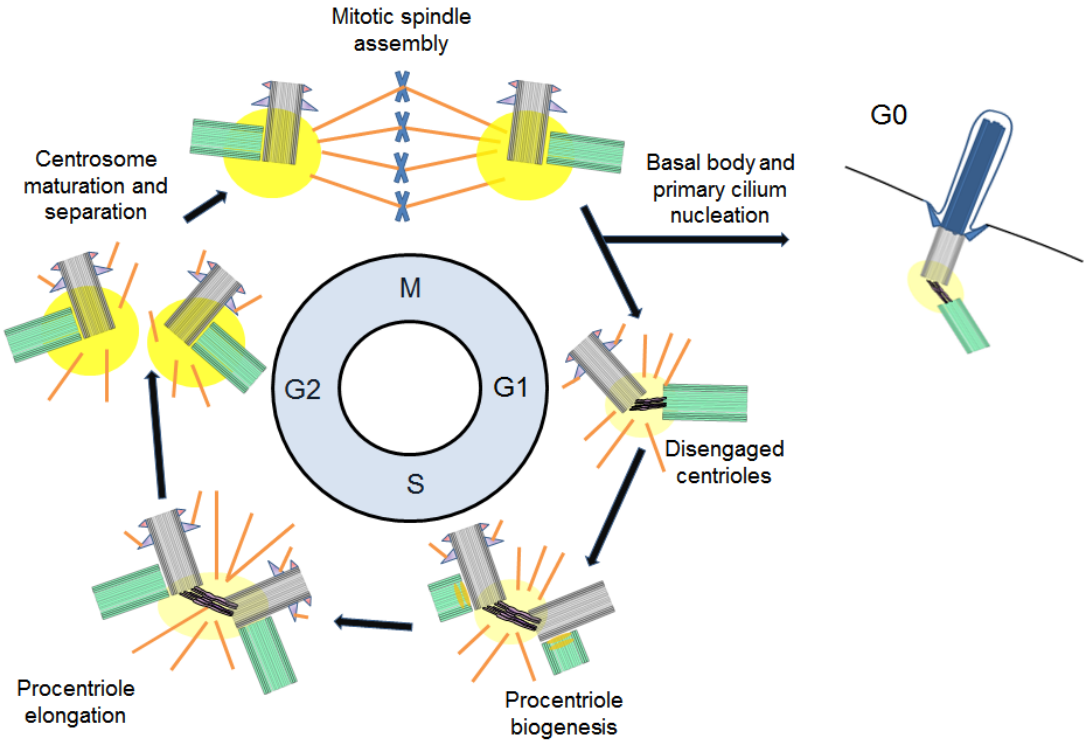

Figure 1.5 The centrosome duplication cycle.
A diagrammatic representation of centriole behaviour during the cell cycle. At the end of mitosis each new daughter cell inherits one centrosome composed of two disengaged centrioles. Cells then undergo quiescence and enter G0 or enter G1.In proliferating cells the centrioles duplicate in S phase, with newly formed procentrioles (light green) remaining tightly engaged with their mother centrioles (grey) and gradually elongating throughout S and G2. At the G2/M transition, the centrioles accumulate more pericentriolar material (PCM, yellow) and the two centrosomes start to separate from one another, eventually forming the poles of the spindle in mitosis. Adapted from (Nigg and Raff, 2009)

1.4.2. Centriole disengagement

Centriole disengagement is the term used to describe the orthogonal arrangement the mother and daughter centrioles occupy prior to duplication. For duplication to occur efficiently this arrangement is lost through a licencing step. Centriole duplication takes place during S phase at the proximal end of the mature centriole. The new centriole assembles orthogonally to the mother centriole and is engaged to it through a poorly defined linker until the end of mitosis (Paintrand et al., 1992). During telophase this linker is disengaged, licencing the centrosome for another round of centriole duplication in the following S-phase (Tsou and Stearns, 2006; Wang et al., 2011). The regulation of centriole disengagement is mediated by a number of proteins which also have a role in the regulation of chromosome segregation. Separase is a cysteine protease well-known for cleaving cohesin at the chromosomes at the onset of anaphase (Hauf et al., 2001). It has also been shown

that separase promotes centriole disengagement, with its loss leading to significant delays this process (Chestukhin et al., 2003; Tsou and Stearns, 2006). While the centrioles do eventually disengage in the absence of separase, when combined with Plk1 inhibition this process is completely blocked demonstrating that Plk1 and separase activity are essential for disengagement (Tsou et al., 2009). The substrate for separase on chromosomes is Scc1 and recent data has confirmed this is present and cleaved at the centrosome (Schockel et al., 2011). Separase is active during mitosis while Plk1 functions in late G2, suggesting that they act at different times during the cell cycle to ensure the centrioles are disengaged.

At the chromosomes, separase activity is known to be controlled through cyclin B1 and securin. However, additional factors appear to be involved at the centrosome, including Aki1 and astrin. These were deemed to be inhibitors of centrosomal separase as their depletion causes premature disengagement (Nakamura et al., 2009; Thein et al., 2007). Shugoshin (Sgo1), a protein responsible for preventing the premature separation of sister chromatids, has also been shown to have a role at the centrosome. Specifically, it is a splice variant sSgo1 which is recruited to the centrosome by Plk1 (Tsang and Dynlacht, 2008; Wang et al., 2008). This exact mechanism by which sSgo1 acts at the centrosome is yet to be made clear. Recently the PCM component, pericentrin has been reported to be a substrate of separase (Lee and Rhee, 2012; Matsuo et al., 2012). It was shown that cleavage-resistant pericentrin blocked centriole disengagement. However while efficient separase cleavage of Scc1 is dependent on Plk1, this is not the case for pericentrin. This indicates that Plk1 controls separase activity via regulating its substrate affinity at centrosomes (Agircan and Schiebel, 2014). While the intricacies of the centriole disengagement process are still being unravelled, it is indisputably a vital stage of the centrosome duplication process.

1.4.3. Procentriole biogenesis and elongation

When the centrioles are disengaged, they have the ability to begin procentriole biogenesis. This is a highly conserved process throughout eukarya (Carvalho-Santos et al., 2011; Nigg and Stearns, 2011). The serine/threonine kinase Plk4 is the major regulator of centriole assembly, as demonstrated by the effects of its overexpression or depletion in cells. Overexpression leads to the nucleation of numerous procentrioles off the mother, while depletion inhibits the centriole

assembly process entirely (Habedanck et al., 2005; Kleylein-Sohn et al., 2007; Wong et al., 2015). With such dramatic effects on centriole number, it is not surprising to find this kinase is highly regulated through phosphorylation and ubiquitination. (Cunha-Ferreira et al., 2009; Guderian et al., 2010; Holland et al., 2010; Kleylein-Sohn et al., 2007; Sillibourne et al., 2010). To initiate procentriole formation, Plk4 is recruited to the proximal end of the mature centriole by the combined efforts of Cep152 and Cep192 (Cizmecioglu et al., 2010; Sonnen et al., 2013). As discussed previously, it is here where a scaffold of proteins is thought to interact to promote the formation of the cartwheel structure (Pelletier et al., 2006; Pelletier et al., 2004).

After the formation of the cartwheel the centriole elongates to a specific length. This process is regulated by the interaction Cep120 and CPAP. Forced overexpression of either induces the assembly of overly long centrioles while their depletion reduces length. (Lin et al., 2013). However, the regulation of this centriole length is not solely dependent on Cep120 and CPAP, as other proteins such as POC1 and POC5 have also been shown to be involved in this process (Azimzadeh et al., 2009; Keller et al., 2009).

1.4.4. Centrosome maturation

Centrosome maturation begins in G2 with the recruitment of PCM proteins, an increase in microtubule nucleation activities and the assembly of appendages on the newly formed mother centriole. Plk1 is a core effector of the maturation process with its inhibition resulting in monopolar spindles and impaired microtubule nucleation capacity (Lenart et al., 2007; Santamaria et al., 2011). Plk1 kinase activity induces the recruitment of numerous proteins to the centrosome such as Cep192, γ-tubulin, NEDD1 and Aurora A (Haren et al., 2006). Plk1 is also required for the assembly of distal appendages, as its inhibition restricts the accumulation of appendage proteins, while unscheduled Plk1 activity accelerates the appendage process allowing the formation mature centrioles earlier in the cell cycle (Kong et al., 2014).

1.4.5. Centrosome separation

As has been discussed, the centrioles disengage at the end of mitosis through the severance of a linker. This linker forms from the wall of the mother to the base of the procentriole. Somewhat counterintuitively, the severance of this linker allows the formation of a second, longer linker (referred to as a tether) between the bases of the disengaged centrioles. Proteins involved in the composition of the tether have been identified through protein interactions and siRNA screens that affect centrosome cohesion. The two best studied tether proteins are C-Nap1 and rootletin (Fry et al., 1998a; Mayor et al., 2000; Yang et al., 2006). The sites at which these dock on the centriole are reported to be provided by the Cep135 at the base of the centriole (Kim et al., 2008). One can imagine that the base of one centriole is inaccessible as a docking site before disengagement. Cep135 has two separate domains: the N-terminal targets the protein to the centriole and the C-terminal has been shown to bind C-Nap1 (Kim et al., 2008). Furthermore, C-Nap1 can bind to rootletin and thus recruit it to the centriole. The kinase Nek2 was originally shown to cause centrosome splitting when overexpressed. However, targets of this kinase have since been identified as C-Nap1 and rootletin. At the onset of separation these targets become phosphorylated, to allow for centrosome migration to the spindle poles (Bahe et al., 2005; Fry et al., 1998a; Fry et al., 1998b).

1.4.6. Centrosome cycle perturbations

Although the centrosome cycle is highly regulated, deviations from this duplication process do occur and can have catastrophic consequences for the cell. These deviations occur when one or more of the proteins involved in the centrosome cycle process become dysregulated.

1.4.6.1. Centrosome amplification

As early as 1887, Boveri realised the implication of a multipolar spindle and the effects it could have on the distribution of the genetic material (Figure 1.6). Although Boveri never studied tumorigenesis directly he postulated that many features of cancer were due to the chromosomal aberrations (Boveri, 1887).

We now have a deeper understanding of the role of centrosome amplification in the formation of abnormal spindles, chromosome mis-segregation and aneuploidy

(Sluder and Nordberg, 2004). Centrosome amplification often arises as a result of over-duplication of centrioles. Although only one procentriole forms per mature centriole under normal circumstances, this restriction can be lifted after proteasome inhibition, extended S-phase delay, viral oncogene expression or Plk4 overexpression (Duensing et al., 2007; Guarguaglini et al., 2005; Kleylein-Sohn et al., 2007). In these conditions, multiple daughters can form around a single mother.

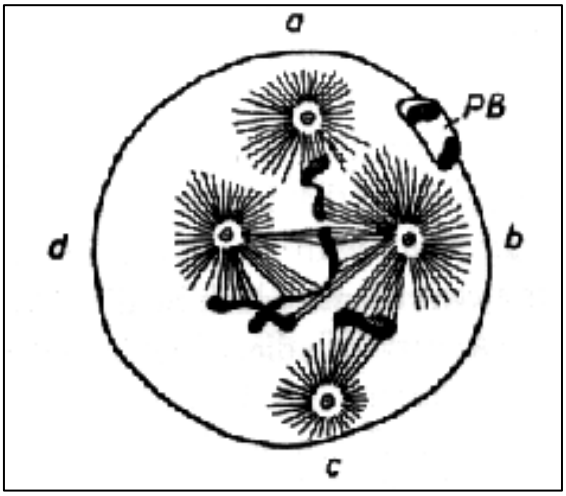

Figure 1.6 A tetrapolar cell as drawn by Boveri.
The cell depicted is an egg of *Ascaris megalocephala* bivalens in which the chromosomes are unequally segregated to the four poles (Boveri, 1887).

Cells treated with HU can amplify their centrosomes without DNA replication, demonstrating that the centrosome cycle is not strictly dependent on DNA replication (Balczon et al., 1995). However, both these processes have been shown to be blocked by Cdk2 inhibitors (Matsumoto et al., 1999). Further work in *Xenopus* identified Cdk2/cyclin E activity as a key regulator of the centrosome cycle providing a link with the DNA replication cycle (Hinchcliffe et al., 1999). Studies in mouse cells have shown an increase in centrosome amplification upon p53 depletion (Fukasawa et al., 1996). This has been suggested to arise through an increase in Plk4 expression levels, as p53 controls the recruitment of the inhibitor HDACs to Plk4 (Li et al., 2005). However, this could also be a result of abnormal Cdk2 activity in the absence of p53, along with a p53-independent cell cycle arrest to provide sufficient time for amplification (Fukasawa, 2008). As an increase in tetraploidization is also evident in p53-deficient cells under these conditions, it is worth bearing in mind that many roads may lead to centrosome amplification in this background (Borel et al., 2002; Meraldi et al., 2002).

1.4.6.2. DNA damage induced centrosome amplification

Early work demonstrating the effects of ionising radiation on centrosomes date back over 30 years (Sato et al., 1983). In this study, electron microscopy showed a high percentage of irradiated mouse cells did not contain paired centrioles and pericentrosomal material typical of a normal centrosome. In a later study in human cells, it was confirmed that irradiation resulted in centrosome amplification (Sato et al., 2000).

Following DNA damage, ATM/ATR activation leads to a G2/M checkpoint arrest as part of the DNA damage response (DDR) (Sancar et al., 2004). Chk1/Chk2 subsequently becomes activated and Plk1 is inhibited. This results in Cdc25 inhibition and the prevention of Cdk1 activation, a necessary step for mitotic entry. While DNA replication is stalled to allow the repair of damage, the centrosome can continue to duplicate resulting in centrosome amplification (Hochegger et al., 2007; Steere et al., 2011). Several DNA damage proteins have been reported to localise to the centrosome during the cell cycle including ATM, ATR, ATRIP, CHK1, CHK2, CSC25B, cyclin B/CDK1 and MCPH1 (Shimada and Komatsu, 2009). Dysfunction of these proteins can lead to centrosome amplification but the exact mechanism is still unclear. Dysregulation of proteins directly involved in the normal centrosome duplication cycle is also likely to play an important role in centrosome amplification after DNA damage.

1.5. DNA damage response

1.5.1. Introduction

Maintaining the integrity of the genome is essential for the proper function and survival of an organism. Damage to the genetic material from exogenous and endogenous sources is a recurring threat to a cell's ability to faithfully replicate its DNA. Endogenous DNA damage sources include reactive oxygen species (ROS) from cell metabolism and replication errors such as stalled and collapsed forks. Exogenous sources include ultraviolet radiation (UV), ionising radiation (IR) and chemical agents. The DNA lesions induced by these sources include single-strand and double-strand DNA breaks (SSBs and DSBs, respectively), bulky DNA adducts (pyrimidine dimers and 6–4 photoproducts) and DNA crosslinks. To counteract these various genetic insults, repair mechanisms have evolved that target specific lesions. Homologous recombination (HR) or non-homologous end joining (NHEJ) are the two mechanisms employed to repair DSBs, the most hazardous form of DNA damage (West, 2003). Nucleotide excision repair (NER) is used to correct pyrimidine dimers or 6–4 photoproducts, which although not as dangerous, occur approximately 1000 times more often than DSBs (Ciccia and Elledge, 2010). Once DNA damage is detected, the cell delays or arrests the cell cycle and initiates the appropriate response pathway. This process is coordinated by a DNA damage checkpoint (Jackson and Durocher, 2013; Polo and Jackson, 2011).

1.5.2. DNA damage repair checkpoint

When DNA damage is incurred, cell cycle progression is delayed in order to repair the damage. A family of proteins knowns as PIKKs (Phosphoinositide 3-kinase-related kinases) are responsible for controlling this delay and are also instrumental in the DNA repair process itself. Following DNA damage, the PIKK family kinases, and ATR are recruited to lesions where they become activated and phosphorylate target proteins at serine and threonine residues (Sancar et al., 2004). The PIKK targets act as mediators of DNA damage signalling, participating in a signal cascade that activates effector proteins such as Chk1 and Chk2 (Lukas et al., 2011). Activated Chk1 and Chk2 phosphorylate Cdc25A in G1-S phase and Cdc25C in G2-M phase, arresting the cell cycle. ATM and ATR also act to regulate the transcriptional activity of p53, causing increased levels of the CDK inhibitor p21 and

keeping the cell arrested to allow the DNA repair process to proceed (Bartek and Lukas, 2007).

There are four main checkpoints activated in response to DNA damage: the G1-S checkpoint, the intra-S checkpoint, the G2-M checkpoint and the spindle assembly checkpoint. As previously alluded to, Chk1 and Chk2 are important factors in distributing damage signals and arresting the cell cycle.

1.5.3. G1-S checkpoint response

If cells are damaged during G1, they are prevented from entering S phase. DSBs predominantly activate the ATM-Chk2-Cdc25A pathway while pyrimidine dimers and 6–4 photoproducts activate the ATM-Chk1-Cdc25A pathway. Activation of either pathway results in p53 becoming phosphorylated thus inducing the transcription of the cyclin dependent kinase inhibitor CDKN1A (p21). The expression of p21 inhibits the cyclin B/Cdk2 complex, preventing entry into S phase (Craig et al., 2003; Schon et al., 2002).

1.5.4. The intra-S phase checkpoint

If DNA damage is incurred in S-phase, or if cells have evaded G1-S arrest they are then subject to the intra-S-phase checkpoint, whereby replication is halted. Activation of this checkpoint after DNA damage requires the MRN complex, ATM and BRCA1, to both sense the damage and initiate the signalling cascade. There are parallel pathways which are known to proceed at this point (Falck et al., 2002; Yazdi et al., 2002). One is the ATM-Chk2-Cdc25A-Cdk2 pathway, whereby phosphorylation of Cdc25A leads to its degradation, thus inhibiting Cdk2 activation. Another possible pathway involves the cohesin subunit SMC1, which becomes phosphorylated by ATM upon DNA damage and acts to inhibit cell cycle progression and aids repair (Kim et al., 2002). However, this is a very poorly understood pathway with more needed to fully resolve it. Upon UV light induced DNA damage ATR-ATRIP senses the DNA damage and once again evokes a signalling cascade leading to the inhibition of Cdk2 (Rohaly et al., 2005).

1.5.5. The G2-M checkpoint

Entry to mitosis is delayed in the presence of DNA damage. Cdc25C becomes phosphorylated from the upstream activities in an ATM/ATR dependent manner and binds the 14-3-3 proteins. The binding of Cdc25C sequesters it in the cytoplasm preventing the activation of Cdk1/cyclin B complex, thus inhibiting entry into mitosis (Kumagai and Dunphy, 1999; Peng et al., 1997). During this checkpoint, $p21^{CIP1}$ is also upregulated through ATM-activated p53. This upregulation can inhibit Cdk2/cyclin A and Cdk4/6/cyclin D preventing the expression of genes by E2F (Bunz et al., 1998; Slansky and Farnham, 1996).

1.5.6. The spindle-assembly checkpoint

To ensure chromosomes are properly segregated during mitosis the spindle assembly checkpoint (SAC) exists. The SAC ensures appropriate attachment of the microtubules to the kinetochores. During the SAC, Cdc20 is sequestered from the APC/C such that the degradation of Cyclin B and Securin is prevented. As Securin degradation is necessary for the activation of separase and thus cleavage of the cohesin ring, sister chromatids are not separated, preventing anaphase entry (Uhlmann et al., 1999). The SAC is terminated when all chromosomes are bi-orientated between spindle poles on the metaphase plate.

1.5.7. DNA double-strand break repair

As previously mentioned, DSBs are the most hazardous form of DNA lesion. Failure to properly repair these lesions can lead to the loss of genetic information and genome instability. In eukaryotes, there are two principal pathways for the repair of DSBs, homologous recombination (HR) and non-homologous end joining (NHEJ). (Takata et al., 1998)

1.5.7.1. Non -homologous end joining

Non-homologous end joining is an error-prone repair pathway that occurs in G1/G0. The erroneous nature of the pathway results from not using a template strand to base the repaired sequence on. This often results in the addition or deletion of some base pairs which can put a gene out of frame (Jackson, 2002). The first step in NHEJ is the recognition and binding to the DSB by Ku70/Ku80 . This recruits DNA-

PK which acts to prevent DNA end resection, regulates chromatin structure and facilitates DSB repair by protein phosphorylation (Mahaney et al., 2009; Meek et al., 2008). Additional proteins recruited to the DSB in NHEJ include: XRCC4, DNA ligase IV, XLF and Artemis (Jackson, 2002). These act to remove damaged bases and stimulate DNA end-ligation. DNA polymerases μ and λ carry out the gap-filling functions (Mahaney et al., 2009). The end result is repaired DNA, often with base pairs added in or deleted from the original sequence.

1.5.7.2. Homologous recombination

Homologous recombination is utilised predominantly in S and G2 (Takata et al., 1998). In contrast to NHEJ, HR has a low error rate when repairing DSBs. This is due to the use of a homologous template from either the sister chromatid or the homologous chromosome to repair the damage (Bernstein and Rothstein, 2009). In the initial stages of HR, the endonuclease activity of the MRN complex together with Exo1 and DNA2 resect the 5' ends of DSBs to facilitate strand invasion. RPA prevents the single-stranded 3' end from degradation. Rad51 is subsequently recruited with the aid of mediator proteins such as BRCA2 and several Rad51 paralogues (Heyer et al., 2010). Once recruited Rad51 finds the homologous sequence and a joint DNA structure is formed whereby the damaged DNA invades the other strand. The information is copied precisely from the template strand, extending the 3' invading strand. The subsequent Holliday junction is resolved through the coordination of a number of proteins which can result in cross-over or non-cross-over repaired DNA (Heyer et al., 2010).

1.5.8. Nucleotide excision repair

The NER pathway is responsible for the repair of bulky, helix-distorting DNA adducts, particularly those generated by ultraviolet (UV) light. Deficiencies in NER lead to several human diseases, including xeroderma pigmentosum (XP), in which patients have a marked sensitivity to sunlight (UV damage) and a predisposition to skin cancer (de Laat et al., 1999; Wood, 1996). Two principal NER subpathways resolve the 6-4 photoproducts and cyclobutane pyrimidine dimers that arise after UV damage. One is termed transcription-coupled NER, and acts quickly to remove DNA distortions that block transcription and the other is global genome repair, which,

while not as rapid, acts genome-wide (Bohr et al., 1985; Mellon et al., 1987). Although both methods of NER are similar in their basic mechanism, one major difference exists in the initial recognition of DNA damage. In transcription-coupled NER, the DNA lesion is recognised by the stalling of RNA polymerase II at lesions (Selby and Sancar, 1993), whereas in global genome NER, the damage is initially detected by the XPC-hRad23-centrin2 protein-containing complex (Sugasawa et al., 1998). The initial detection is dependent on the type of distortion. 6-4 photoproducts are predominantly recognised by XPC but cyclobutane pyrimidine dimers are detected more robustly by the UV-DDB complex before XPC is recruited. The steps subsequent to the initial recognition are common to both modes; XPC recruits TFIIH through interaction with one of its subunits, XPB (Bernardes de Jesus et al., 2008). DNA is then unzipped near the lesion by helicase actions of TFIIH in the presence of XPA, XPG and replication protein A (RPA) (Egly, 2001). This allows structure-specific endonucleases, namely XPF-ERCC1 and XPG, to excise a short region around the lesion by cleaving at both 5' and 3' of the damage, removing approximately 25-30 base pairs. The resulting gap is then resolved by DNA polymerase (δ or ε), and the nick is joined by DNA ligase I (de Laat et al., 1999; Sugasawa, 2010; Wood, 1996).

1.6. Centrosome functions

1.6.1. Introduction

The importance of the centrosome to the animal cell is underlined by its ubiquitous nature. Some planarians and the female germline of several species represent a few of the only examples where this MTOC is not present (Azimzadeh et al., 2012; Debec et al., 2010). The processes to which the centrosome has been linked include: microtubule nucleation and organisation, cell polarity, cell signalling and ciliogenesis.

1.6.2. Microtubule organisation and cytokinesis

Being pivotal for microtubule nucleation, it was assumed that the centrosome was indispensable for cell survival, especially considering its role in forming the mitotic spindle. However work in *Drosophila* has demonstrated that the absence of centrioles still allows the development of this organism, to a certain point. Shortly after birth, the flies die due to a lack of cilia on their sensory neurons (Basto et al., 2006). In this case, the cells produce acentriolar mitotic spindles via a pathway involving Ran, a small GTPase. When in the vicinity of chromatin, Ran-GTP has the ability to activate the γ–tubulin ring complex and initiate microtubule nucleation (Kalab and Heald, 2008). While this shows that the centrosome may be redundant for spindle assembly, it is considered essential for asymmetrical division where it orientates the mitotic spindle along this axis and localize cell fate determinants to one side of the cell (Betschinger and Knoblich, 2004). A further study in vertebrate DT40 cells in which centrioles were disrupted showed a high rate of chromosome instability and aneuploidy with a significant delay in bipolar spindle assembly (Sir et al., 2013). So while cells may be able to compensate for a lack of centrosomes through acentriolar spindle assembly, they are significantly impaired in chromosome segregation.

As previously mentioned, the γ-tubulin ring complex is key to nucleating microtubules at the centrosome (section 1.2.3). When nucleated, their growth takes place at the (+) end in a GTP dependent manner. The α- and β-tubulin dimers bind GTP when extending while they are depolymerised upon hydrolysation to GDP (Etienne-Manneville, 2010). When the microtubules are fully extended, a scaffold

forms in which motor proteins such as dynein and kinesin can bind, creating the dynamic microtubule network required for all microtubule-related functions (Badano et al., 2005). While the cartwheel nucleates microtubules to form the triplet, the PCM and the subdistal appendages are the locations from which this microtubule network is thought to emanate (Bornens, 2002).

1.6.3. The centrosome and cell signalling

The centrosome is increasingly appreciated for its roles outside microtubule organisation. As a dynamic organelle, it responds to cellular cues. On such cues it duplicates, relocates to conduct a bipolar spindle and if needs be, can become a basal body during ciliogenesis. However, in addition to a response to cues, the centrosome is now being considered as a centre from which such signals emanate. Cell cycle progression and DNA damage two particular areas where the MTOC may act as a signalling centre.

1.6.3.1. Centrosomes as a signalling centre during cell cycle progression

Early evidence indicating the centrosome could trigger cell cycle events came from the demonstration that the injection of purified centrosomes into mature starfish oocytes was sufficient to overcome interphase arrest (Picard et al., 1987). A similar experiment in *Xenopus laevis* corroborated this work and taken together indicated a role for the centrosome in the initiation of mitosis (Klotz et al., 1990). Entry into mitosis is regulated by the activation of a Cdk1-cyclin B complex (Masui and Markert, 1971). Through the generation of a phospho-specific antibody to phospho-Chk1 it has been shown that this activation occurs at the centrosome, although this point is still contested (Jackman et al., 2003; Matsuyama et al., 2011). Interestingly, the Cdk1-activating phosphatase, Cdc25B, has been shown to be regulated at the centrosome by Chk1, Mcph1 and pericentrin (Kramer et al., 2004; Loffler et al., 2007; Tibelius et al., 2009). Other cell cycle factors such as Cdc25C, Plk1 and Aurora A have also been localised to the centrosome at the G2/M transition (Bailly et al., 1989; Dutertre et al., 2004; Golsteyn et al., 1995). The localisation of these kinases and phosphatases to the MTOC supports the idea of it acting as a signal platform.

1.6.3.2. Centrosomes as a nexus for DNA damage response signalling

In addition to the role the centrosome has in normal cell cycle progression, there is also evidence of it being involved in signalling during the DNA damage response (DDR). A number of proteins which have a role in the DDR pathway have been shown to localise to the centrosome such as: ATM, ATR, Chk1, Chk2, BRCA1, BRCA2 and PARPs. In attempting to assess the significance of these localisations it is worth considering that the centrosome has the ability to delay the cell cycle, thus allowing sufficient time for the repair of any DNA damage before mitosis. Therefore, this localisation of DNA repair proteins provides an interesting avenue of research with regards to the centrosomes involvement in the DDR. One hypothesis is that these proteins may converge at the centrosome to interact or become modified (Yue et al., 2008). These interactions could neatly promote both cell cycle delay and DNA repair. In fact, recent research on Chk1 provides some evidence to support this, although due to the promiscuity of the antibody used in initial studies, some controversy ensued. Briefly, an antibody (DCS-310) used in a 2004 study was shown to localise Chk1 to the centrosome where it acts to regulate CCDC25B, and thus Cdk1-cyclin B. The localisation with this antibody was confirmed in a range of cell lines including fibroblasts, carcinoma and ES cells (Katsura et al., 2009; Koledova et al., 2010; Loffler et al., 2007). A further study cast doubt on this hypothesis by showing the centrosomal localisation of DCS-310 persisted in Chk1 null cells and that the antibody actually cross reacts with Ccdc21 (Matsuyama et al., 2011). As other studies using a combination of specific antibodies and exogenously-expressed Chk1 constructs have also localised this protein to the centrosome it seems likely that while the initial study may have been flawed, the conclusion drawn is credible (Antonczak et al., 2015; Jilani et al., 2015).

The phosphatidylinositol-3 (PI-3) family-related DNA damage checkpoint kinases ATM and ATR have been localised to the centrosome during mitosis in human cells (Oricchio et al., 2006; Zhang et al., 2007). However, the exact function of these proteins at the centrosome is somewhat contentious with difficulty in asserting whether the phosphorylated forms of the proteins act here. A prominent theory is that these DNA damage checkpoint proteins may control the formation of gamma-tubulin and/or the kinetics of microtubule formation at the centrosomes, and thereby couple them to the DNA damage response (Zhang et al., 2007).

Other bona fide DDR proteins to localise to the centrosome include the PARPs and both BRCA1 and BRCA2. These proteins are well-characterised for their roles in the DDR but have also been shown to cause aberrant centrosome numbers when absent (Augustin et al., 2003; Kanai et al., 2000; Xu et al., 1999). As to whether these aberrations are the result of defects in DNA repair or in centrosome control remains to be clarified.

In addition to DDR proteins being localised at the centrosome there is also evidence of centrosomal proteins with a role in the DNA damage response. Centrin2 is the best example of this to date as although it is a highly conserved centriolar protein that is required for proper ciliation, it has also been shown to be indispensable for proper nucleotide excision repair (NER) in chicken DT40 cells (Dantas et al., 2011; Prosser and Morrison, 2015). During NER, centrin2 binds to XPC and Rad23 and has been shown to aid the function of this damage recognition complex when UV-induced genotoxic stress is incurred (Araki et al., 2001; Sugasawa et al., 1998). However, although centrin2 is generally regarded as a centrosomal protein, only 10% of the total cellular protein has been shown to localise here (Paoletti et al., 1996). Therefore, it is possible that separate functions exist for centrin2 rather than it being a centrosomal protein modulating a nuclear repair function. This issue could be addressed with separation of function analyses. Cep164 is another centrosomal protein linked to the DDR and is discussed in more detail in section 1.7.

1.6.4. Cilia and ciliogenesis

Cilia and flagella are evolutionarily conserved structures which project from the surface of almost all cells. There are two types of cilia, defined by their capacity to move. Motile cilia, which have the ability to move, are found on the respiratory epithelia or the sperm flagellum where they are required to create flow or generate propulsion. Immotile cilia, or primary cilia as they are more commonly known, were initially regarded as an obscure structure with little significance. However they are now understood to have a broad range of functions in development and homeostasis and can cause disease (Gerdes et al., 2009). Though motile cilia are crucial for the proper functioning of an organism, the focus here will be on primary cilia (referred to interchangeably as “cilia”).

While the primary cilium was first described in 1898, only recently have studies gained momentum regarding its function as a sensory organelle (Zimmerman, 1898). It is now understood that primary cilia can detect mechanical and chemical signals from the extracellular environment and elicit a response within the cell, a theory that was initially postulated by Barbara Barnes (Barnes, 1961). Key to understanding this were genetic studies conducted on vertebrate development (Huangfu et al., 2003). Mice that had mutations in two intraflagellar transport (IFT) proteins showed abnormal embryonic morphology and dysfunctional cilia. The dysfunction resulted in a disruption in Hedgehog signalling, which is required by embryonic cells for proper development (Echelard et al., 1993). Aside from the Hedgehog signalling pathway, primary cilia have also been reported to be involved in Wnt and platelet-derived growth factor signalling pathways (Corbit et al., 2008; Schneider et al., 2005). As these pathways are all extremely important to proper cell function, it is not surprising that cilium assembly is a tightly-controlled, cell cycle specific event.

1.6.4.1. Making a primary cilium

The primary cilium forms from a docked mother centriole at the plasma membrane. This process occurs during G0/G1 and the cilium is resorbed before mitosis to accommodate the role that the centrosome has in organising a mitotic spindle. When the mother centriole docks it becomes redefined as a basal body. The biochemical steps leading to this docking have been the focus of many studies recently, although a carefully conducted electron microscopy study expertly detailed the physical steps in the 1960's (Figure 1.7) (Sorokin, 1968).

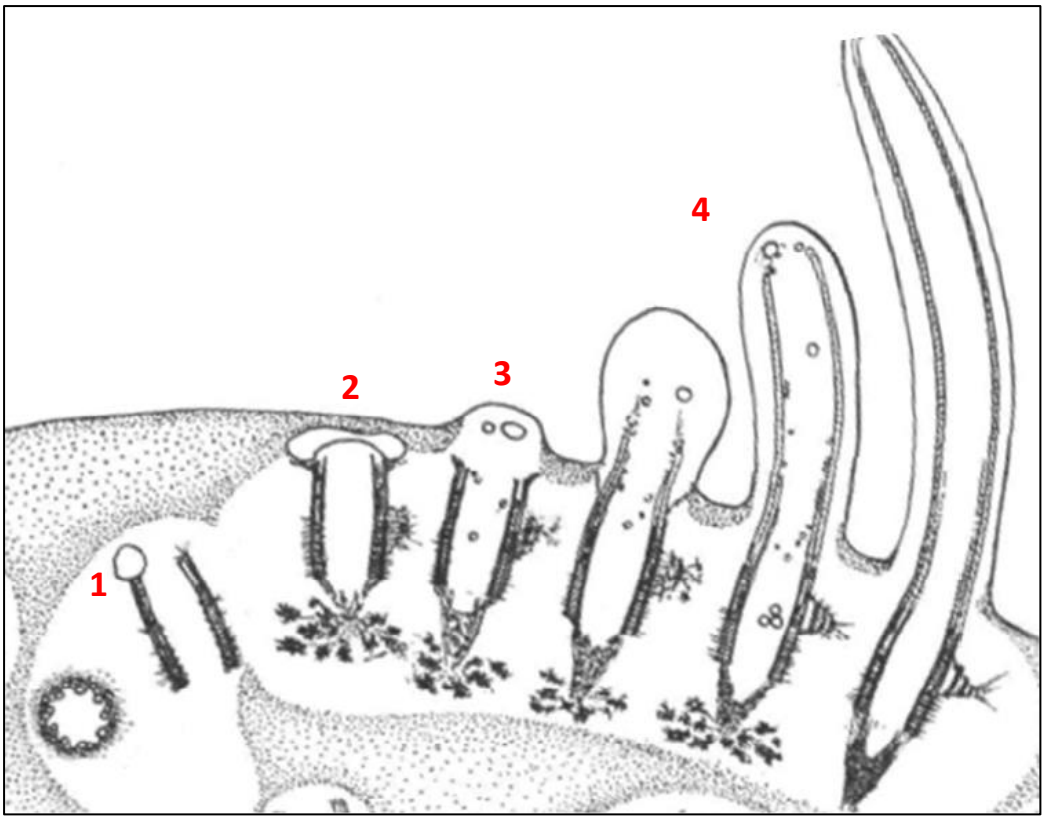

Figure 1.7 Physical stages of ciliogenesis drawn by Sorokin in 1968
The physical stages of ciliogenesis are distinct under electron microscopy. Vesicles localise to the distal end if the mature centriole (1). These then combine to form one enlarged ciliary vesicle (2). Following this, the centriole binds to the plasma membrane, becoming a basal body (3) and the axoneme is extended (4). Illustration adapted from Sorokin, 1968

1.6.4.2. Vesicle assembly and fusion

During the initial stages of ciliogenesis, small distal appendage vesicles (DAVs) localise to the mature centriole (Figure 1.8). These vesicles need to bind to each other and the mature centriole to form a ciliary vesicle and initiate ciliogenesis. Electron microscopy has shown that the DAVs initially bind to the distal end of the mature centriole in a process reliant on a number of distal appendage proteins (Ye et al., 2014). Cep164, Cep89, Cep83 SCLT1 and FBF1 are all distal appendage proteins required for this process and appear to act in a hierarchal order (Figure 1.3) (Tanos et al., 2013). When the DAVs are bound to the distal end of the mother centriole, the kinase TTBK2 is recruited. This recruitment is essential to remove the CP110 cap, which acts as an inhibitor of cilliogenesis (Goetz et al., 2012; Spektor et al., 2007). The removal of CP110 allows the distally bound DAVs to merge and form the ciliary vesicle. This step has recently been shown to involve endosomal membrane trafficking proteins, EHD1 and EHD3. Knockdown of these proteins was

shown to significantly reduce ciliation and, on further inspection, this was deduced to be the result of a failure to recruit a vesicle fusion mediator, SNAP29 (Lu et al., 2015).

1.6.4.3. Vesicle extension

When the ciliary vesicle is formed it becomes extended. While Rab GTPases are known to be involved in this process, specific details about their localisation and interactions at primary cilia have only gained momentum recently (Feng et al., 2015; Lu et al., 2015). Rab8 is plays an important role in tubulovesicular trafficking and has been shown to be required for the ciliary extension during ciliogenesis (Nachury et al., 2007; Peranen et al., 1996). In order for Rab8 to function properly, the guanine exchange factor (GEF) Rabin 8 is required. Recruitment of Rab8 to CV is dependent on Cep290, while Rabin8 is localised via Rab11 (Knodler et al., 2010; Westlake et al., 2011).

1.6.4.4. Axoneme extension and Intraflagellar transport

As all protein synthesis is restricted to the cytoplasm, continued growth of the axoneme is dependent on the transport of ciliary proteins to and from the tip by Intraflagellar transport (IFT). IFT was first observed by enhanced digital interference microscopy (DIC) microscopy of immobilised *Chlamydomonas* flagella. It was seen as a continuous movement of granular particles (IFT particles) which move bidirectionally underneath the flagellar membrane (Kozminski et al., 1993). This process of IFT transport was subsequently found to be mediated by motor proteins. These act in opposing directions with the outward or anterograde movement powered by kinesin-2 and the inward or retrograde movement driven by cytoplasmic dynein-2 (Pazour et al., 2005; Pedersen and Rosenbaum, 2008). Two subcomplexes of IFTs have been identified, IFT-A and IFT-B. Each subcomplex is composed of several individual IFT proteins with mutations in these components attributed to a range of ciliopathies (Taschner et al., 2012). In order to get to the cilium tip, the IFT complexes must first pass through the base. While this is a poorly understood process it is thought to be mediated in part by the distal appendage component FBF1 (Wei et al., 2013). When ciliary growth is complete there is a continuous turnover of tubulin at the tip. This balance determines the length of the cilia and demonstrates

that many of the elements necessary for assembly are also required for maintenance (Marshall and Rosenbaum, 2001).

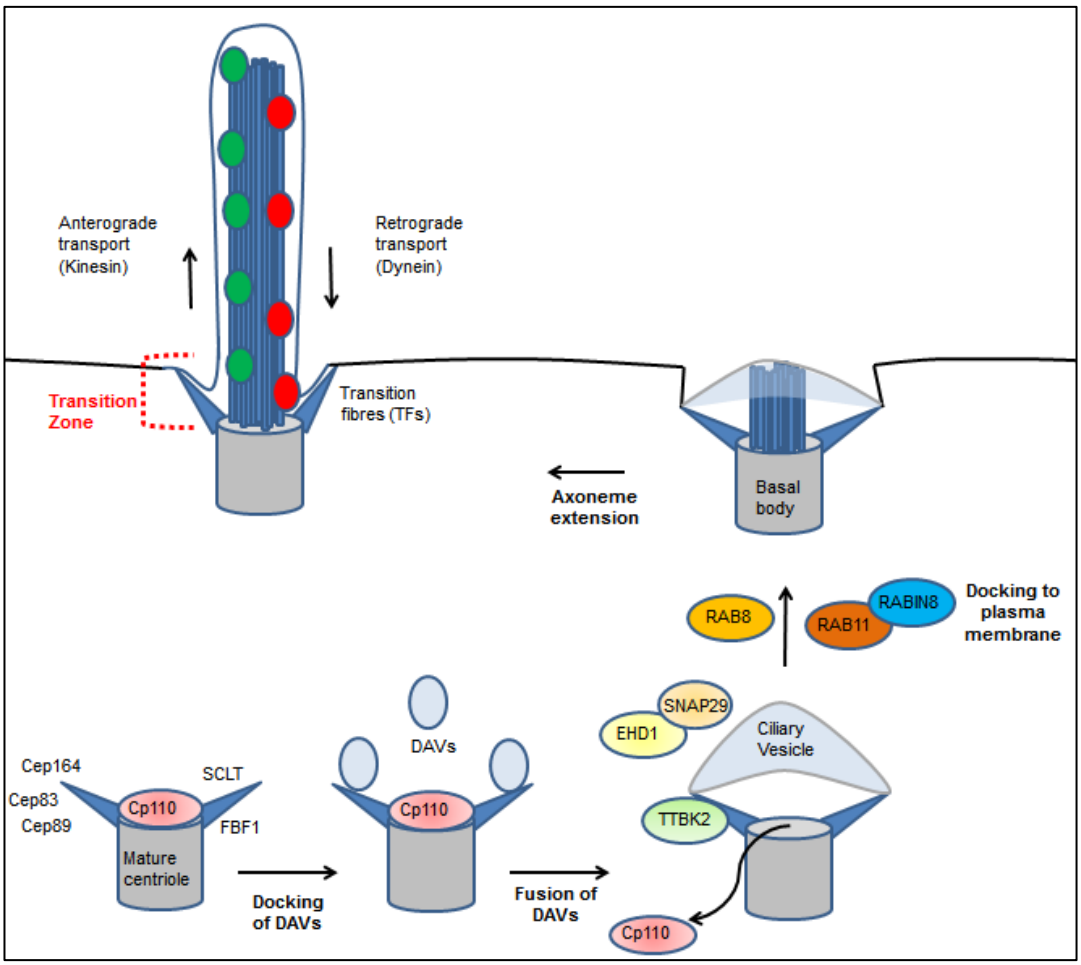

Figure 1.8 The biochemical steps necessary for ciliation
During the very early stage of ciliogenesis, small DAVs first dock to the DAs of the mother centriole through an unknown mechanism (1). EHD1 and SNAP29 then regulate the fusion of DAVs into the large PCV (2). During the formation of PCV, TTBK2 is recruited to TFs by CEP164 to remove microtubule cap protein CP110 to initiate axoneme elongation. Then the interaction between Rabin8/Rab8 complex and CEP164/Cby complex mediates the recruitment of more Rab8 positive vesicles to support membrane extension of the PCV (3). Meantime, the TZ starts to form, the basal body-PCV migrates to the plasma membrane, and then the PCV fuses with the cell membrane through an unknown mechanism (4). Lastly, IFT regulates the extension of the axoneme. FBF1 acts as the functional component on TFs to facilitate the ciliary import of assembled IFT complex. Polarized vesicle trafficking and exocytosis have been implicated in mediating ciliary cargos targeting to periciliary membrane, and then these cargos enter into cilia through lateral diffusion. But, whether TFs play a role in this process is not clear. In other cell types, an alternative ciliogenesis pathway (5) may be employed: the basal body directly docks to the plasma membrane independent of DAV/PCV route. TFs, transition fibres; TZ, transition zone; DAs, distal appendages; DAVs, distal appendage vesicles; PCV, primary ciliary vesicle.

1.6.4.5. Primary cilium disassembly

Primary cilia are regarded as incompatible with mitosis and have to be disassembled before that phase of the cell cycle can occur. Nek2, a protein involved in centrosome separation, has also been shown to be required for the timely resorption of the cilium (Spalluto et al., 2012). Nek2 localises to the distal end of the mature centriole during G2, where it facilitates disassembly. It is at the distal end where it is reported to interact with and phosphorylate the kinesin Kif24. This phosphorylation promotes a conformational change in Kif24 and allows it to depolymerise specifically the cilium microtubules (Kim et al., 2015). Microinjection of Aurora A into cells has also been shown to also promote cilium disassembly in a process dependent on HEF1 (Pugacheva et al., 2007). The HEF1-Aurora A complex is thought to be stabilised by Plk1 (Lee et al., 2012). As is evident primary cilia disassembly involves multiple distinct pathways interconnected with each other.

1.7. Cep164

Cep164 was initially identified through a proteomic analysis of purified centrosomes in 2003 (Andersen et al., 2003). However, it was 2007 before a function was attributed to Cep164. In an siRNA screen of several centrosomal proteins, ciliogenesis was significantly impaired upon Cep164 depletion. Through the use of antibodies against Cep164, it was seen to localise to the mother centriole by immunofluorescence microscopy. This was further specified with immunogold-electron microscopy placing Cep164 at the distal appendages of the mother centriole (Graser et al., 2007). The significance of Cep164 to human disease was realised in patients with Nephronophthisis-related ciliopathies (NPHP-RC). In these disease-affected individuals, mutations are present in the coding sequence of Cep164, abrogating localisation at the mother centriole and preventing ciliation (Chaki et al., 2012). A combination of siRNA and electron microscopy has provided more insight into the exact function of Cep164 during ciliogenesis. At a mechanistic level, the absence of Cep164 results in the failure of mother centrioles to dock distal appendage vesicles. In addition, two components of the vesicle transport machinery, the small GTPase Rab8 and its guanine–nucleotide exchange factor Rabin8, were identified as interaction partners of Cep164 (Schmidt et al., 2012). Recently TTBK2

has been shown to form a complex with Cep164 at the mother centriole, an essential step for efficient ciliogenesis, as TTBK2 removes the CP110 cap which prevents this process (Cajanek and Nigg, 2014).

In addition to its role in ciliogenesis, Cep164 has also been implicated in the DNA damage response. A BLAST search of the human exome using sequence from UVSB (an ATR interacting homologue in *Aspergillus nidulans)* identified Cep164 as sharing homology and therefore potentially having a role in DNA repair (Sivasubramaniam et al., 2008). To further investigate this, antibodies were generated against Cep164. These antibodies showed a nuclear localisation of Cep164 in HELA cells and upon UV or HU treatment foci were detected within the nucleus. Cep164 was shown to interact with ATR and ATM and reported to be essential for the phosphorylation of H2AX, MDC1, CHK2, and RPA upon UV and IR (Sivasubramaniam et al., 2008). Another study has implicated Cep164 in the nucleotide excision repair pathway (NER), with its depletion sensitising cells to UV damage. In the NER pathway Cep164 is reported to interact with XPA and become localised to cyclobutane pyrimidine dimers (Pan and Lee, 2009).

With links to the DNA damage response, the centrosome and nephronophthisis (the most common genetic cause of childhood kidney failure), Cep164 provides an interesting avenue of research in which to explore the mechanism that links ciliary dysfunction with defects in the DNA damage response. As the centriolar protein centrin2 has recently being shown to be indispensable for proper nucleotide excision repair, the potential for exploring this NER link further with regard to Cep164 is especially interesting.

1.8. Aims of the study & model system selection

1.8.1. Aims of study

Despite the clear link between the centrosome and the DNA damage response, much is unknown about how and why this connection has manifested. Cep164 is a known distal appendage protein and has an essential role in ciliogenesis. There are also reports of Cep164 having a role in the DNA damage response, specifically NER. In this study we aimed to clarify the exact role of Cep164 in the DDR. We wanted to investigate the link between NER and the centrosome and to address if the potential role of Cep164 in this pathway was related to the role of centrin2 as a factor in the NER recognition complex. To do this we decided to use a reverse genetic analysis approach in both chicken and human model systems. Initially our study was to be conducted solely in chicken DT40 cells but advances in gene targeting technology made using a human cell line feasible. In the chicken DT40 model system we insert a degradable and fluorescent tag at the endogenous *CEP164* locus. We investigate the effect of Cep164 depletion on cell viability and proliferation in addition to centrosome integrity and duplication. We also test the response of Cep164 deficient cells to DNA damaging agents, IR and UV radiation.

To corroborate our results in chicken we also disrupt the *CEP164* locus in human hTERT-RPE-1 cells. In these Cep164 null cells, we again monitor any changes in cellular/centrosomal function and DNA damage response. We also investigate the impact on ciliogenesis in the absence of Cep164.

1.8.2. Model system selection and comparison

While it is estimated to be ~300 million years since the last common ancestor of human and chicken, many orthologous genes are present between the species, especially in relation to basic cell functions such as DNA damage (Brown et al., 2003; International Chicken Genome Sequencing, 2004). This is not surprising as many genes which have an essential function in these cellular processes have been conserved from yeast to vertebrates (Nyberg et al., 2002; Zhou and Elledge, 2000). In comparing DDR research, findings from work conducted in DT40 and human cell lines have shown that the major players are conserved with regard to function. ATM, ATR, BRCA1, 53BP1, MCPH1 and MDC1 are just some examples of DDR proteins that have all been studied in the DT40 model, with research has been driven

by the ease at which gene ablation and point mutation studies could be carried out in this model system (Sato et al., 2012; Yamazoe et al., 2004). Extensive comparisons of phenotypes of HR-deficient mutants have revealed no significant difference between DT40 cells and murine cells, a mammal model relatively genetically similar to humans (Yamazoe et al., 2004).

Studies on centrosome function and composition have also been conducted in a range of species, including DT40. The relevance of these studies to human cell functions is supported by an evolutionary analysis of 53 centriolar proteins in which it was found that many of the functions of centrosomal proteins are ancestral and that the composition of the centriole is highly conserved between vertebrates (Hodges et al., 2010). Indeed some seminal work has been produced in the field of centrosome biology in DT40 including the first genetic ablation of the centrioles and the first knock-out of CHK1 (Sir et al., 2013; Zachos et al., 2003).

As discussed in section 1.8.1 we undertook this study in both chicken DT40 and human hTERT-RPE-1 model systems. The relative ease of performing gene targeting in the chicken DT40 model has resulted in it being widely used for gene function analysis (Winding and Berchtold, 2001). This along with the well-established protocols for ablating and/or modifying a gene made DT40 an ideal model to conduct our studies (Takata et al., 1998). In addition to being highly genetically tractable in a directed and targeted manner (before CRISPR technology), DT40 also have the benefit of a stable karyotype in culture and a relatively fast cell cycle of ~8h. One drawback of the DT40 B-lymphocytes is there comparatively small size (7-12μm) which makes imaging difficult.

In comparison to DT40, hTERT-RPE1 cells have the advantage of being a human cell line, thus allowing more reliable conclusions to be made with regard to human cell function. The ability of these cells to readily ciliate also provided another avenue of investigation with regards to Cep164 function. The larger cell size compared to DT40 is also advantageous when conducting microscopy although the slower cell cycle (~24h) results in longer experimental procedures.

While there are obvious differences between the chicken DT40 and human cell lines, the similarities between systems supported our choice to undertake this study in both models and would allow us to make meaningful interpretations of our results.

Chapter 2. Materials & methods

2.1. Chemical reagents

The chemicals used throughout this study were of analytical grade and were purchased from Sigma (Arklow, Ireland), Fisher (Leicestershire, UK) or GE Healthcare (Buckinghamshire, UK). All common solutions and buffers used in this study were prepared using ddH_2O or MilliQ- purified water (Millipore, Billerica, Massachusetts) and were autoclaved/filtered before use if necessary. These are listed in Table 2.1 (alphabetical order).

Table 2.1. Common reagents and buffers

Solutions and reagents	Composition	Notes and use
Blocking solution (immunofluorescence microscopy)	1% BSA in 1x PBS. Filter sterilise and store with 0.1% Sodium azide	For blocking cells and diluting antibody
Blocking solution (Southern blot)	10% caseine in maleic acid wash buffer	For blocking of Southern blot membranes
Blocking solution (Western blot)	1x PBS, 0.1% Tween-20, 5% dried milk	To decrease the unspecific binding of antibodies
1x Ca^{2+} buffer	10mM HEPES pH 7.5, 140mM NaCl, 2.5mM $CaCl_2$	For AnnexinV staining
Church hybridistion buffer	0.5M NaPi, 7% SDS	For Southern blot hybridisation
Church wash buffer	40mM NaPi, 1% SDS	For Southern blot washes
Coomassie brilliant blue	0.5% Coomassie in 35% Methanol, 14% Acetic acid	For SDS-PAGE analysis
2x Cytoskeleton buffer (CB)	137mM NaCl, 5mM KCL, 1.1mM Na_2HPO_4, 0.4mM KH_2PO_4, 2mM $MGCl_2$, 2mM EGTA, 5mM PIPES, 5.5mM Glucose pH to 6.1	To prepare fixation and permeabilisation buffers for immunofluorescence microscopy, filter sterilized
DABCO (1,4-diazabicyclo [2.2.2]octane)	2.5% DABCO, 50mM Tris base pH 8, 90% Glycerol	For mounting slides
Denaturation solution	1.5M NaCl, 0.5M NaOH	For the denaturation of DNA in Southern gels
DEPC water	0.1% DEPC in ddH_2O	For RNA work
Depurination solution	250mM HCl	For fragmenting DNA in Southern gels
Detection buffer	0.1M Tris base pH 9.5, 0.1M NaCl	To bring the Southern membrane to the right pH before DIG probe detection
Coomassie destain solution	30% methanol, 10% acetic acid	For destaining Coomassie-stained gels

6x DNA loading dye	20% sucrose, 0.1M EDTA pH 8.0, 1% SDS, 0.25% Bromophenol blue, 0.25% Xylene cyanol.	For loading of DNA samples on agarose gels
Immunofluorescence fixation solution	4% paraformaldehyde in 1x CB	For fixation of cells for immunofluorescence microscopy
Immunofluorescence fixation solution	Methanol supplemented with 5 mM EGTA or 4% Paraformaldehyde in CB buffer	For fixation of cells for immunofluorescence microscopy
Immunoprecipitation buffer	50mM HEPES pH 7.3, 150mM NaCl, 2mM EDTA, 0.5% NP-40, 10% Glycerol	For immunoprecipitation of endogenous and tagged proteins
High stringency buffer	0.5x SSC, 0.1% SDS	For Southern blot membrane washes
Low stringency buffer	2x SSC, 0.1% SDS	For Southern blot membrane washes
Luria-Bertani (LB) Medium	1% Tryptone, 0.5% yeast extract, 1% NaCl, pH 7.0	For growth of bacteria (*Escherichia coli*) cultures
Neutralization solution	1.5M NaCl, 0.5M Tris base, pH 7.5	For neutralization of Southern gels
Maleic Acid Washing Buffer	100mM Maleic acid pH 7.5, 150mM NaCl, 0.3% Tween-20	For membrane washes in non-radioactive Southern blot
Permeabilisation buffer	0.15% Triton-X-100 in 1x CB or PBS	For permeabilisation of cells for immunofluorescence microscopy after PFA fixation
1x Phosphate buffered saline (PBS)	137mM NaCl, 2.7mM KCl, 1.4mM NaH_2PO_4, 4.3mM Na_2HPO_4, pH 7.4	For washing cells
PBS-Tween	1x PBS with 0.1% Tween-20	For washing Western blots
Ponceau S	0.5% Ponceau S., 5% Acetic acid	For staining Western blot membranes
Primary antibody dilution buffer	1x PBS, 0.1% Tween-20, 1% Milk	For dilution of primary antibody for Western blot
Primary antibody dilution buffer	1x PBS,0.1% Tween-20, 5% BSA	For dilution of primary phospho-antibodies for Western blot
RIPA buffer	50mM Tris base pH 7.4 (with HCl), 1% NP-40, 0.25% Sodium deoxycholate, 150mM NaCl, 1mM EDTA	For extraction of proteins
Running buffer	1x TG, 0.1% SDS	For running acrylamide gels
3x Sanple buffer	150 mM Tris base pH 6.8, 45% Sucrose, 6mM K-EDTA pH 7.4, 9% SDS, 0.03% Bromophenol blue.	For loading western samples on SDS-PAGE gels
10x Salt-sodium citrate (SSC)	1.5M NaCl, 0.15M Sodium citrate, pH adjust to 7.0 with Citric acid	For transfer of DNA from Southern gels to nylon membranes

SCac buffer	0.1M Sodium cacodylate buffer pH 7.2	To wash cell pellets for TEM
Super Broth	0.5% Tryptone, 2% Yeast extract, 0.5% NaCl, pH 7.5	To grow bacterial cultures
1x TAE buffer	40mM Tris base, 20mM Acetic acid pH 8.0, 1mM EDTA	For preparation and running of agarose gels
1x Tail buffer	50mM Tris base pH8.8, 100mM EDTA, 100mM NaCl, 1%SDS	For extraction of genomic DNA
1x TE buffer	10 mM Tris base, 1 mM EDTA	To elute DNA
1x TG buffer	25mM Tris base, 192mM Glycine, pH 8.3	For making running buffer and transfer buffer for western blot
1x Transfer buffer	1x TG buffer, 20% Methanol, 1%SDS	For wet transfer of proteins from SDS-PAGE gels to nitrocellulose membranes
1x Transfer buffer	1x TG 20% methanol, 1% SDS	For wet transfer
1x Washing buffer	0.1M Maleic acid, 0.15M NaCl, pH 7.5, 0.3% Tween-20	For washing Southern blot membranes

2.2. Molecular biology reagents

The restriction enzymes used for DNA digestion and ligation were obtained from New England Biolabs (NEB, Herfordshire, UK). The DNA polymerases KOD and SigmaTaq used for polymerase chain reactions (PCR) were obtained from Novagen (Darmstadt, Germany) and Sigma, respectively. Shrimp Alkaline Phosphatase (SAP) was obtained fom USB (Cleveland, Ohio). DNA 1kb ladder was supplied by Invitrogen and protein size markers by NEB and Fermentas (Glen Burnie, Maryland).

The bacterial strain used in this study for general subcloning was *E. coli* Top10 and has the following genotype: F^- *mcrA*Δ*(mrr-hsdRNS-mcrBC)* ϕ*80lacZ*Δ*M15* Δ*lacX74deoR recA1 araD139* Δ*(ara-leu)7697 galU galK rpsL(*Str^R*) endA1 nup***.*** *Escherichia coli (E. coli)* clones were selected using ampicillin (50μg/ml) or kanamycin (30μg/ml) antibiotics (Sigma). The molecular biology commercial kits used during this study are listed in Table 2.2.

Table 2.2. Molecular biology kits used in this study

Name	Use	Supplied by
GenElute Mammalian Genomic DNA Miniprep Kit	Small scale genomic DNA extraction	Sigma
GenElute Plasmid Miniprep Kit	Small scale plasmid DNA extraction	Sigma
Midi Prep Kit (Endotoxin-free)	Large scale plasmid DNA extraction	Qiagen (West Sussex, UK)
QIAquick Gel Extraction Kit	Extraction and purification of DNA fragments from the agarose gel	Qiagen
QIAquickPCR Purification Kit	Purification of DNA fragments	Qiagen
SigmaSpin™ Sequencing Reaction Clean-Up	Purification of DNA fragments	Sigma
Superscript First-Strand Synthesis for RT-PCR kit	cDNA synthesis	Invitrogen
PCR DIG Probe Synthesis Kit	Labeling probe for Southern blot	Roche (Mannheim, Germany)

Several plasmids were acquired for this project. A list of the cloning and expression plasmids used is shown in Table 2.3.

Table 2.3. Commercial or provided plasmids used in this study

Plasmid name	Use	References
pGEM-T Easy	General subcloning and for assembly of knock out targeting vectors	(Promega, Wisconsin)
pBlueScript(SK/KS)		Stratagene (California)
pEGFP-C1/N1	Expression in vertebrate cells	Clontech (California)
pcDNA 3.1	Expression in vertebrate cells	Invitrogen
pANMerCreMer	Recombine loxP sites to recycle resistance cassettes	(Arakawa et al., 2001)
pX330	SpCas9 and chimeric guide RNA expression plasmid.	(Cong et al., 2013)

The antibodies (Abs) used throughout this study were mainly employed for immunodetection in Western blot (WB) and imaging of cells by immunofluorescence (IF) and are listed in Table 2.4 (primary Abs) and Table 2.5 (secondary Abs).

Table 2.4. Primary antibodies used in this study

Antigen	Reference No.	Host species	Dilution for IB	Dilution for IF	Source
α-tubulin	B512	Mouse	1:10000	1:10000	Sigma
Acetylated Tubulin	T 6793	Mouse		1:2000	Sigma-Aldrich
Arl13B	17711-1AP	Rabbit		1:1000	Proteintech (Chicago, Illinois)
ATM	Ab78	Mouse	1:1000		Abcam (Cambridge, UK)
Centrin	20H5	Mouse		1:1000	Millipore
Centrin-3	M01 3E6	Mouse		1:1000	Abnova (Taipei, Taiwan)
Cep135		Mouse		1:5000	(Ohta et al., 2002)
Cep135	1420 739	Rabbit		1:1000	Alex Bird (Bird and Hyman, 2008)
Cep164	HPA037606	Rabbit	1:1000	1:1000	Sigma
Cep164	1C3 A10	Mouse		1:200000	Dr David Gaboriau, CCB
Cep290	1C3 G10	Mouse	1:500	1:200	Dr David Gaboriau, CCB
GFP		Mouse	1:1000	1:500	Roche
γ-tubulin	GTU88	Mouse		1:600	Sigma
γ-tubulin	T3559	Rabbit		1:600	Santa Cruz (Santa Cruz)
Myc	9E10	Mouse	1:1000		Ciaran Morrison, CCB
Ninein	ab4447	Rabbit		1:200	Abcam
OFD1	NBP1-32843	Rabbit	1:500	1:500	Novus Biologicals (Colorado)
PCM-1	817	Rabbit		1:10000	(Dammermann, 2002)
p-ATM S1981	Ab81292	Rabbit	1:1000		Abcam
p-Chk1 S345	2348	Rabbit		1:1000	Cell Signaling
p-H2AX	JBW103	Rabbit	1:1000	1:1000	Millipore

Table 2.5. Secondary antibodies used for this study

Antibody	Conjugation	Host species	Dilution for IB	Dilution for IF	Source
Rabbit IgG (H+L)	Rhodamine Red	Goat		1:1000	Jackson Labs (Bar Harbor, Maine)
Rabbit IgG (H+L)	FITC (fluorescein isothiocyanate)	Goat		1:1000	Jackson Labs
Rabbit IgG (H+L)	FITC	Donkey		1:1000	Jackson Labs
Mouse IgG (H+L)	Texas Red	Goat		1:1000	Jackson Labs
Mouse IgG (H+L)	FITC	Goat		1:1000	Jackson Labs
Mouse IgG (H+L)	FITC	Donkey		1:1000	Jackson Labs
Goat IgG (H+L)	Rhodamine Red	Donkey		1:1000	Jackson Labs
Rabbit IgG (H+L)	HRP (horseradish peroxidase)	Goat	1:10000		Invitrogen
Mouse IgG (H+L)	HRP	Goat	1:10000		Invitrogen
Goat IgG (H+L)	HRP	Donkey	1:10000		Abcam

2.3. Tissue culture reagents and conditions

This study was carried out using the chicken DT40 B-lymphocyte cell line and human retinal epithelial cells immortalized with telomerase (hTERT-RPE1). DT40 cells have a doubling time of 8-10 hours under normal culture conditions of 39.5^{o}C with 5% $CO_{2.}$ (Takata *et al.*, 1998). The reagents used to culture these cell lines include Roswell Parl Memorial Institute (RPMI) 1640 media (Lonza, Basel, Switzerland), Dulbecco's Modified Eagle Medium/Nutrient Mixture F-12 (DMEM/F-12) (Lonza) fetal bovine serum (FBS) (Lonza) (10%), chicken serum (1%) (Sigma) and penicillin-streptomycin antibiotics (1%) (Sigma).

All sterile plasticware used for cell culture was obtained from Sarstedt (Numbrecht, Germany), Corning (Riverfront Plaza, NY), Fisher and Sigma. Unless otherwise stated, cell culture reagents were obtained from Sigma. Cell density was

determined by counting the cells with a haemocytometer (Sigma) as described in the manufacturer's protocol.

Several antibiotics were used for resistance selection in the generation of stable chicken DT40 cell lines. These are listed in Table 2.6 together with the working final concentrations.

Table 2.6. Antibiotics used for selection of stable cell lines

Name of the drug	Final concentration
Blasticidin	25μg/ml
Geneticin (Invitrogen)	2mg/ml
G418 (Invivogen)	2mg/ml
Puromycin	0.5μg/ml

For the treatment of cells with ionising radiation (IR), a 137Cs source at 23.5Gy/min was used (Mainance Engineering, Hampshire, UK) while for UV-C (Ultra-Violet type C) irradiation, cells were irradiated using a 254nm UV-C lamp at 23J/m2/min (NU-6 lamp; Benda, Wiesloch, Germany).

2.4. Cell biology techniques

2.4.1. Cell culture and growth maintenance

Unless otherwise stated cells were spun down and harvested at a speed of 250*g* for 5 mins. Chicken DT40 cells were maintained in exponential growth by adding a minimum of 10^5 cells to 10ml of fresh media and cell density was not allowed exceed 10^6 cells/ml. Human cells were maintained in a humidified 5% CO2 atmosphere at 37°C. DT40 the RPE1 cells used in this study were obtained from American Type Culture Collection (ATCC, Manassas, Virginia).

For freezing and storage, $3x10^6$ DT40 cells were spun down, the supernatant was removed and the cells were resuspended in 300μl FBS supplemented with 10% DMSO. These cells were kept at -80^{o}C for short term storage or stored in liquid nitrogen for longer periods. For RPE-1 cell storage, $1x10^6$ cells were spun down and the supernatant removed. The pellet was subsequently resuspended in freezing media composed of 70% FBS, 20% normal culturing media and 10% DMSO. The cells were then frozen at a -1^{o}C/min gradient in a Mr.Frosty freezing container (Thermo Fisher Scientific, Wilmington, Delaware) until at -80^{o}C where they were kept for

short term storage or transferred to liquid nitrogen for longer storage. To wake up either DT40 or RPE-1 cells, the contents of a frozen vial were warmed in a 37^{o}C water bath before being transferred to 10ml prewarmed media.

For proliferation analysis, cell lines were plated at equal cell densities and counted every 24hrs for 72hrs. Cells were replated at the initial cell density after each count and this dilution factor was taken into consideration when plotting the cell number.

2.4.2. Stable transfections

Stable transfections were peformed to insert foreign or altered DNA into the endogenous genome of chicken or human cell lines.

2.4.2.1. DT40 stable transfections

To generate DT40 cell lines that stably expressed a cloned gene (cDNA) or to target a locus for integration, electroporation was performed. In this procedure the plasmid DNA to be transfected was linearised by overnight digestion (with a specific endonuclease), ethanol precipitated and reconstituted to 1μg/μl. 1x10^{7} cells were then harvested, washed in PBS and resuspended in 0.5ml of PBS. 20μg of the linearised plasmid DNA was then mixed with these cells. The cell and DNA mixture was transferred to a Bio-Rad 0.4μm cuvette and was incubated on ice for 10 mins. Subsequently, the cells were electroporated at 550V/25μF, using a gene pulsar apparatus from Bio-Rad (Hertfordshire, UK) and incubated on ice for a further 10 mins to recover. The cells were transferred from the cuvette to a plate containing 20ml media and incubated for 24 hours. After this period a further 20ml of media was added with the appropriate antibiotic (see Table 2.6.) and the culture was plated in 4x96-well plates where colonies were incubated for approximately 10 days. When the colonies were 2mm in diameter, the contents of the wells were expanded to 3ml cultures in 12-well plates and further incubated for 2-3 days. When confluent, half of the culture was frozen while the other half was used to extract protein or genomic DNA.

2.4.2.2. RPE-1 stable transfections

To generate RPE-1 cell lines that stably expressed a cloned gene, lipofection was performed. In this procedure cells where plated in antibiotic-free media on a

10cm dish to be 80-90% confluent at the time of transfection. Before transfection 5μg linear DNA was mixed with 10μl Lipofectamine 2000 (Invitrogen) in Opti-MEM Reduced Serum Medium (Invitrogen) and allowed to form complexes for 20 mins. This mixture was then added to the cells and they were incubated for 6 hours before the media was changed. The cells were then allowed to recover from the transfection for a further 24 hours before being typsinised and serial diluted in 5 10cm dishes containing conditioned media (filtered media taken from 50% confluent cells) with antibiotic selection. 10-14 days later, single colonies were expanded using 3mm Scienceware cloning discs (Sigma). Clones were screened by WB or IF as appropriate.

2.4.3. DT40 transient transfections

For protein expression in DT40 cells, transfections were carried out using the Amaxa nucleofection system (Lonza, Basel, Switzerland). Using this system, $5x10^6$ cells were harvested, resuspended in 100μl of solution R (supplied with kit) and 5μg of endotoxin-free circular plasmid DNA (see section 2.5.2. for plasmid preparation) was added. This mixture was then transferred to an Amaxa transfection cuvette and nucleofection was performed using the Amaxa program B-23. The cells were transferred to 5ml of media and incubated for 24hrs before being harvested for analysis by IF or WB.

2.4.4. RPE-1 transient transfections

In this procedure RPE-1 cells were plated to be ~70% confluent at the time of transfection. 2-5μg of DNA was mixed with 4-10μl Lipofectamine 2000 (Invitrogen) in Opti-MEM Reduced Serum Medium (Invitrogen) and allowed to form complexes for 20 mins. The lipid-DNA mixture was then added dropwise to the plate and it was returned to the incubator in media without serum. 6 hours post transfection fresh media was put on the cells (containing serum) which were then analysed between 24-48 hours after transfection.

2.4.5. RNA mediated interference

RNA mediated interference was carried out to knock down messenger RNA transcripts in RPE-1 cells. Briefly, cells were seeded the day before transfection to

be 50-60% confluent at the time of transfection. siRNAs were resuspended in RNA-free water to yield a final concentration of 20μM. The siRNAs were transfected using Lipofectamine 2000 as outlined in section 2.4.4.

2.4.6. Clonogenic survival assays

Clonogenic survival assays were performed to assess the effect of DNA damaging agents on cell survival in selected cell lines. For DT40 cell lines these were performed as previously described in (Takata et al, 1998). The composition of the methylcellulose media used to grow the colonies was: 1.5% methylcellulose, 1x Dulbecco's Modified Eagle Medium F-12 (DMEM/F-12) with L-glutamine (Gibco, Invitrogen) and filter sterilised 1.5% chicken serum, 15% FBS 1%, pen/strep and 50μM β-mercaptoethanol. A final concentration of 500μM auxin (3-Indoleacetic acid) (Sigma) was also added to any media in which a Degron tagged protein was to be depleted. Due to the viscosity of the media it was left to stir overnight at 4^{o}C before 7ml was dispensed into each compartment of a 3-section Y-petri dish. The plates were left for 1 hour in the incubator to equilibrate before cells were plated. Cell lines were grown to similar cell densities (5-8x10^{5} cells/ml) and then diluted to 1x10^{5} cells/ml as a stock from which cell numbers could be accurately dispensed onto plates.

2.4.6.1. Gamma radiation clonogenic survival in DT40

To test the sensitivity of DT40 cell lines to gamma radiation an appropriate number of cells were plated onto the methylcellulose medium in each Y compartment of the petri dish. These cells were subsequently exposed to various doses of ionising radiation (0; 2; 4; 8Gy) using a ^{137}Cs source and returned to the incubator.

2.4.6.2. UV radiation clonogenic survival in DT40

To test the sensitivity of DT40 cell lines to UV-C radiation 2.5x10^{6} cells were pelleted, resuspended in 0.5ml of PBS and treated with various doses of UV-C irradiation (0; 5; 10; 20J/m^{2}). After irradiation the cells were serially diluted and plated at the appropriate cell number onto the methylcellulose medium and returned

to the incubator. For any experiment on methylcellulose media the assays were performed in triplicate for each cell line and each treatment dose. Colonies were counted when clearly visible after 8-12 days. Cell survival was expressed as the percentage plated cells that were viable and was normalized to the untreated controls.

2.4.6.3. UV radiation clonogenic survival in RPE-1

For clonogenic survival assays performed in the adherent cell line RPE-1, cells were plated on a 10cm to be 70-80% confluent the next day. These cells were then trypsinised and counted before being serially diluted to appropriate concentrations for plating on 10cm dishes. The cells in each dish were allowed to adhere for 6 hours before the media was removed and they were treated with UV-C irradiation of varying doses (0; 5; 10; 20; 40J/m^2). Conditioned media was used to replenish the dishes and they were returned to the incubator.

2.4.7. Immunofluorescence microscopy

To study DT40 cells under immunofluorescent microscopy, approximately $5x10^5$ cells were centrifuged, resuspended in 200µl media and allowed to adhere on poly-L-lysine coated slides (Thermo Fisher Scientific) for 15 minutes at room temperature. For RPE-1 cells, $5x10^4$ cells were plated on glass coverslips and allowed to incubate overnight. For both cell types the media was subsequently aspirated and the cells were fixed and permeabilized in -20^{o}C 95% methanol with 5mM EGTA for 10 minutes. Alternatively, cells were fixed with 4% paraformaldehyde in cytoskeleton buffer (CB) for 10 minutes and permeabilized with 0.15% Triton X-100 in CB for 30 seconds. After fixation and permeabilisation, cells were incubated in blocking buffer for 45 minutes at room temperature. The cells were then incubated with the appropriate primary antibody (see Table 2.4.) diluted in blocking buffer for 1 hour at 37^{o}C. The slides/coverslips were washed 3 times in PBS for 5 minutes and then incubated with fluorophore-conjugated secondary antibody diluted in blocking buffer at 37^{o}C in the dark. The slides/coverslips were washed again 3 times in PBS for 5 minutes before being

mounted in DABCO supplemented with 1μg/ml DAPI. Coverslips were placed on slides, sealed with nail varnish and stored at 4 ^{o}C.

Images were captured with an Orca AG camera (Hamamatsu Photonics, Hertfordshire, UK) under oil at room temperature on a 1X71 microscope (Olympus, Essex, UK), 100x oil objective, NA 1.35, using Volocity software (PerkinElmer). Merges and individual channel images were exported as TIFFs for publication. Images were then cropped using Photoshop CS6 (Adobe Systems, California).

2.4.8. Electron Microscopy

The protocol for electron microscopy of DT40 and RPE-1 cells was adapted from (Liptrot and Gull, 1992). Unless otherwise stated, all the following steps were carried out at room temperature and each wash consisted of 5 minute incubations with 0.1M sodium cacodylate pH7.2 (SCac) buffer.

$3x10^6$ DT40 or $5x10^6$ RPE-1 cells were pelleted, washed once in PBS followed by two washes in SCac buffer before being fixed with a solution of 2% glutaraldehyde and 2% paraformaldehyde in SCac buffer overnight at 4^{o}C. The next day the pellet was again washed twice with SCac buffer and fixed for a second time with a solution of 1% osmium tetroxide in SCac buffer. The secondary fix was left until the osmium had penetrated through the entire pellet and turned it dark brown. The secondary fix was subsequently drawn off into a 2% solution of ascorbic acid for safe disposal and the cell pellet was washed 3 times in SCac buffer. The pellet was subsequently dehydrated through 2x15 minute incubations of increasing concentrations of ethanol as follows: 30%, 60%, and 90%. This was followed by 3x30 minute incubations of 100% ethanol. The pellet was then treated with propylene oxide for 30 minutes and incubated overnight in a 1:1 mixture of propylene oxide and Agar low viscosity resin (Agar Scientific, Essex, UK). The cell pellet was then embedded in 100% resin for 24 hours with fresh resin replacements every 3 hours for the first 12 hours and at the end of the incubation. After the last resin change, the pellet was incubated for 2 days at 60^{o}C to allow the resin to fully polymerise. Ultra-thin sections (~90nm thickness) were cut from the resulting block using a Reichert-Jung Ultracut E microtome (Leica, Hesse, Germany) and collected onto copper grids. The grids were then loaded into a Leica EM AC20 Ultrastainer for staining using a preset programme. Briefly, the grids were washed in ddH_2O and stained in 0.5% aqueous uranyl acetate for 20 minutes at 20^{o}C. After a new ddH_2O

wash, the grids were stained in lead citrate solution for 10 minutes at 22^{o}C and washed in ddH_2O again. Upon removing the grids from the ultrastainer, the excess water was removed carefully with filter paper and the grids were allowed to air-dry before TEM viewing. Samples were imaged with an H-7000 Electron Microscope (Hitachi, Maidenhead, UK) with an ORCA-HRL camera (Hamamatsu city, Japan) and processed using AMT version 6 (AMT Imaging, Danvers, Massachusetts).

2.5. Nucleic acid techniques

Most of the nucleic acid techniques used in this study were performed as previously described (Sambrook and Russell, 2001).

2.5.1. Agarose gel electrophoresis

To separate DNA fragments by size they were run on agarose gels of 0.6-1%. The gel was made in TAE buffer supplemented with 0.5μ/ml ethidium bromide and were run in Hoefer HE33 tanks (Amersham), in TAE buffer at 60-110V, until the required separation was achieved. The DNA fragments in the gels were then visualized using a UV light transilluminator and images were captured with the attached digital camera (AlphaImager HP system, Protein Simple, California). For DNA extraction, bands were cut out of the agarose gel with a clean scalpel blade. The DNA was then purified using the Qiagen QIAquick Gel Extraction Kit according to the manufacturer's instructions.

2.5.2. Plasmid DNA preparation

Mini and midi plasmid DNA isolation was carried out using GeneElute plasmid MiniPrep kit (Sigma) and NucleoBond Xtra Midi Kit Endotoxin free (Qiagen), respectively. In both procedures, plasmid DNA was prepared according to the manufacturer's instructions. Briefly, bacterial cell cultures were grown overnight at 37^{o}C under agitation in the presence of a selective antiobiotic. For mini plasmid preparations 2ml of an overnight *E. coli* culture was used while for a midi this was increased to 100ml. The resultant DNA pellet was resuspended in MilliQ H_2O and the concentration was quantified using a Nanodrop 2000 (Thermo Fisher Scientific).

2.5.3. CRISPR/Cas9 plasmid generation

To generate CrispR/Cas9 plasmids, gRNAs were designed and ordered as oligos. These were annealed by heating to 95^{o}C for 5 minutes then cooled slowly 1 ^{o}C/min. The annealed oligos were subsequently phosphorylated with T4 Polynucleotide Kinase (New England Biolabs, MA, USA) as per manufacturer's instructions. The pX330 plasmid was obtained from Addgene (MA, USA), digested with BbsI and desphosphorylated with Calf Intestinal Phosphatase (NEB). Annealed oligos were then ligated into the digested pX330 plasmid confirmed by sequencing.

2.5.4. Sequencing

DNA samples were sent to Source Bioscience (Waterford, Ireland) for commercial sequencing. As per recommendation 5ul of 100ng/µl DNA was sent to be sequenced and 5ul of 5pM primer if necessary.

2.5.5. Restriction enzyme digestions

All restriction enzymes used throughout this study were supplied by New England Biolabs (NEB). The reactions were performed using the 10x buffer provided and were supplemented with 0.1mg/ml BSA when necessary. Digestions were performed in accordance with the manufacturer's guidelines on a thermo-stable block for 1-16 hours depending on the amount of DNA being digested.

2.5.6. DNA purification or precipitation

Linearised plasmid DNA was precipitated before transfections by adding 1/10 volume of 3M sodium acetate, pH5.2 and 1 volume of isopropanol. This was mixed and the DNA was centrifuged at 16000g. The pellet was then was then washed with 70% ethanol and pelleted again. The ethanol was removed and the pellet was allowed to air dry before being resuspended in an appropriate volume of MillQ H_2O.

2.5.7. DNA ligations

Digested DNA used for cloning was purified using SigmaSpin Sequencing Reaction Clean-Up columns (Sigma) to remove restriction enzymes and buffers. To prevent self-ligation, digested DNA was dephosphorylated with shrimp alkaline

phosphatase at 37^{o}C for 1 hour, followed by a 20 minute heat inactivation step at 65^{o}C. The ratio of vector and insert fragment used in ligations ranged between 1:1 and 1:10. The ligations were performed using T4 DNA ligase in 1x DNA ligase buffer at room temperature for 4 hours. Reactions were subsequently transformed into competent *E. coli* cells.

2.5.8. Preparation of competent *E. Coli*

To prepare competent *E. coli* cells, a 5ml culture was grown under agitation overnight at 37^{o}C. This culture was then added to 500ml of LB and was left to further incubate until the culture reached an OD_{600} of 0.35-0.4. All subsequent steps were carried out in a cold room to maximise the competency of the cells. The *E. coli* cells were incubated on ice for 5 minutes and centrifuged at 5000g for 15 minutes at 4^{o}C. The supernatant was decanted and the pellet was resuspended in ice cold 0.1M $CaCl_2$ and incubated on ice for 30 minutes. Subsequently the cells were pelleted, resuspended in 0.1M $CaCl_2$ supplemented with 15% glycerol, aliquoted and stored at -80^{o}C.

2.5.9. *E. coli* transformation

To insert foreign DNA into *E. coli*, 50µl of competent Top10 cells were thawed on ice, mixed with ~50ng plasmid DNA and incubated on ice for 20 minutes. After this incubation they were heat shocked at 42^{o}C for 90 seconds and placed on ice for 2 minutes to recover. 1ml of LB broth was added to the cells and they incubated under agitation for 40 minutes at 37^{o}C. Following this, the cells were spun down at 6000g for 1 minute and resuspended in a small volume before being spread on LB agar plates containing an appropriate antibiotic selection and incubated overnight at 37^{o}C. Colonies were picked and grown overnight in LB broth cultures with antibiotics at 37^{o}C and used for DNA preparations the next day.

2.5.10. RNA extraction

Any solutions used for RNA work were treated with 0.1% diethyl pyrocarbonbate (DEPC). To extract RNA, $4x10^5$ cells were pelleted and resuspended in 1ml of TRIzol reagent (Invitrogen). 200µl of chloroform was added and this mixture was centrifuged at 12000g for 15 minutes at 4^{o}C. The aqueous top layer was carefully pipetted off and the RNA was ethanol precipitated and resuspended in a

small volume DEPC-treated ddH_2O. The RNA concentration was determined by reading the 260nm absorbance using a Nanodrop 2000 (Thermo Fisher Scientific) and samples were stored at -80°C or used to make cDNA.

2.5.11. cDNA synthesis

cDNA synthesis was performed using the High Capacity RNA to cDNA kit (Invitrogen) according to the manufacturer's instructions. Briefly 2µg of RNA was mixed with the reverse transcriptase from the Moloney Murine Leukemia Virus (M-MuLV) and the supplied reaction buffer. This mixture was then incubated at 37^{o}C for 60 minutes followed by 95^{o}C for 5 minutes.

2.5.12. Polymerase chain reaction (PCR)

PCRs were performed on a TGradient block (Biometra, Göttingen, Germany) using Sigma Taq or KOD Hot Start polymerases (for higher proof-reading activity). Tables 2.7 and 2.8 show PCR conditions and the concentrations of reagents used.

Table 2.7. PCR reagents and concentrations

Reagent	**Final concentration**	
	Sigma Taq	KOD Hot Start
PCR buffer	1x	1x
Mg^{2+}	1x (2mM)	1.5-2.25mM
dNTP's	200µM	200µM
Primers	0.25µM	0.4µM
Template	1-4ng/µl	1-4ng/µl
Enzyme	0.02U/µl	0.02U/µl

Table 2.8. PCR condtions

PCR step	**Temperature and duration**	
	Sigma Taq	KOD Hot Start
Initial denaturation	94°C - 2 min	95°C - 2 min
Denaturation	94°C – 1 min	95°C - 20 sec
Annealing*	60°C - 30 sec	60°C - 30 sec
Extension	70°C - 30 sec/kb	68/72°C - 30 sec/kb
Final extension	70°C - 5 min	72°C - 5 min
Cycle No.	30	30

*Adjusted if necessary

2.5.13. Genomic DNA extraction

Genomic DNA was extracted from cells to amplify genomic regions interest or to screen for gene targeting. To perform this, 1.5ml of confluent cells were pelleted, resuspended in 0.5ml of Tail buffer (supplemented with 0.5mg/ml proteinase K) and incubated at 37^{o}C overnight. Following this, each sample was shaken vigorously for 5 minutes and 200µl of 6M NaCl was added. This was shaken again for 5 minutes and then centrifuged at 16000*g* for 10 minutes. The supernatant was collected and the DNA was ethanol precipitated and air dried before being resuspended in 70µl MillQ H_2O.

2.5.14. Southern blotting

Southern blotting was carried out to verify genetic insertions made in DT40 cells. To carry out this protocol 35µl of genomic DNA (prepared as in 2.5.12) was digested overnight with a given endonuclease in the presence of RNaseA (0.1mg/ml). The samples were run on a 0.7% agarose TAE gel at 100V for 3-4 hours until a suitable resolution of DNA fragments was achieved. The gel was then imaged, depurinated in 0.25N HCL for 20 minutes, incubated in denaturation buffer for 30 minutes and finally, soaked in neutralisation buffer for an additional 20 minutes. The DNA fragments were transferred to a Hybond-N nylon membrane by upward capillary transfer with 10x SSC buffer. Following transfer, the DNA and membrance were UV cross-linked (300J/cm^2) with a UV Cross-linker (Hoefer UVC500, GE Healthcare).

The probes used for hybridisation in this study were labelled with digoxigenin nucleotides using the PCR DIG Probe Synthesis kit. The typical reagent concentration and reaction conditions used are shown in Table 2.9.

Table 2.9. DIG PCR reagent concentration and conditions

Reagent	Final concentration	PCR step	Temperature and duration
10X PC buffer with $MgCl_2$	1x	Initial denaturation	95°C – 2 min
Dig probe synthesis mix	1x (including 70µM DIG-11-dUTP)	Denaturation	95°C – 30 sec
dNTP's from kit	200µM	Annealing	60°C – 30 sec
Primers	0.4µM	Extension	72°C – 40 sec

Template	0.2-2pg/µl	Final extension	72°C – 5 min
Enzyme provided	0.05U/µl	Cycle No.	30

The membrane was incubated with prehybridisation buffer to warm it to the correct temperature, which was calculated according to the length and GC content of the probe (Roche) before 15µl of the DIG labelled probe was added. The membrane was incubated overnight at the same temperature hybridisation temperature. The following day the membrane was washed twice with low stringency buffer for 5 minutes at room temperature and twice in high stringency buffer for 15 at 65^{o}C. Afterwards, the membrane was blocked with Roche Blocking Solution for 30 minutes at 25^{o}C and then incubated in the same buffer supplemented with anti-digoxigenin antibody (1:10000) for an additional 30 minutes at 25^{o}C. The membrane was then washed twice in maleic acid washing buffer for 15 minutes at 25^{o}C and incubated with Detection Buffer for 2 minutes at 25^{o}C. The membrane was subsequently incubated with CSPD substrate for 10 minutes at 37^{o}C and exposed to autoradiograph (Hartenstein, Germany) for 4-24 hours and then developed (CP 1000 AGFA, Brentford, UK).

2.6. Protein Methods

2.6.1. Protein sample preparation

To prepare whole cell extracts, cells were pelleted, washed once in PBS and pelleted again. After removing the PBS wash, cell pellets were resuspended in an appropriate volume of RIPA (lysis) buffer (60µl /3x10^{6} chicken cells; 60µl/1x10^{6} human cells) and incubated on ice for 30 minutes, vortexing every 10 minutes. The lysed cells were then centrifuged at 16000g for 10 minutes at 4^{o}C and the protein containing supernatant was collected. The protein concentration was determined by diluting 1µl of the sample in 1ml of Bradford reagent (Sigma) and measuring the absorbance at 595nm using a Nanodrop 2000 (Thermo Fisher Scientific). A standard curve was then used to convert this absorbance to a protein concentration.

2.6.2. Sodium dodecyl sulfate-polyacrylamide gel electrophoresis (SDS-PAGE)

For SDS-PAGE 25-100μg protein was supplemented with 3x sample buffer containing 10% β-mercaptoethanol. Samples were boiled at 95^{o}C and loaded alongside a prestained broad range protein marker to determinine molecular wight. The percentage of Acrylamide mix in the SDS-PAGE gel varied depending on the size of the target protein, with higher percentage gels being favoured for low molecular weight proteins (composition in Table 2.10). Gels were run at 150V for 90-120 minutes in running buffer using a the Hoefer mini VE equipment.

Table 2.10

Reagent	**Running gel**		**Stacking gel**
30% Acrylamide mix (37.5:1)	8-10%	12-15%	5%
Tris-HCl pH 8.8 / 6.8	375mM	375mM	125mM
Sodium dodecyl sulfate (SDS)	0.1%	0.1%	0.1%
Ammonium persulfate (APS)	0.1%	0.1%	0.1%
Tetramethylethylenediamine (TEMED)	0.04%	0.04%	0.1%

2.6.3. Semi-dry and wet protein transfer

When the proteins were appropriately separarted by gel electrophoresis, they were transferred to a nitrocellulose membrane (GE Healthcare) using a semi-dry transfer unit (Hoefer TE 77) (GE Healthcare) or a wet transfer unit (BioRad Trans-Blot Cell) (Hercules, California, USA). For either procedure the SDS-PAGE gel was placed on a nitrocellulose membrane between 4 sheets of Whatman paper that had been soaked in transfer buffer. The semi-dry transfer was carried out for 90 minutes at 1 mA/cm^2 while wet transfer was done at 350 mA for 3 hours.

2.6.4. Western blotting

Post transfer, the membrane was rinsed in ddH_2O and stained in Ponceau S solution for 10 minutes to visualise the protein. A picture was taken as a reference of transfer quality and protein loading. The stain was removed by washing for 5

minutes in PBS and the membrane was then incubated in blocking solution for 45 minutes at room temperature on a rocking platform. After blocking, the membrane was incubated with primary antibody in 1% milk PBS-Tween solution overnight at 4^{o}C. Excess primary antibody was washed off with three 5 minute washes in PBS-Tween. The membrane was then incubated with a HRP-conjugated secondary antibody in 1% milk PBS-Tween for 45 minutes at room temperature. Three washes were once again conducted and the membrane was covered with a 1:1 mix of the ECL solutions and incubated for 2 minutes followed by autoradiograph film exposure and development.

2.7. Computer programmes

Immunofluorescence microscopy images were saved as Adobe Photoshop CS version 8.0 files and combined using Adobe Ilustrator CS3 (Adobe) DNA subcloning and plasmid maps were designed with the pDRAW32 software (Acaclone, www.acaclone.com). DNA sequence files were viewed using Chromas software (version 2.31, Digital River GmbH, Shannon, Ireland).

The following databases and programmes were used for bioinformatics:

- The NCBI gene database (http://www.ncbi.nlm.nih.gov/gene/)
- The Ensembl chicken database (http://www.ensembl.org/Gallus_gallus/Info/Index)
- the ESTs (expressed sequence tags) database (http://www.ncbi.nlm.nih.gov/dbEST/),
- Blast (http://www.ncbi.nlm.nih.gov/BLAST)
- ClustalW2 (http://www.ebi.ac.uk/Tools/msa/clustalw2/).

GraphPad Prism 5 (La Jolla, California) was used to performed statistical analysis.

Chapter 3. Reverse genetic analysis of Cep164 in chicken DT40 cells

3.1 Introduction

Cep164 is a centrosomal protein associated with the distal appendages of the mature centriole (Graser et al., 2007). At the distal end, Cep164 is part of a network of proteins that make up appendages circumscribing the centriole. These distal appendages are known to play a key role in ciliogenesis with loss of their components leading to loss of ciliation (Avasthi and Marshall, 2012). Cilia are highly conserved microtubule-based organelles that protrude from the surface of most cell types. B-lymphocytes, such as chicken DT40 cells were originally thought not to form cilia but recent work has described their presence in this cell for the first time (Prosser and Morrison, 2015).

Although initially noted for its role in ciliogenesis, Cep164 has also been reported to have a function in the DNA damage response (DDR) (Graser et al., 2007; Sivasubramaniam et al., 2008). This function was postulated to involve Cep164 acting as a "mediator" in the maintenance of genomic stability, whereby its phosphorylation regulates a DNA damage-activated signaling cascade. Another report has implicated Cep164 in the Nucleotide Excision Repair (NER) pathway of DNA repair, as an interactor of XPA. This interaction is reported to mediate the localisation of Cep164 to UV induced DNA damage (Pan and Lee, 2009).

Centrosomal proteins having roles in the DDR is not unprecedented. With the clear link between centrosome number and genome stability it is unsurprising to find that centrosomal proteins are showing a link to DNA damage. The centriolar protein centrin2 plays a significant part in the NER pathway with its ablation leading to a hypersensitivity to UV light (Dantas et al., 2011). MCPH1, a protein which has been shown to have a role early in the DNA damage response (Lin et al., 2005), also limits centrosome amplification upon ionizing radiation (Brown et al., 2010). Why centrosomal proteins have DDR activity is a key question in this field.

In order to fully investigate the role of Cep164 in the DDR pathway and its other cellular functions we decided to carry out a reverse genetic study in the hyper-recombinogenic DT40 model cell line (Buerstedde and Takeda, 1991). In this part of the study we describe the insertion of an inducible system for the rapid degradation of Cep164 in DT40 cells. To achieve this, we first identified and characterised the

CEP164 locus using the available databases. With this information we could design a suitable targeting strategy and clone the cDNA.

In this chapter we report the successful alteration of the DT40 *CEP164* locus to contain both an auxin inducible degron (AID) and GFP tag and demonstrate no significant effect on cell function upon Cep164 depletion.

3.2 Characterisation and cloning of chicken *CEP164*

3.2.1 Analysis of *CEP164* locus in chicken

To analyse the *CEP164* locus in the chicken genome we used the NCBI database. We searched for the gene that was annotated as *CEP164* and also used the human sequence to search for orthologues. This analysis revealed that both the putative gene in the database and the protein BLAST analysis matched the same sequence in the chicken genome. This confirmed that there is one locus for *CEP164* in chicken, located on chromosome 24, with a number of predicted isoforms. Comparing this chicken locus with its human (and other species) equivalent we examined the exonic structure (using longest predicted sequence) and synteny (Table 3.1).

Gene	Organism	Chr	Upstream locus	Downstream locus	No. of Exons	mRNA length (bp)	CDS length (bp)	Protein length (AA)	Sequence ID
CEP164	Human (Confirmed)	11	*BACE1*	*DSCAML1*	30	5628	4383	1460	NM_014956
	Monkey (Predicted)	14	*BACE1*	*DSCAML1*	33	4937	4374	1457	XM_001094990
	Dog (Predicted)	5	*BACE1*	*DSCAML1*	32	6015	4338	1445	XM_546507
	Mouse (Provisional)	9	*BACE1*	*DSCAML1*	30	5487	4002	1333	NM_001081373
	Rat (Predicted)	8	*BACE1*	*DSCAML1*	30	5474	3978	1325	XM_008766182
	Cow (Predicted	15	*BACE1*	*DSCAML1*	34	6386	4848	1615	XM_010812396
	Chicken (Predicted)	24	*BACE1*	*DSCAML1*	31	5744	4536	1512	XM_417909.3
	Turkey (Predicted)	26	*BACE1*	*DSCAML1*	45	5978	4386	1461	ENSMGAG00000003462
	Xenopus (Predicted)	-	*BACE1*	*DSCAML1*	30	5160	4140	1379	XM_002932927

Table 3.1 Comparison *CEP164* loci across species
This table shows the location, synteny, exonic structure and mRNA/protein length. bp-base pairs; AA-amino acids.

We found that the *CEP164* locus spans 39kb in chicken compared to 91kb in human, with both genes composed of a similar number of exons (31 versus 30) and a comparable coding sequence length. The discrepancy in intron size is in line with the smaller genome size of chicken (1.2×10^6 bp versus 3×10^6 bp) compared to human. The synteny between human and chicken *CEP164* is consistent between both, with an upstream locus of *BACE1* and the downstream locus of *DSCAML1*.

Comparing the protein homology between the human and predicted chicken sequences we found that while the sequence identity in some parts was high, the overall homology was only 28% (Figure 3.2). This suggests that some parts of the protein are more resistant to change than others and may have been conserved to protect function. We compiled the Cep164 protein sequence comparisons from a number of animals in Figure 3.1 and created a molecular phylogenetic tree as shown in Figure 3.2.

Human	-							
Monkey	95	-						
Mouse	62	63	-					
Cow	68	68	52	-				
Dog	74	55	48	66	-			
Rat	52	52	60	55	53	-		
Chicken	28	28	27	38	41	41	-	
Turkey	45	45	23	35	44	46	76	
Frog	20	11	21	26	28	34	9	-
	Human	Monkey	Mouse	Cow	Dog	Rat	Chicken	Frog

Figure 3.1 Comparison of Cep164 protein sequence in selected animals.
The level of conservation is measured by the % of identical residues found in the analysed sequences multiplied by the coverage. The referred values do not account for erroneously predicted sequence information. The proteins used for this comparison and their NCBI Protein database accession number are as follows: Human: NP_055771; Monkey: XP_001094990.2; Mouse: NP_001074842.2; Cow: XP_010810698.1; Dog: XP_546507.3; Rat: XP_008764404.1; Chicken: XP_417909.3;Turkey ENSMGAT00000003898; Frog; XP_002932973.1. Note that NP denotes a confirmed protein sequence whereas XP a predicted protein sequence.

From the sequence comparison of Cep164 between a number of animals we can conclude that it has varying conservation and that chicken has a relatively low sequence conservation. The size of the sequence is similar between all indicating that structural elements of the protein may have been maintained while the specific

sequence was allowed to change, except where important motifs are present (Figure 3.3).

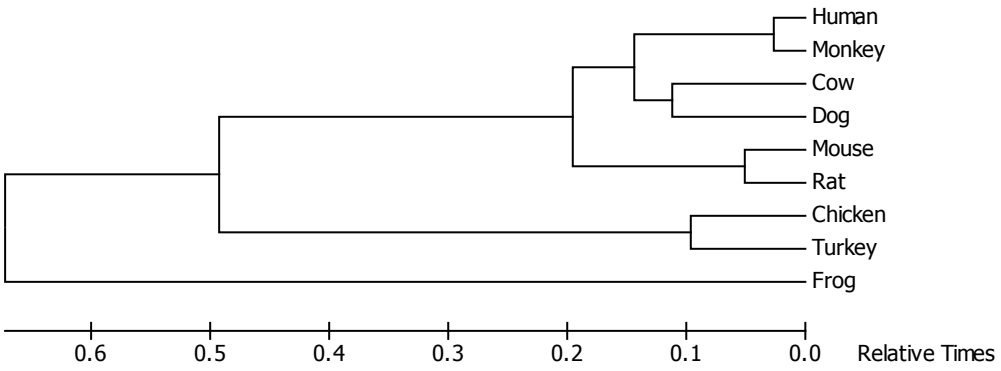

Figure 3.2 Molecular phylogenetic analysis of Cep164.
The tree shown was generated using the RelTime method (Tamura et al., 2012). Divergence times for all branching points in the topology were calculated using the Maximum Likelihood method based on the JTT matrix-based model (Jones et al., 2012). The estimated log likelihood value of the topology shown is -14127.0268. The tree is drawn to scale, with branch lengths measured in the relative number of substitutions per site. The analysis involved 8 amino acid sequences. All positions containing gaps and missing data were eliminated. There were a total of 1217 positions in the final dataset. Evolutionary analyses were conducted in MEGA6 (Tamura et al., 2013).

As expected, the Cep164 sequence-derived phylogenetic tree mirrors the divergence of these animals from the last common ancestor. In Figure 3.2, we can see the different clades the animals fall into when the sequence is compared. This provides a good picture of how the Cep164 protein has diverged over time. On closer inspection of the homology between chicken and human it is evident that a large region in the middle is conserved. No functional domains were detected in this area and it appears to be a coiled-coil region of the protein (Figure 3.3). A small area at the beginning of the protein is also conserved between sequences. This was identified as a WW tryptophan domain which are known to be important for protein-protein interaction (Salah et al., 2012).

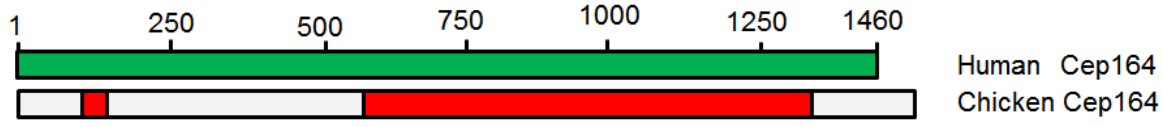

Figure 3.3 Alignment of human and chicken Cep164 protein.
The above schematic is an overlay of the confirmed sequence of human and the predicted sequence of chicken Cep164. The red boxes depict areas of homology over 50% between the chicken and human Cep164 protein sequence. The smaller red box corresponds to a tryptophan domain conserved between both sequences.

3.2.2 Cloning of chicken Cep164

As the chicken Cep164 was a predicted version from the NCBI database we searched the expressed sequence tags (ESTs) using the longest predicted chicken sequence (XP_417909.3) to verify its expression. The chicken ESTs in the NCBI database are derived from sequencing cDNA of various chicken tissues including the trunks (torso), testis and brain so tissue specific expression (if any) could also be crudely analysed. The resulting alignment (Figure 3.4) revealed ~85% coverage with one major gap of 500bp from 750-1250 and some minor ones elsewhere. As the putative start and end of the sequence was well covered, they were used to design primers to these sites and amplify the gene from chicken cDNA.

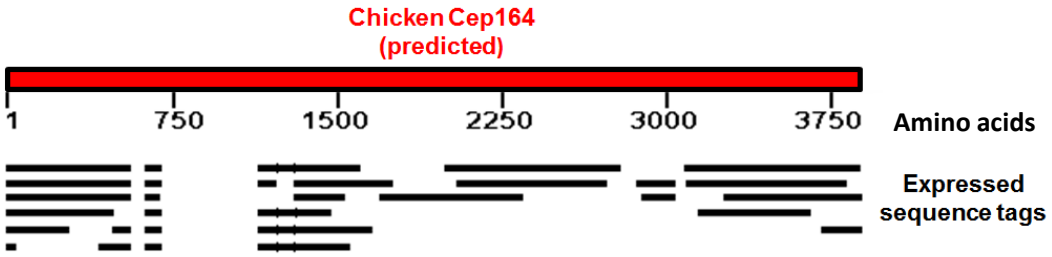

Figure 3.4 Schematic depicting sequence blast of predicted chicken Cep164 against chicken EST database.
Schematic representing the predicted amino acid sequence in red (XM_417909.3) against the EST database for chicken (black) we can see that most of the sequence can be accounted for. One major gap can be seen at position 750-1250 amino acids and a couple of minor gaps elsewhere. Coverage at the start and end of the predicted sequence is suitable for primer design to these areas for *CEP164* cDNA cloning.

To alter the endogenous *CEP164* locus at the 3'end later in the project, the cDNA was cloned in and put it into the pGFP-N1 plasmid. This would allow insight into how the Cep164 protein would function when it was tagged at the C-terminus. To achieve this, a reverse primer was designed that would abrogate the naturally occurring stop codon of Cep164 and therefore allow translation into the GFP tag.

The RT-PCR of *CEP164* using these primers and cDNA from DT40 was successful (Figure 3.5A). We can see from the agarose gel that two similar sized, but distinct bands are present, indicating at least two isoforms of *CEP164*. We then proceeded to clone these into pEGFP-N1 for sequencing and verification. The sequencing results confirmed two isoforms of 3528bp and 3438bp. The differing sizes were due to the presence/absence of two exons, VI and XXII, or 192bp

sequence (Figure 3.5B). Comparing these sequenced isoforms to the predicted gene indicate that the large gap missing in the expressed sequence tags is also missing in both these isoforms. This strongly suggests it is an artefact of the prediction programme (Figure 3.4).

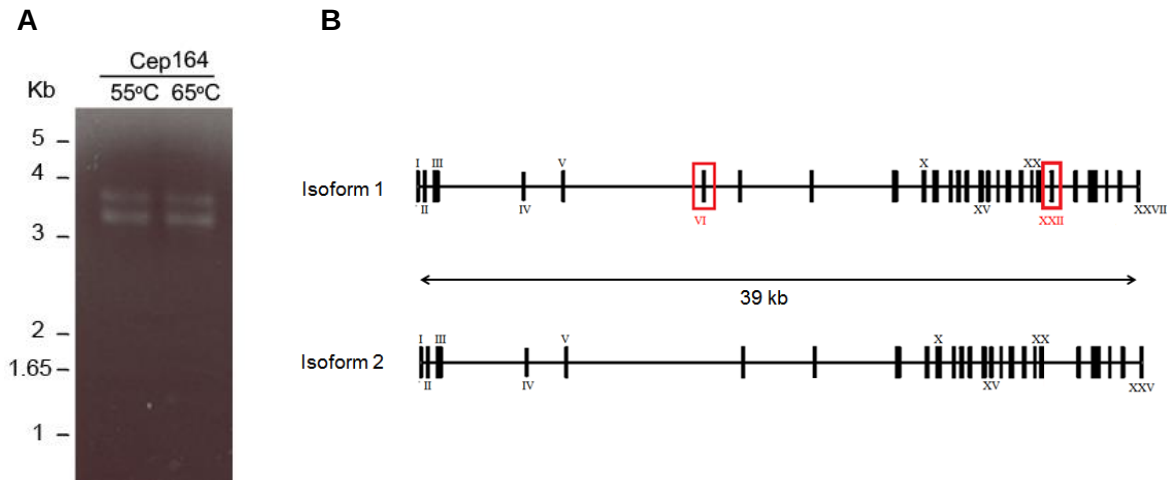

Figure 3.5 Cep164 confirmed size and exon structure
(A) RT-PCR amplification of chicken Cep164. Two bands are evident from the PCR of Cep164 from chicken cDNA. This indicates the presence of at least two isoforms of the protein.
(B) The exonic structure of the sequenced Cep164 isoforms. The larger isoform (1) contains 27 exons composed of 3528bp while the small isoform (2) contains 25 exons composed of 3336bp. The red squares indicate exons present in isoform 1 that are missing from isoform 2.

From the verified sequence we calculated that the translated size protein (without GFP) would equate to roughly 135kDa. To check if this tagged protein was functional and did not affect protein localisation, we transiently overexpressed it in DT40 cells and carried out immunofluorescence microscopy and Western blot (Figure 3.6).

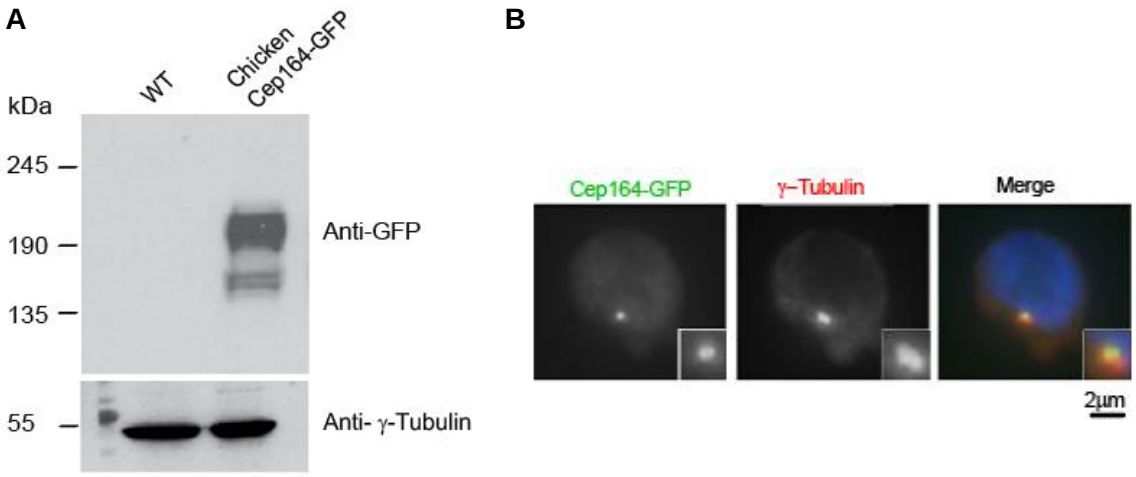

Figure 3.6 Transiently expressed Cep164 localises to the centrosome and is visible by Western blot.
(A) Immunofluorescence microscopy analysis of transiently expressed Cep164-GFP in WT DT40 shows localisation with centrosomal markers centrin2 and γ–Tubulin. **(B)** Western blot of transiently expressed Cep164 shows bands in a range from 150-200 kDa (using Roche anti-GFP). These multiple bands may suggest post-translational modifications.

Exogenously expressed Cep164-GFP localised to the centrosome (Figure 3.6), as has been previously reported (Graser et al., 2007) and was detected by Western blot. The calculated size of the cloned Cep164 cDNA with the GFP tag is ~165 kDa, which is lower than the bands observed on the Western blot. However, it is not uncommon for proteins to migrate anomalously in an SDS-PAGE (Rath et al., 2009). This result was important as when we were initially analysing Cep164 with a commercial antibody (Sigma), we did not observe localisation to the centrosome (Figure 3.7). Thus this was the first confirmation of Cep164 localising to the centrosome in chicken.

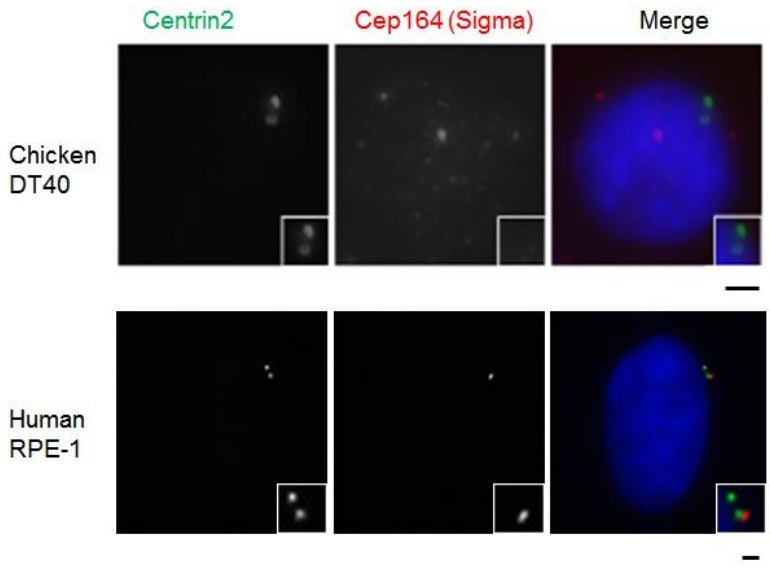

Figure 3.7 Polyclonal antibody raised against human Cep164 does not recognise the chicken protein under IF.
Immunofluorescence microscopy analysis of DT40 WT cells stained for Cep164 and centrin2 shows no co-localisation at the centrosome thus a lack of reactivity across species. Scale bars 2μm.

From the transient overexpression of cloned Cep164 we confirmed the GFP tag did not affect the localisation to the centrosome (Figure 3.6A). This result combined with the fact that the commercial antibody did not recognise the chicken protein encouraged us to incorporate a GFP tag as part of the targeting strategy of the endogenous Cep164 locus.

3.3 Modifying the endogenous Cep164 locus

3.3.1 Targeting strategy and generation of targeting vector

To assess the importance of Cep164 in cellular functions we planned on performing gene targeting in the DT40 cell line. This hyper-recombinogenic cell line is known to produce a relatively high ratio of targeted to non-targeted cells after transfection, if the strategy is designed correctly (Buerstedde and Takeda, 1991). Our targeting strategy (Figure 3.8) was designed to remove the endogenous stop codon and replace it with an auxin-inducible degron (AID) and a GFP tag (Nishimura et al., 2009). The logic behind introducing both an AID and GFP tag is that the endogenous Cep164 protein could be both tracked and depleted.

The unperturbed localisation of transiently expressed Cep164-GFP (Figure 3.6) supported the strategy of targeting the 3' end of the endogenous locus. Flanking 5' and 3' targeting arms were generated and cloned together into one plasmid containing the AID-GFP and resistance cassette. As Southern blotting was the screening method for successful targeting, we also amplified a short stretch of DNA 5' of the targeting construct to be used as a probe (Figure 3.8).

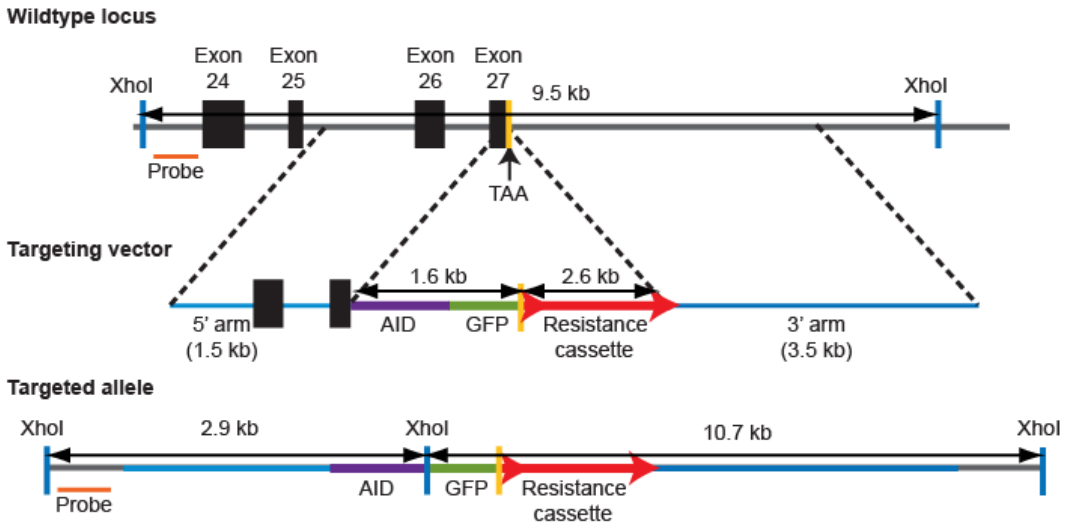

Figure 3.8 Schematic depicting targeting strategy of endogenous Cep164 genomic locus. Successful targeting will integrate an Auxin-Inducible Degron (AID) and GFP tag in place of the stop codon of the last exon. A resistance cassette for selection is also included after the GFP tag. This AID-GFP insert would create a new XhoI site which would change the size of the fragment detected by the 5' probe after restriction digest. This change is visible with a Southern blot and could be confirmed with a Western blot.

The overall change to the endogenous *CEP164* locus is an insertion of ~1400bp AID-GFP to the coding sequence and a separate resistance cassette which is transcribed under its own promoter (Figure 3.8). Significantly for the screening of successfully targeted clones, the alteration introduces new restriction sites which change the band sizes that are visible by Southern blot. Taking the XhoI restriction site in Figure 3.7 we can see that before targeting, the 5' probe would detect a band of 9.5kb, in comparison to a targeted allele where a 2.9kb fragment would be detected.

Non-radioactive Southern blotting was performed using an amplified probe labelled with digoxigenin (Figure 3.9A), a highly antigenic molecule, to visualise the bands bound by the probe. Once this was achieved we tested the probe with a

number of different restriction enzymes that were predicted to produce fragments of a certain size according to the genomic sequence on the NCBI database (Figure 3.9B, C)

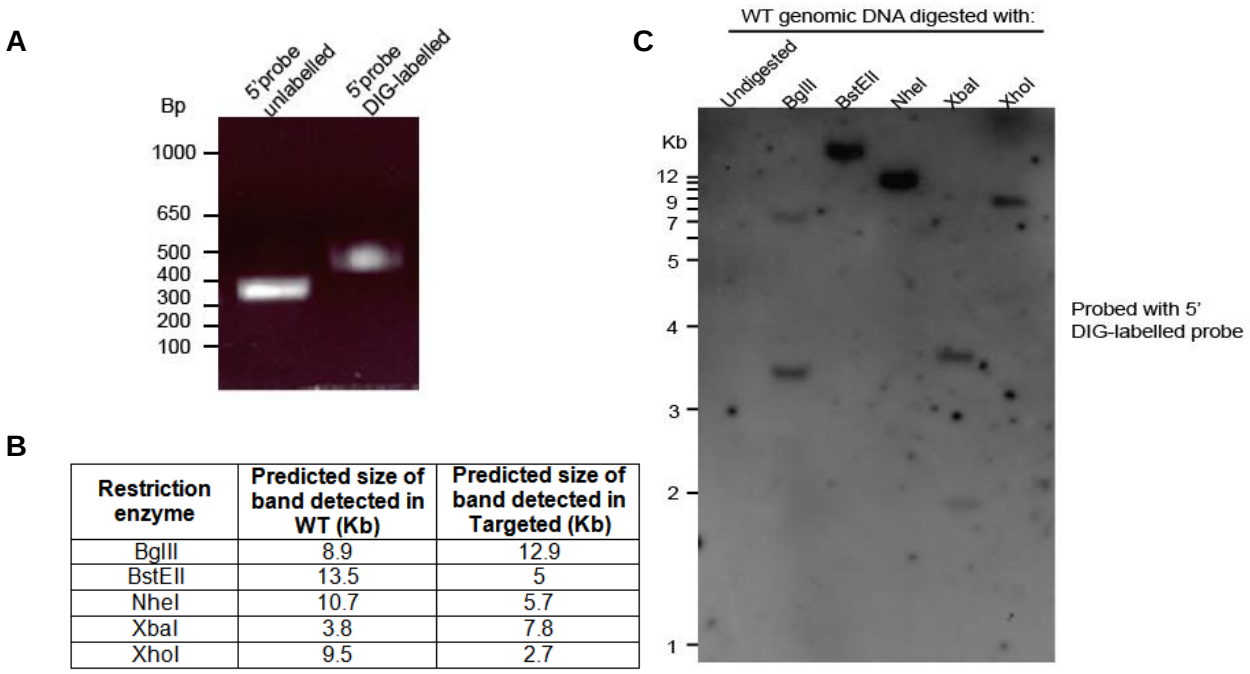

B

Restriction enzyme	Predicted size of band detected in WT (Kb)	Predicted size of band detected in Targeted (Kb)
BglII	8.9	12.9
BstEII	13.5	5
NheI	10.7	5.7
XbaI	3.8	7.8
XhoI	9.5	2.7

Figure 3.9 Labelling and testing of 5'probe confirms suitability for Southern blot screening. (A) Successful PCR and labelling of 5'probe is confirmed by slower migration of the DNA band through an agarose gel. (B) Table showing size of bands that should be detected by Southern blot based on predicted chicken genomic sequence and size that would be detected after targeting. (C) Southern blot test with the DIG-labelled 5'probe on WT genomic DNA. BstEII, NheI, XhoI all show bands in agreement with their respective predicted sizes. However, BglII and XbaI produced extra bands at ~3.5 and ~1.9kb.which were not predicted for WT.

All 5 of the enzymes tested produced a band at the appropriate size. However 2 of these, BglII and XbaI, also produced lower bands than were predicted. This is likely due to extra restriction sites in the genomic DNA that are not accounted for in the NCBI database (possibly due to single nucleotide polymorphisms). Nonetheless, it was clear that the probe was detecting the correct sequence and we would proceed with it for screening potentially targeted clones.

3.3.2 Verification of successful targeting of Cep164 in DT40

After the probe testing, the targeting vector was transfected into DT40 wild-type cells by electroporation (as described in section 2.4.2.1). Thirty-two resistant clones were isolated and their genomic DNA was extracted and digested using XhoI, one of the successfully tested probe enzymes. The 6 clones were screened using the

5'probe and heterozygous clones were identified by the presence of a 2.7 kb band by Southern blot (Figure 3.9b). Two of the heterozygous clones were transfected again with the targeting vector (with different resistance cassette) to alter the second allele. 4 homozygous targeted clones were once again verified by Southern blot by the absence of the 9 kb band (Figure 3.10).

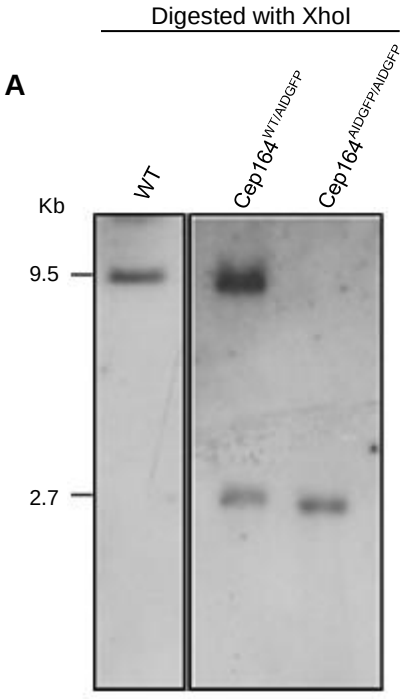

B

Cep164	Resistance used	No. of clones screened	No. of targeted clones	Targeting efficiency
1st allele	Blasticidin	32	6	19%
2nd allele	Puromycin	35	4	11%

Figure 3.10. Southern blots confirming the generation of heterozygous and homozygous targeted clones.
(A) Southern blots showing the successful targeting of the endogenous *CEP164* locus. Genomic DNA was extracted from clones and digested with XhoI. The lower band at 2.7kb is indicative of successful insertion of the AID-GFP tag. (B) Table showing the targeting efficiency of the first and second round of targeting. These were carried out with different resistance cassettes.

For the degron tag to effectively degrade Cep164 in homozygous clones, the F-box protein TIR1 (transport inhibitor response 1) must also be expressed. As this gene is absent in vertebrate cells we inserted a myc-tagged version into the chicken genome by transfection. We then screened clones using a myc antibody to verify TIR1 expression in the cells (Figure 3.11).

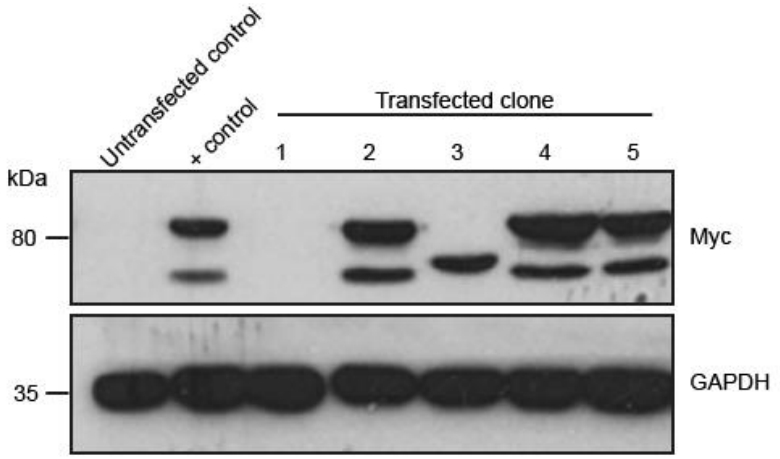

Figure 3.11. Western blot confirming the expression of Myc tagged TIR1 in Cep164 altered clones.
TIR1-Myc (with neomycin resistance cassette) was transfected into *CEP164*$^{AIDGFP/AIDGFP}$ cells. Protein from the obtained clones was blotted for with Anti-Myc. We can see that in addition to our positive control, clone 2, 4 and 5 show the same two bands. Clone 1 is negative while an unknown band is present in clone 3. The expected size of TIR1-Myc is ~70kDa.

As there was a TIR1-expressing DT40 cell line in the lab (Eykelenboom et al., 2013) we used it as a positive control for the Western blot. We obtained a number of clones which shared the same expression pattern as our positive control, so we proceeded to test for the degradation of Cep164 upon auxin addition.

3.3.3 Validation of *CEP164*$^{AIDGFP/AIDGFP}$ localisation and depletion

To verify the expression and the ability to deplete the endogenously tagged Cep164 we treated targeted cells with IAA (Indole-3-acetic acid), the plant hormone which triggers the degradation of AID tagged proteins (Nishimura et al., 2009). We then carried out an immunoblot using a GFP antibody (Roche), similarly to when we were testing the overexpressed protein in Figure 3.6B.

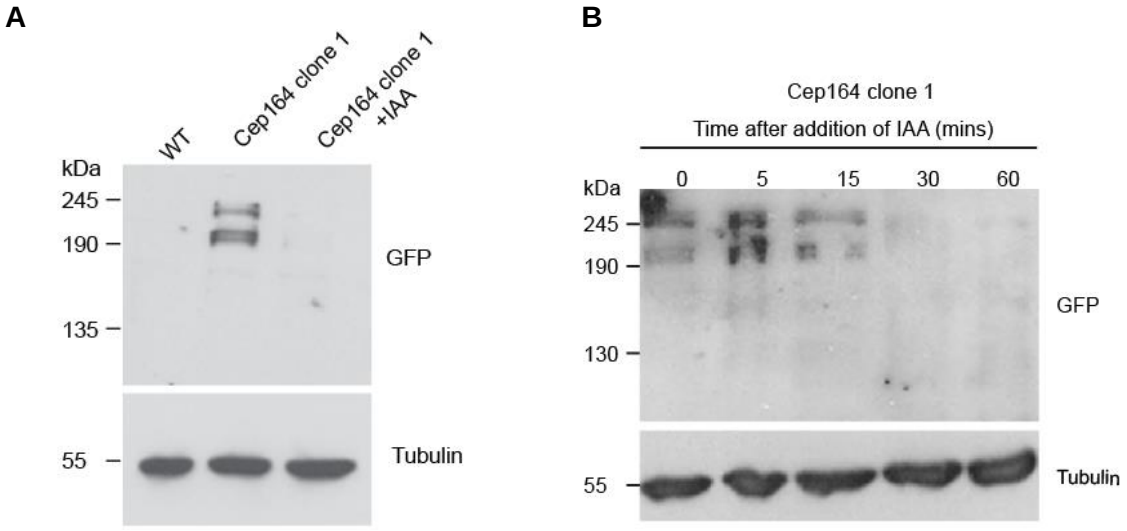

Figure 3.12. Confirmation of the depletion of Cep164-AIDGFP protein upon IAA addition. (A) Immunoblot confirms the expression of Cep164-AIDGFP in the created cell line. The presence of multiple bands is consistent with the overexpression data from Figure 3.6 and may represent other isoforms. 24hrs after the addition of 500μM IAA, all bands corresponding to Cep164-AIDGFP are totally depleted. (B) Immunoblot detection of Cep164-AIDGFP at the indicated time after IAA addition.

The presence of multiple bands in the Cep164$^{AIDGFP/AIDGFP}$ protein extract is consistent with the overexpression data in Figure 3.6. The addition of 500μM IAA depletes all these bands in rapid and effective manner (Figure 3.12) confirming that they are tagged forms the Cep164 protein. The reason for numerous bands is unknown, but may be due to multiple uncharacterised isoforms or post-translational modifications which affect the protein's mobility in the gel.

With confirmation of the efficient depletion of Cep164 upon IAA addition, the localisation of the endogenous protein was tested in our clone under the microscope. As the locus is tagged with GFP the green channel was used to view Cep164 and other channels to co-stain with centrosomal markers. We also treated some cells with IAA 24hrs prior to staining to verify that Cep164-AIDGFP disappears by immunofluorescence in agreement with the Western result (Figure 3.12).

Immunofluorescence microscopy verified the depletion of Cep164 24hrs after IAA addition. The co-markers stained a broad range of centrosomal structures including the centrioles, pericentriolar material and distal appendages. We did not observe any noticeable difference in centrosomal structure between normal and Cep164 depleted cells (Figure 3.13).

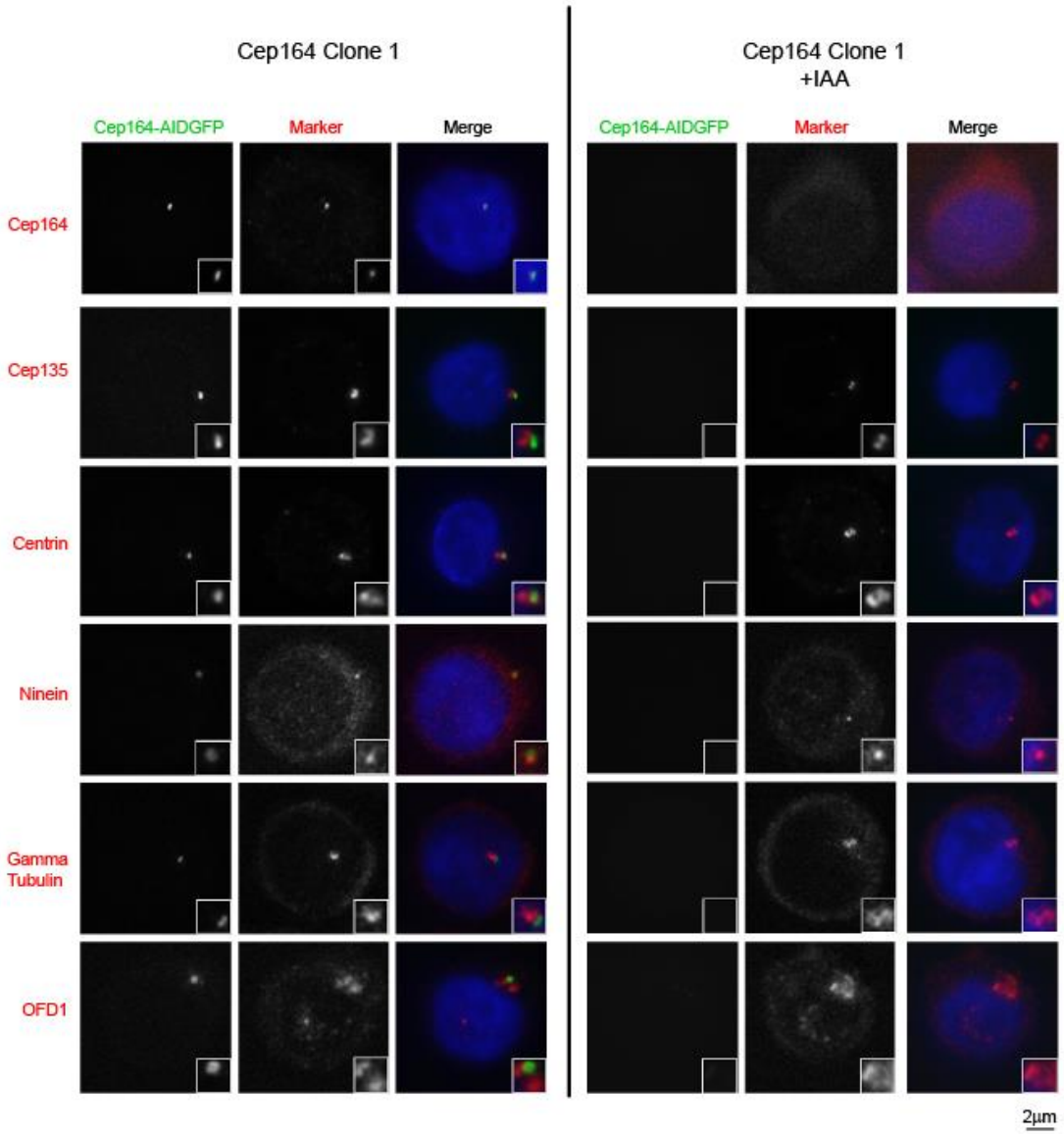

Figure 3.13. Cep164 depleted cells show normal recruitment of various centrosomal proteins during interphase.
Immunofluorescence microscopy shows the depletion of Cep164-AIDGFP 24 hours after the addition of 500µM IAA. Centrosomal co-markers: Cep135, Centrin, Ninein, Gamma Tubulin and OFD1 show no effect in the absence of Cep164. A Cep164 monoclonal also confirms the depletion (The production of this antibody is described in more detail in chapter4).

Taken together, the Western and immunofluorescence microscopy analyses confirm the rapid and effective depletion of endogenous Cep164. As the immunofluorescence analysis was undertaken in interphase cells we decided to also investigate mitotic cells to see if there was any noticeable difference in centrosomal proteins after Cep164 depletion in this phase of the cell cycle (Figure 3.14).

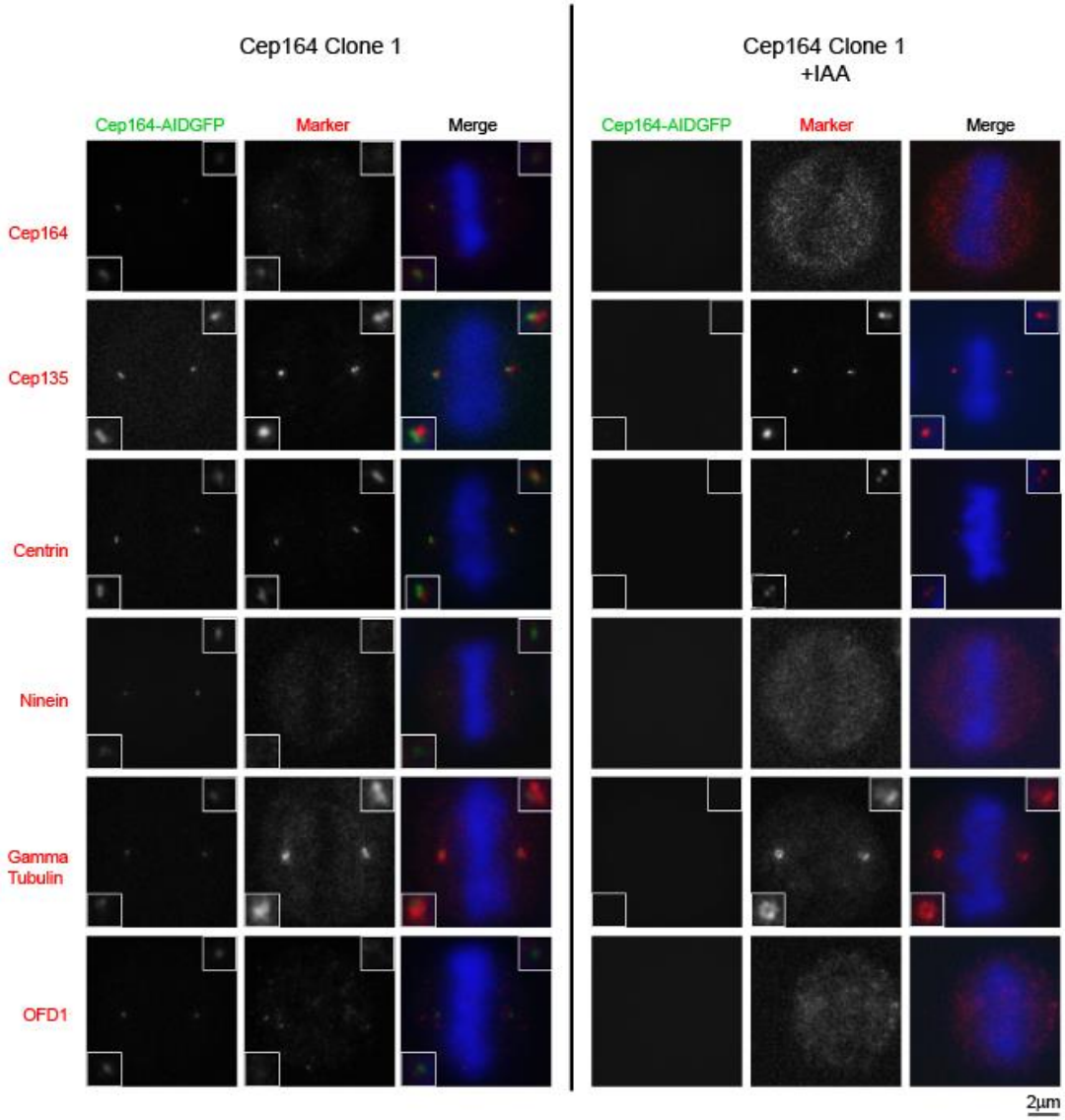

Figure 3.14. Cep164-depleted cells show normal recruitment of various centrosomal proteins during mitosis.
Immunofluorescence microscopy shows the depletion of Cep164-AIDGFP 24 hours after the addition of 500µM IAA. Centrosomal co-markers: Cep135, Centrin, Ninein, Gamma Tubulin and ODF1 show no effect in the absence of Cep164 during metaphase.

Recruitment of centrosomal factors was not impaired during mitosis after Cep164 depletion (Figure 3.14). The Cep164 signal intensity is notably weaker

during mitosis, but this is consistent with previous results tracking the expression during the cell cycle (Slaats et al., 2014).

Cep164-deficient cells showed no obvious defect in centrosome compositon. Thus we decided to proceed with electron microscopy in order to gain further insight into the centrosomal ultrastructure in Cep164-depleted cells.

3.3.4 Ultrastructure of Cep164 deficient centrosomes appears normal

The centrosome is composed of two barrel shaped centrioles made up of 9 microtubule triplets surrounded by a proteinaceous matrix, the pericentriolar material (PCM). Of the two centrioles present in a centrosome, one is at least a cell cycle older than the other, defined as the mature centriole. The mature centriole is distinguished by the presence of distal and subdistal appendages which allow the centrosome to dock to the plasma membrane in ciliating cells. Immuno-EM of Cep164 has previously localised it to the distal appendages (Graser et al., 2007). We decide to investigate the ultrastructure of the centrosome after Cep164 depletion (Figure 3.15).

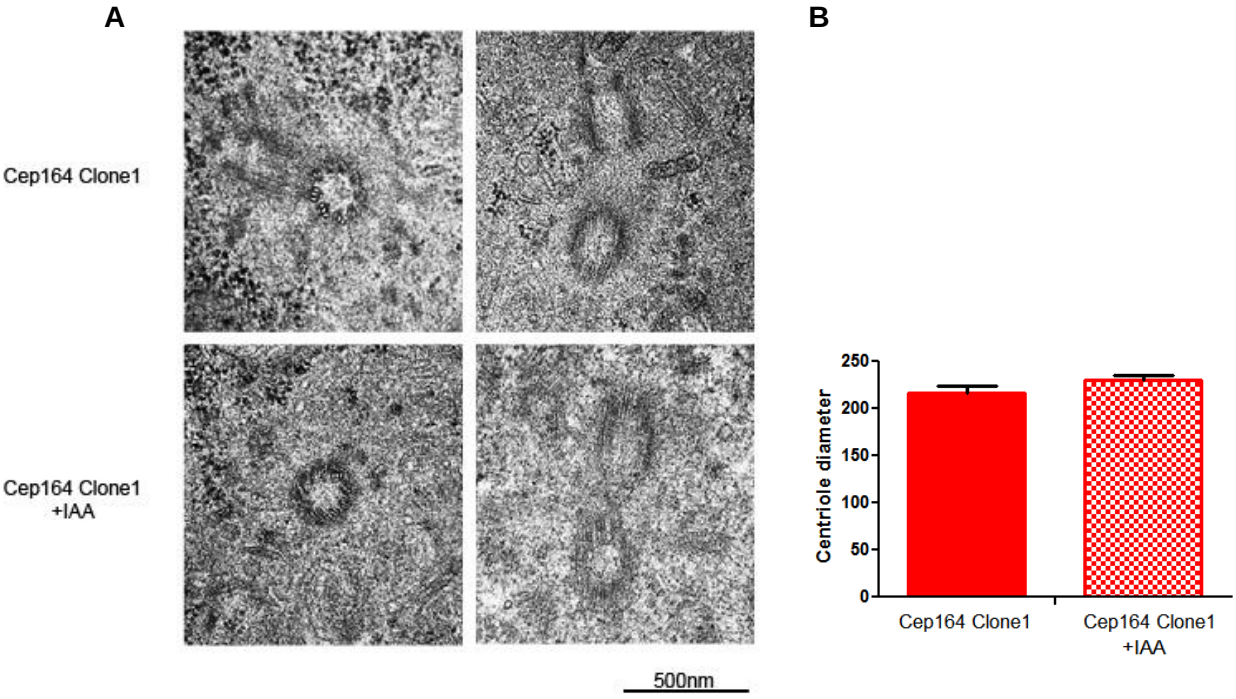

Figure 3.15. Cep164 depleted cells show normal ultrastructure of centrosome.
(A) Comparison of centrosomes from cells with Cep164 versus cells without Cep164 shows no noticeable difference in ultrastructure. The 9 microtubule triplets are present in cells from both samples and the centrosome structure in general seems unaffected upon Cep164 depletion. (B) Diameter of centrioles. N=3. P< 0.01

There is no noticeable difference in centrosomal structure between cells with and without Cep164 using transmission electron microscopy. Centriole length and diameter appear normal as do the microtubule triplets. The appendages were difficult to image and thus it is hard to make any qualitative conclusions about their structure in the absence of Cep164.

3.3.5 Cep164 deficient DT40 cells show normal proliferation

To analyse the proliferative properties of Cep164 deficient cells we did counts every 24 hours for a period of 96 hours. To control for any effect the addition of auxin may have on cell proliferation we also treated WT cells with this hormone. We then plotted the cell numbers on a graph and compiled their respective doubling times (Figure 3.16).

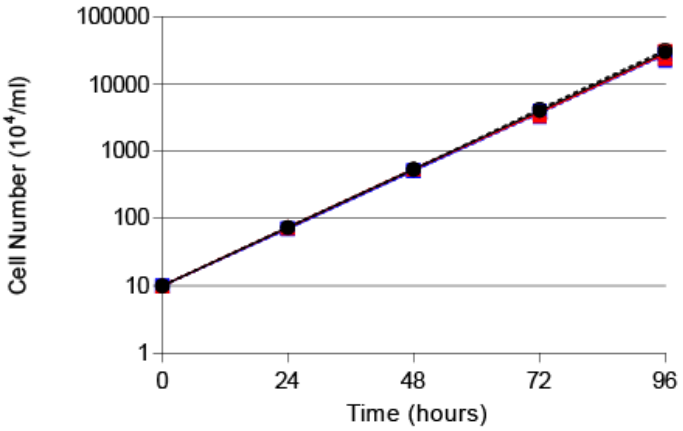

Cell line	Doubling time(hrs)
WT	8.32
WT +IAA	8.25
Cep164 Clone1	8.37
Cep164 Clone1+IAA	8.34
Cep164 Clone2	8.39
Cep164 Clone2+IAA	8.29

Figure 3.16. Cep164 depleted cells show normal proliferative capacity.
Growth curve analysis of cells and condition indicated. Cep164 refers to the Cep164$^{AIDGFP/AIDGFP}$ genotype. Doubling times of the clones are also shown in hours. Data points show mean of 3 separate experiments ± SD.

Cell proliferation remained unaffected after the depletion of Cep164 in DT40 cells, although a recent report claims a 25% decrease in cell cycle duration in RPE-FUCCI cells after siRNA inhibition of Cep164 (Slaats et al., 2014). The reason for this discrepancy in result is unclear.

3.3.6 Cep164 deficient DT40 cells show normal sensitivity to DNA damage

Cep164 has been reported to be a player in the DNA damage response pathway (DDR) through siRNA studies in human cells (Sivasubramaniam et al., 2008). A further study placed it as having an important role during Nucleotide Excision Repair (NER) (Pan and Lee, 2009). We wanted to investigate these roles further in our DT40 chicken model so performed various assays to assess the importance of Cep164 to the DDR.

Centrosome amplification is often incurred after IR radiation (Fukasawa, 2005). We tested the ability and frequency of centrosome amplification in Cep164-deficient cells by exposing cells to gamma radiation and counting the over-amplified centrosomes 24 hours later (Figure 3.17).

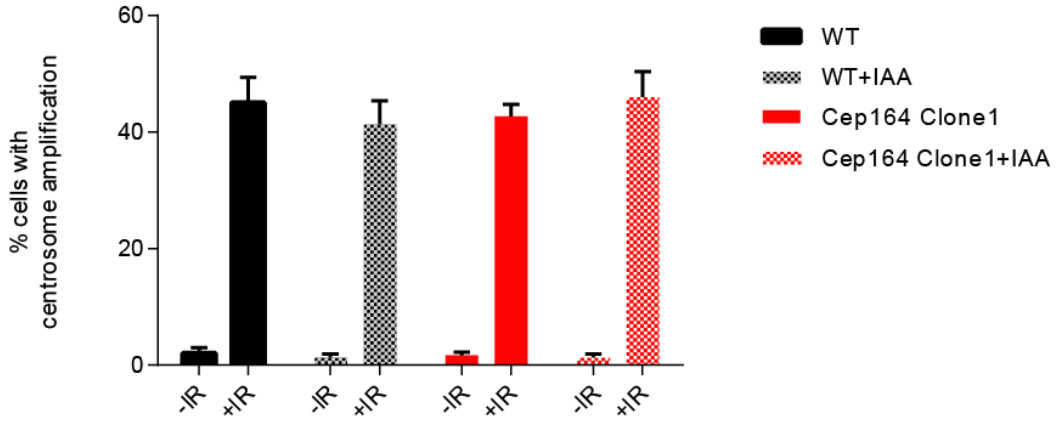

Figure 3.17. DNA damage induced centrosome amplification is normal in Cep164 deficient cells.
Quantitation of cells with aberrant centrosome number in cells of the indicated genotype and conditions. Briefly, cells were treated with 10Gy gamma radiation and the number of centrosomes was determiined by counting the number of gamma-tubulin spots 24 hours later. Histogram shows mean of 3 separate experiments in which 100 cells were counted + SD. P< 0.01

No change in the ability or severity of centrosome amplification was present in the Cep164 deficient cells. We next decided to perform clonogenic survival assays to test impact of DNA damage on cell survival in our clones (Figure 3.18). To ensure the addition of auxin was not affecting the DNA response we tested WT and two Cep164 clones with and without auxin. To induce DNA double strand breaks, we treated cells with gamma radiation while to induce the NER pathway we treated cell with UV-C light.

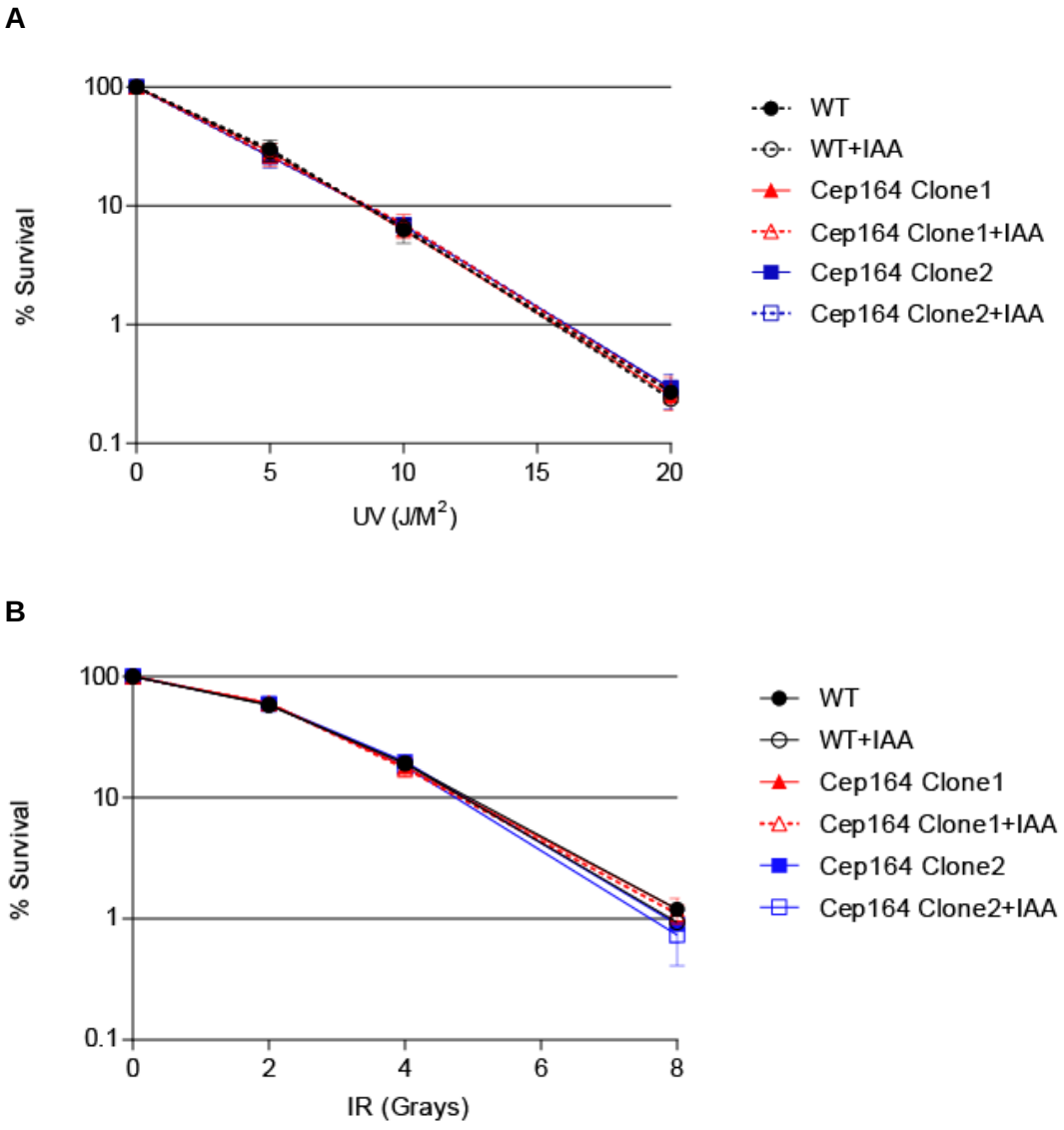

Figure 3.18. Cep164 deficient cells show normal sensitivity to UV and IR.
A. Clonogenic survival assay of cells ± IAA with the indicated doses of UV-C irradiation.
B. Clonogenic survival assay of cells ± IAA with the indicated doses of IR irradiation. Data points show mean ± SD of the survival fractions in 3 seperate experiments.

Surprisingly, and contrary to published data (Pan and Lee, 2009; Sivasubramaniam et al., 2008) we did not detect a difference in the survival of Cep164 depleted cells. While we did not include a UV-sensitive cell line in this assay may have been included, it is clear that the cells are not surviving and have been exposed to UV stress. On reflection, a suitable control could have been an auxin-depletable Centrin2 transgene expressed in the Centrin2 null UV sensitive cell line. At this stage we were concerned that the depletion of Cep164 by the AID system was not effective enough to remove all the protein and that residual protein

was protecting the cells from sensitivity to our assays. We began to explore other options to tackle this problem and decided the best route would be to change model and ablate Cep164 in a human cell line.

Chapter 4. Reverse genetic analysis of Cep164 in human RPE1 cells

4.1 Introduction

It has been reported that Cep164 has a role in the DNA damage response, acting as a mediator of genome stability and being necessary for the efficient removal of UV- induced DNA lesions (Pan and Lee, 2009; Sivasubramaniam et al., 2008). However, the results we obtained from the chicken DT40 cell line conflicted with this published work. It was unclear as to whether this data represented the bona fide phenotype in this model system or if the AID strategy was leaving residual protein that was sufficient for a normal cellular response to our assays.

To address this, we decided to disrupt the *CEP164* locus so that no viable transcript would be produced, removing any ambiguity about residual levels of Cep164 in the cell. This gene disruption was considered to be conducted in DT40 cells but significant advances in gene editing technologies had been made since the beginning of the project, allowing a potential switch in model organism. While DT40 cells have the advantage of quick growth and ease of handling, they do not readily undergo ciliation, a process to which Cep164 has been linked and we were interested in investigating (Graser et al., 2007). Considering this, we concluded that being able to study ciliation in addition to the DNA damage response would be beneficial to our study as we could investigate any potential link between these processes and Cep164. We decided to proceed with hTER-RPE1 (retinal pigment epithelium) cells, as they were a human cell line which readily ciliated allowing us to investigate ciliogenesis in cells lacking Cep164. The non-transformed nature of this cell line was also beneficial as it lacks the oncogenic mutations and karyotypic re-arrangements that are frequently seen in cancer cells and would allow us to make stronger conclusions with regard to the normal cell.

Aside from the purported role in the DDR, Cep164 is also of note as a key player in ciliogenesis, with its depletion resulting in >90% reduction in ciliation (Graser et al., 2007; Schmidt et al., 2012). Cilia are known for their role in signalling, coordinating key processes during development while also playing a part in other cellular events such as cell cycle re-entry and cell migration (Pedersen et al., 2008). During the early stages of ciliogenesis, vesicles dock at the distal end of the mother centriole (Sorokin, 1968), redefining it as a basal body. A membrane-bound

axoneme composed of 9 doublet microtubules then extends from this basal body to make up the main structure of the cilium. Previous work on Cep164 has reported it as necessary for the initial stages of vesicle docking during ciliogenesis (Schmidt et al., 2012). Further work advanced this hypothesis by showing that Cep164 triggers ciliation by recruiting Tau tubulin kinase 2 to the mother centriole (Cajanek and Nigg, 2014). By creating a Cep164 knockout cell line we could further investigate and test this theory and identify the precise stages of ciliogenesis which are impaired by Cep164 absence.

4.2 Characterisation and cloning of human *CEP164*

4.2.1 Analysis of the *CEP164* locus in human

To analyse the *CEP164* locus in the human genome we used the NCBI database. According to this database there are two confirmed isoforms of human *CEP164*, NM_001271933.1 and NM_014956.4. These isoforms share 99% identity, with the difference between them due to alternate in-frame splice sites in two exons, X and XXVII (Figure 4.1). The 5' UTR is also different in the shorter isoform. The functional significance (if any) of this variation is unclear, but noting the nature and location of the differences was important for any potential gene disruption strategy.

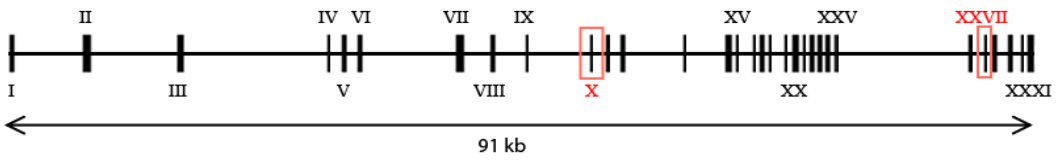

Figure 4.1 Confirmed exon structure of human *CEP164*. 31 coding exons span 91kb to make up the human *CEP164* locus. Exon X and XXVII are marked in red to signify that these contain the differences in amino acid between the confirmed isoforms. Distance between exons to scale.

The difference between the two confirmed Cep164 sequences are minor as they share 1451 amino acids out of 1463. However, there are 25 other mRNA variants of Cep164 predicted on the NCBI database and, while it is unlikely that all these are actually produced, we decided to investigate their composition. We conducted a nucleotide sequence BLAST analysis of each of the variant's mRNA against the longest confirmed isoform of Cep164 (NM_014956.4). We found that the identity between all these sequences and the longest confirmed one was over ≥99% and the coverage >90% with two exceptions; XM_011542689.1 and

XM_011542690.1, which returned a coverage of 15 and 14%, respectively, and encoded truncated proteins. As both of these truncated predictions had a premature stop codon at the end of exon VI or VII, respectively, we conducted an EST search for their expression. Unsurprisingly, no evidence of a stop codon being produced at the end of these exons. Considering these data, there was not enough evidence to suggest that XM_011542689.1 and XM_011542690.1 were truly expressed isoforms but were artefacts of Gnomon, the NCBI gene prediction tool.

4.2.2 Analysis of the Cep164 protein in human

As discussed previously, the human Cep164 protein is composed of 31 coding exons and the locus that encodes it is located on chromosome 11. The translated protein is 1455 amino acids long. Contained within its sequence is a two tryptophan (WW) domain (Figure 4.2), which spans 30 amino acids (59-89). Tryptophan domains are known to be involved in protein-protein interactions, with this one shown to be necessary for the efficient binding of TTBK2 to Cep164 (Oda et al., 2014). This binding is required for proper recruitment of TTBK2 to the mother centriole where it initiates ciliogenesis (Cajanek and Nigg, 2014). Other features of note within the Cep164 sequence include a phosphorylation site at Serine186. This has been reported to become phosphorylated by ATM/ATR upon DNA damage to activate a signalling cascade involving MDC1, RPA, and CHK1 (Sivasubramaniam et al., 2008).

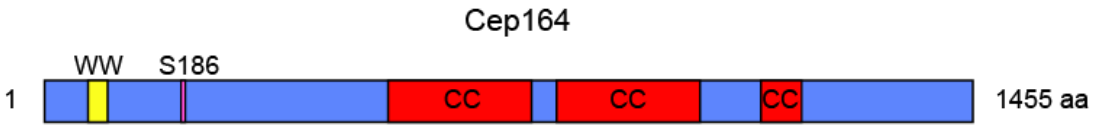

Figure 4.2. Motifs present in Cep164.
Schematic illustrating primary structure of human Cep164. The protein contains an N-terminal WW domain (WW) and three predicted coiled-coil domains (CC). A phosphorylation site at position 186 has also been reported. Predicted using SMART protein domain database (Schultz et al., 2000).

4.2.3 Cloning and overexpression of human Cep164

As we were confident of the confirmed sequence on the NCBI data base, we designed primers which allowed us to clone the entire *CEP164* cDNA. The subsequent RT-PCR was successful at particular annealing temperatures, as displayed in Figure 4.3A.

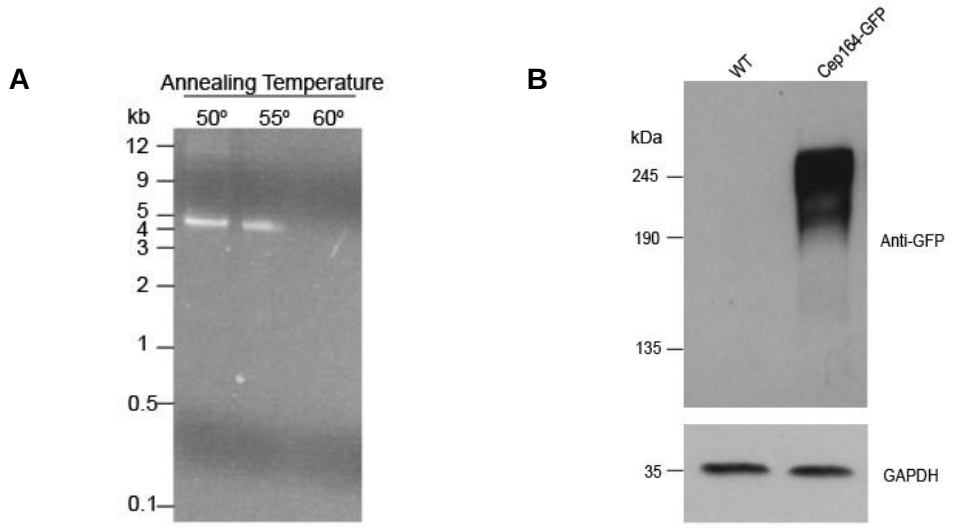

Figure 4.3. RT-PCR of *CEP164* from human cDNA and transient expression in hTERT-RPE1 cells. (A) The successful amplification of *CEP164* from human cDNA resulted in a product of ~4.5kb, as expected. (B) The overexpression of this cDNA tagged at the C-terminus with GFP shows a product of over 190 kDa.

The successfully amplified product was sequenced and cloned into the expression pEGFP-N1. To test the functionality of this plasmid, it was then transfected into hTERT-RPE1 cells and the resulting cell line analysed by Western blot for expression (Figure 4.3B). There are a number of bands present on the film, possibly indicating a mobility shift of the protein after post-translational modifications. This band pattern is comparable to what was observed in DT40 (Figure 3.6B) and may be a result of the GFP tag. To investigate the localisation of the protein we carried immunofluorescence microscopy after transfection (Figure 4.4).

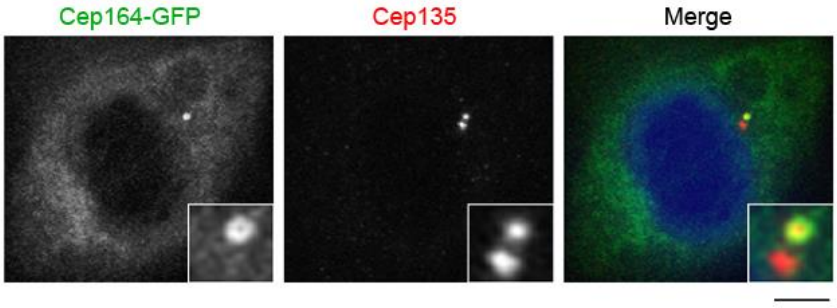

Figure 4.4 Transiently expressed Cep164 localises to the centrosome.
Immunofluorescence microscopy analysis of transiently expressed Cep164 in WT RPE1 cells shows localisation with one centriolar Cep135 focus as expected. Scale bar 5μm

Through immunofluorescence microscopy, we observed the localisation of GFP-tagged Cep164 exclusively at the centrosome. This is in agreement with published work (Graser et al., 2007), although some reports have shown a nuclear localisation, which we did not observe (Sivasubramaniam et al., 2008).

4.3 Verification of a novel monoclonal human monoclonal antibody to Cep164

During the investigation of Cep164, a project running concurrently in our lab was developing mouse monoclonal antibodies. Usefully for this study, an antibody was produced against human Cep164 (1F3G10) (Figure 4.5). As we were planning to ablate the Cep164 protein, this would be a very important reagent to identify any successfully targeted clones. The size and location of the sequence used as an antigen was ~300 amino acids at the N-terminus of the protein.

Figure 4.5. Depiction of the fragment location used for antibody production. The amino acid sequence used as an antigen for the production of a human monoclonal antibody is depicted as a green line in relation to the full length sequence.

After the cloning and initial verification steps were conducted by Dr. David Gaboriau, the Cep164 antibody was purified from a carefully selected hybridoma (Dundee Cell Products). Western blotting on a number of human cell lines was

conducted to confirm the specificity of the antibody (Figure 4.6A). A band consistent across all cells lines is visible at ~200kDa but to confirm this as Cep164 we performed an siRNA mediated knockdown on hTERT-RPE1 cells and once again blotted for Cep164 using the monoclonal antibody (Figure 4.6B). 24 hours after siRNA treatment the band corresponding to Cep164 disappears, confirming the specificity of the monoclonal antibody.

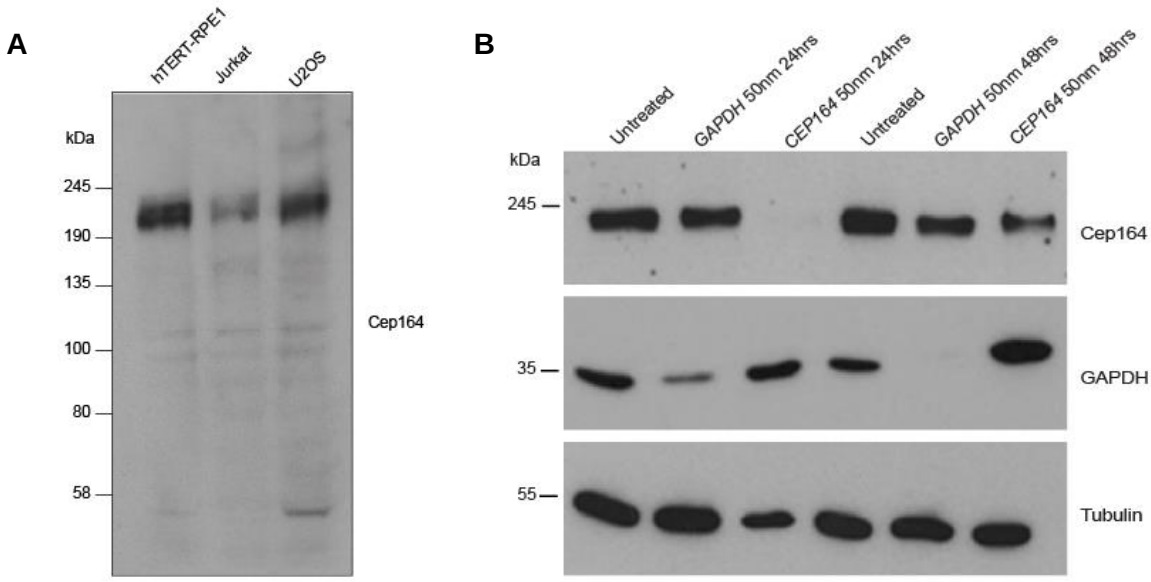

Figure 4.6.Confirming the specificity of the mouse monoclonal Cep164 antibody.
(A) Western blot of Cep164 (1F3G10) on three different human cell lines as labelled. A band is visible in all three lanes at ~200kDa. (B) hTERT-RPE1 cells were transfected for 24 or 48hrs with control (GAPDH) or Cep164-specific oligonucleotide duplexes. Western blot of Cep164 (1F3G10), GAPDH (control siRNA) and Tubulin (loading control) was then conducted. The disappearance of the putative Cep164 band after siRNA treatment 24 hrs confirms the specificity of the antibody.

With the antibody detecting a clean band that was verified by siRNA-mediated knockdown, we decided to investigate its localisation under immunofluorescence microscopy. We used both the centriolar marker, Cep135 and the distal appendage marker, ninein (Mogensen et al., 2000; Ohta et al., 2002) to co-stain with our Cep164 monoclonal (Figure 4.7). As expected and similar to what was seen in DT40 (Figure 3.6), ninein and Cep164 share a tight co-localisation, while Cep164 appears at the end of one Cep135 focus. These data support the view of Cep164 as marking only the mother centriole and confirms its specificity.

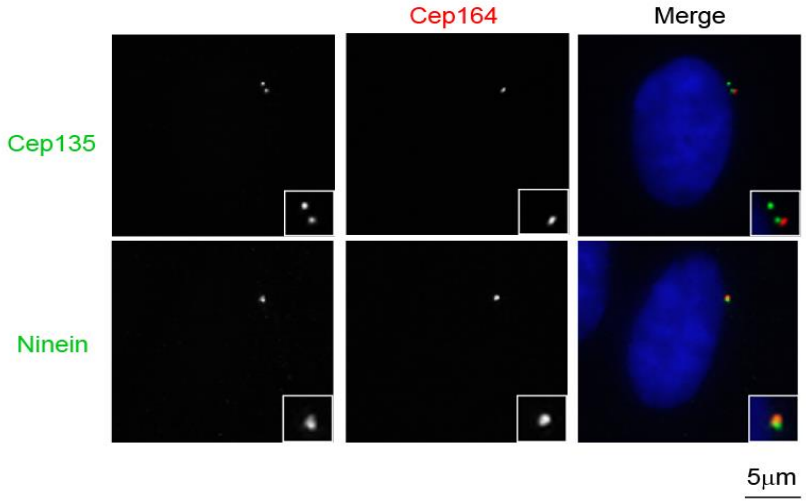

Figure 4.7. **The mouse monoclonal Cep164 antibody detects antigen at the mature centriole.** Immunofluorescence microscopy analysis of the mouse monoclonal Cep164 antibody (1F3G10). Cells were co-stained with antibodies to the sub-distal appendage marker ninein, or the centriolar marker Cep135.

4.4 Disruption of *CEP164* in human hTERT-RPE1 cells using CRISPR/Cas9

CRISPR/Cas9 has become an increasingly popular method for gene disruption. While there are limitations to the sequence that can be targeted using this system, many genes are targetable. Work conducted in 2013 bioinformatically identified >190,000 unique gRNAs adhering to a $GN_{20}GG$ structure (Mali et al., 2013). These gRNAs represented ~40.5% of exons in the human genome. This list was curated and published online at http://arep.med.harvard.edu/human_crispr/. When we initially scanned through this list, we noted 21 sequences that could be used to target *CEP164*. Our previous analysis of the gene locus was useful to decide upon three sequences that would ensure efficient targeting of all isoforms, predicted and confirmed. These sequences were located on exons 3, 4 and 7 (Figure 4.8).

A

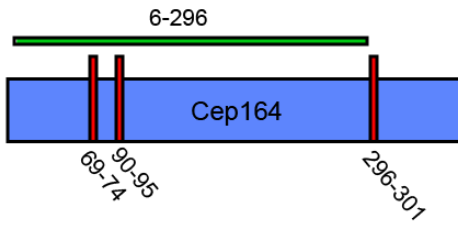

B

Location of gRNA	Sequence of gRNA
Exon 3 (69-74)	GTCCCACATAGACTGCCCGTTGG
Exon 4 (90-95)	GGCTCCTTTACGAGGTCTTGTGG
Exon 7 (296-301)	GCTGTTGGCAAAGGGCGACAGGG

Figure 4.8. Depiction of the gRNA target sequence locations.
(A) Schematic depicting the first 350 amino acids of Cep164 protein in blue. The three target sequence locations chosen as sites for disruption are shown in red. The sequence location of the amino acid fragment used to produce the mouse monoclonal antibody is also depicted in green. (B) Table showing location and corresponding sequence of the three gRNAs. They can all be seen to follow the $GN_{20}GG$ nucleotide structure.

Targeting the gene at the 5' end of the locus was preferred as we hypothesised that this would reduce the possibility that a stable or potentially coding transcript would be produced. We cloned each of the three sequences (Figure 4.8B) into the pX330 plasmid as described in section 2.5.3. The resulting plasmids were subsequently co-transfected with a plasmid containing antibiotic resistance into hTERT-RPE1 cells. For screening the resulting single clones, we initially confirmed potential gene disruptions by lack of Cep164 signal using immunofluorescent microscopy before confirming by Western blot and genomic sequencing. Of the three exons which we attempted to disrupt, only exon 7 was targeted and produced clones that lacked Cep164 signal by immunofluorescence microscopy (Figure 4.9A).

A

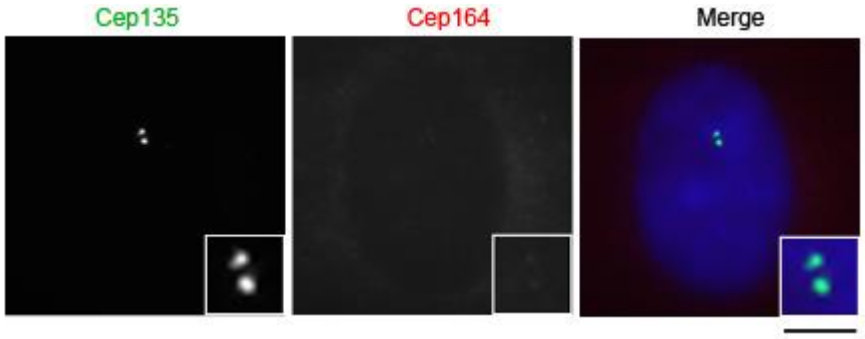

B

CEP164 gRNA location	No. of clones screened	No. Cep164-deficient clones by IF
Exon 3	62	0 (0%)
Exon 4	57	0 (0%)
Exon 7	24	7 (33%)

Figure 4.9. Immunofluorescence microscopy of targeted clone and targeting efficiency of the gRNA sequences.
(A) Immunofluorescence showing the absence of a Cep164 signal in one of seven Cep164-deficient clones. Scale bar-5μm. (B) Table highlighting the efficiency of the three targeting gRNA sequences. Targeting of exons 3 and 4 failed to yield a positive clone for gene disruption (62 and 57 clones screened, respectively) while exon 7 targeting produced 33% positive clones (24 screened clones) by immunofluorescence microscopy.

The underlying reason why targeting exon 3 or 4 was unsuccessful remains unclear, but it may be because they are inaccessible sites on the genome. Nonetheless, analysis was continued with the exon 7 clones. We conducted a Western blot on those which lacked a signal by immunofluorescence to verify the disappearance of the putative Cep164 band (Figure 4.10).

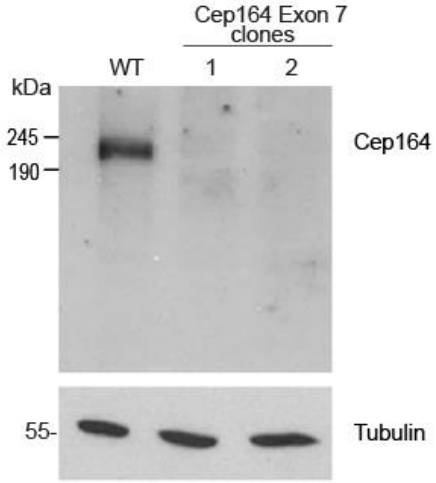

Figure 4.10. Confirming the disruption of Cep164 expression.
Immunoblot of two exon 7 targeted Cep164 clones which showed no signal by immunofluorescence also show no signal at ~200kDa.

Combining the lack of signal observed by immunofluorescence microscopy and Western blot data, we concluded that we had successfully disrupted the *CEP164* locus. To determine the exact nature of this disruption we isolated the genomic DNA from the above clones and sequenced the region that we had targeted (Figure 4.11). As non-homologous end joining was responsible for the disruption we expected an insertion or deletion of some base pairs to put the coding sequence out of frame.

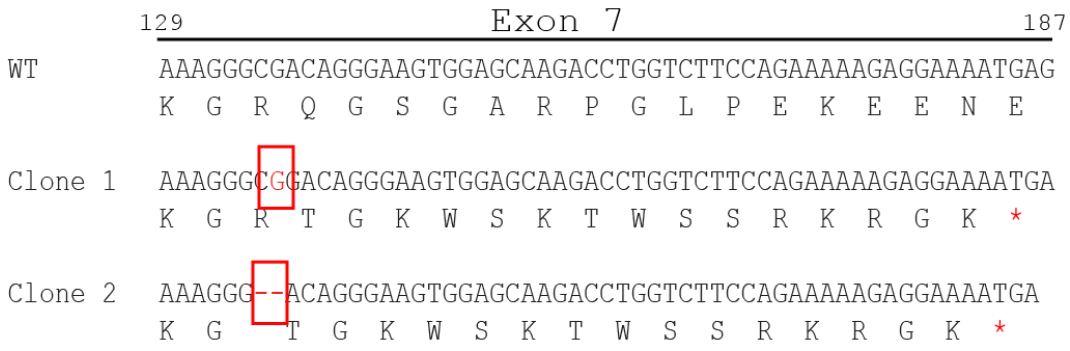

Figure 4.11. Sequencing of exon 7 from WT and *CEP164* clones 1 and 2 reveals insertions/deletions in targeted clones.
The above sequence corresponds to coding sequence in exon 7 of *CEP164*. The targeted clones show a homozygous insertion (clone 1) or deletion (clone 2) (depicted in a red box) that results in a stop codon produced just downstream of the target site (red asterisk).

The resulting sequence data revealed that the two clones sequenced were homozygous for a 1bp insert or a 2bp deletion at the location the guide RNA targeted (7 independent sequence reactions for each clone). The effect of these mutations is a frameshift within amino acid 301 resulting in a premature stop codon at position 317. A quality control system within eukaryotes known as nonsense-mediated decay (NMD) acts unfavourably towards transcripts containing premature termination codons (Kervestin and Jacobson, 2012). By degrading these aberrant transcripts, NMD acts to prevent the production of truncated proteins. This, taken together with the location of the gene disruption, suggests there is little possibility of a functional protein being produced in these two clones.

4.5 Cep164-deficient hTERT-RPE1 cells show normal proliferation

Cep164 has recently been linked to cell cycle progression, with siRNA depletion leading to a significantly shorter G1, G2 and M phase with an increase in time spent in S phase (Slaats et al., 2014). To analyse the cell cycle of our Cep164-

deficient cells, we first analysed the proliferative capacity of our clones by conducting cell counts every 24 hours for a period of 96 hours. We then plotted the numbers on a graph and compiled their respective doubling times (Figure 4.12).

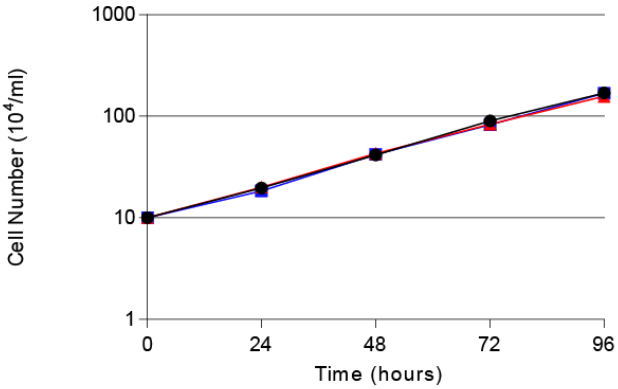

Cell line	Doubling time(hrs)
WT	23.5
Cep164 Clone 1	24.1
Cep164 Clone 2	23.6

Figure 4.12. Cep164-deficient cells show normal proliferative capacity.
Cell growth analysis of WT and Cep164-deficient cells show they exhibit normal proliferation. Doubling times of the clones are also shown in hours. Data points show mean of 3 separate experiments ± SD. Note that the SD are small and not visible on log plot.

No noticeable difference in cell proliferation between Cep164-deficient cells and wild-type was evident. As this does not assess the number of cells in each phase of the cell cycle we also completed flow cytometry on one of the Cep164-deficient clones and compared it to wild-type (Figure 4.13).

A

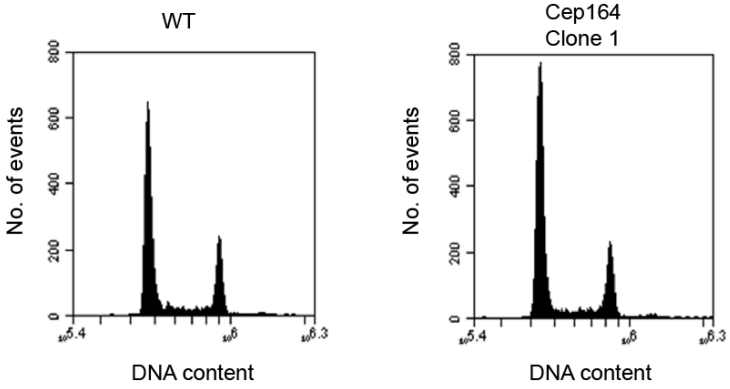

B

Cell line	G1	S	G2/M
WT	62.7%	12.2%	21.9%
Cep164 Clone 1	65.7%	11.2%	20.1%

Figure 4.13. Cep164-deficient cells show normal cell cycle distribution.
(A) FACS analyses of asynchronous cell populations in both wild-type and Cep164-deficient cells using PI to stain for DNA content. 10,000 cells were measured for each plot. (B) The percentage of cells in each cell cycle stage adapted from the cell cycle profiles. The Accuri C6 Sampler software was used for measurement.

While Cep164-deficient cells showed trivial differences in cell cycle stage progression with an increased G1 population and a comparatively lower S and G2/M (Figure 4.13.B), these variances were minor and not worth pursuing. The reason for the discrepancy between our results and the previously published data is not clear but may be due to the cell lines used in each experiment or off-target siRNA effects.

As Cep164 is a distal appendage protein, we next investigated if the localisation of other proteins known to act at this site was disrupted (Figure 4.14).

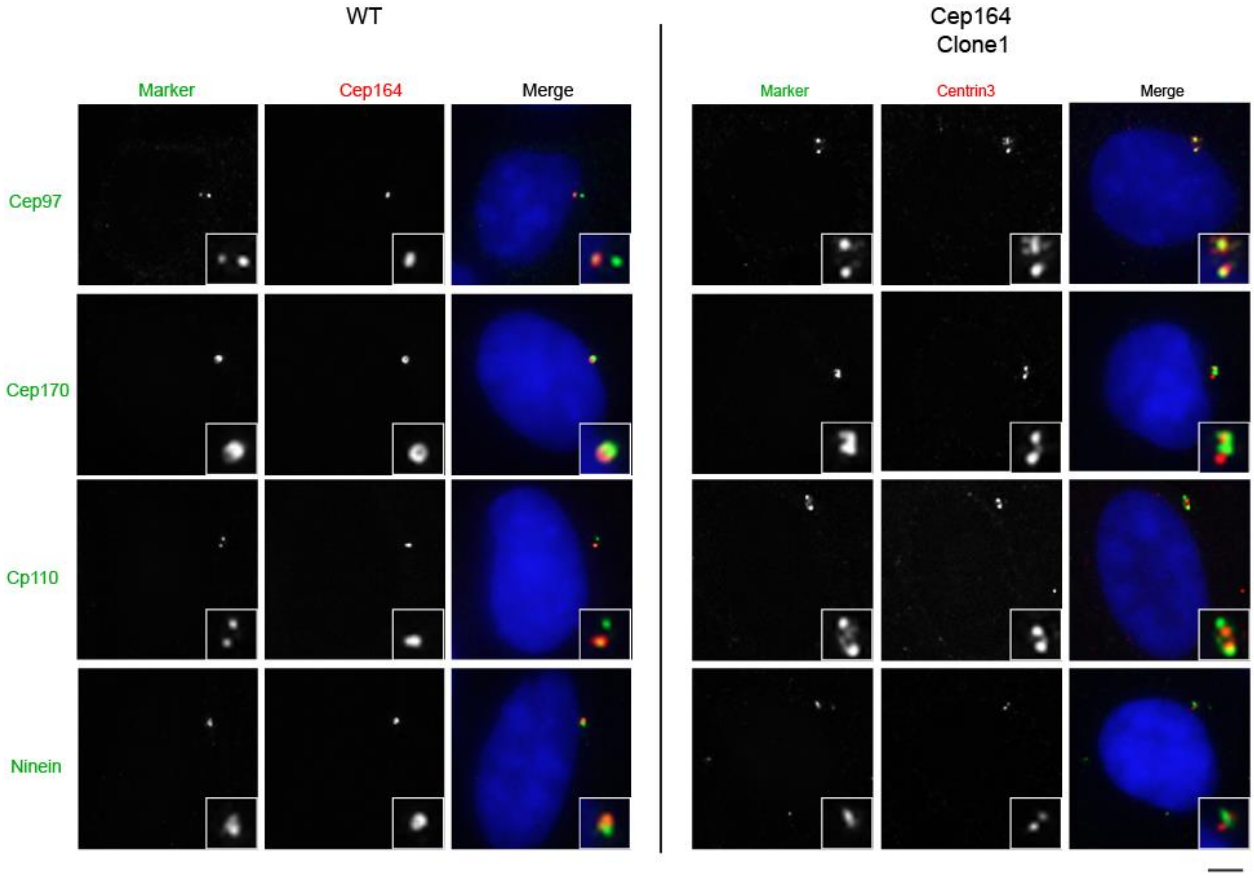

Figure 4.14. Localisation of other distal-end centriole proteins are normal.
Immunofluorescence microscopy shows the absence of Cep164 does not appear to affect the localisation of other distal-end centriolar proteins. Scale bar-5μm.

At this resolution of immunofluorescence microscopy, we could detect no visible difference in the appearance and localisation of the tested centrosomal markers (Figure 4.14). As electron microscopy would give us a closer look at the ultrastructure of the centrosome, we decided to pursue that technique (Section 4.7).

4.6 Cep164 is necessary for ciliogenesis

Ciliogenesis is the process by which cells assemble an antenna-like structure projecting from the cell surface known as a cilium. Cep164 was originally of note due to its being required for this process (Graser et al., 2007). Exit from cell cycle into G0 is known to potentiate ciliogenesis (Dingemans, 1969). To test the ability of Cep164-deficient cells to ciliate we induced quiescence through serum starvation for a period of 72 hours and through immunofluorescence microscopy, counted the number of cilia produced (Figure 4.15).

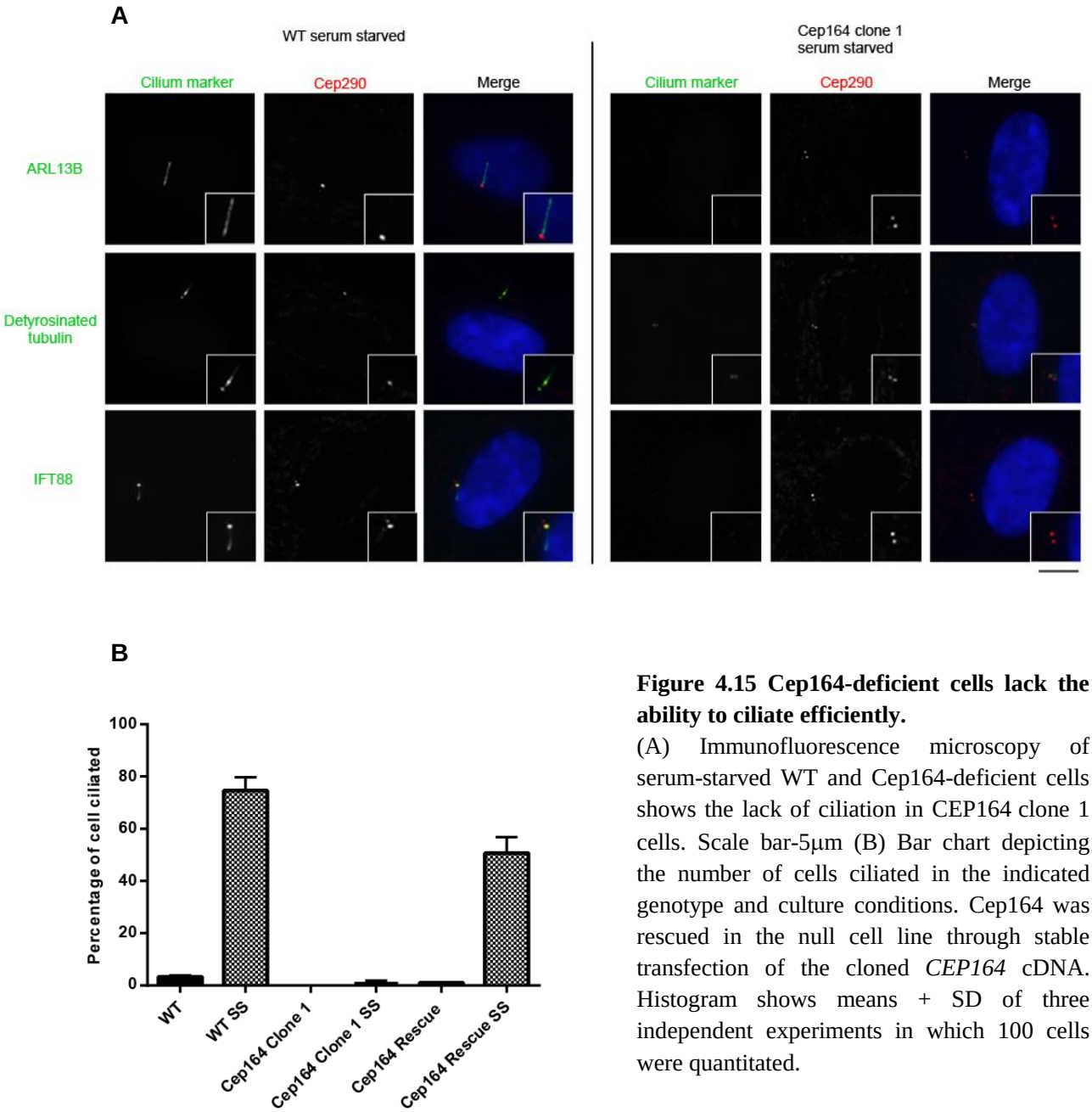

Figure 4.15 Cep164-deficient cells lack the ability to ciliate efficiently.
(A) Immunofluorescence microscopy of serum-starved WT and Cep164-deficient cells shows the lack of ciliation in CEP164 clone 1 cells. Scale bar-5μm (B) Bar chart depicting the number of cells ciliated in the indicated genotype and culture conditions. Cep164 was rescued in the null cell line through stable transfection of the cloned *CEP164* cDNA. Histogram shows means + SD of three independent experiments in which 100 cells were quantitated.

Cep164 is critical for efficient ciliation in hTERT-RPE1 cells. In normally supplemented wild-type cells ~4% are ciliated. This rises to ~80% upon serum starvation. No cilia were detected in normally-supplemented Cep164-deficient cells and when encouraged into quiescence, these cells only produced 1-2% cilia (Figure 4.15). This phenotype was rescued by the re-introduction of Cep164 into the genome of deficient cells. Three makers for ciliation, Arl13b, detyrosinated tubulin and acetylated tubulin were used to stain for cilia to ensure the lack of Cep164 was not merely resulting in a de-localisation of one ciliary protein, while the organelle remained intact.

4.7 Cep164 is necessary for the docking of vesicles to the mother centriole

Ciliogenesis is an ordered process which can be defined by a number of key steps. To demonstrate these steps we serum starved wild type RPE1 cells and carried out transmission electron microscopy (TEM). The images taken are of separate ciliation events at differing stages and neatly demonstrate the process originally described by Sorokin in the 1960's (Figure 4.16). Initially the centrosome becomes re-localised (as a basal body) to the plasma membrane where upon the binding of vesicles it docks to the cell surface via distal appendages (Figure.4.16A-C). This is followed by the extension of axonemal microtubules, which protrude from the cell within the plasma membrane, surrounded by a ciliary pocket (Figure.4.16D&E). Intraflagellar transport is responsible for the continued elongation of the structure which extends the cell surface in an antenna-like manner (Figure.4.16F).

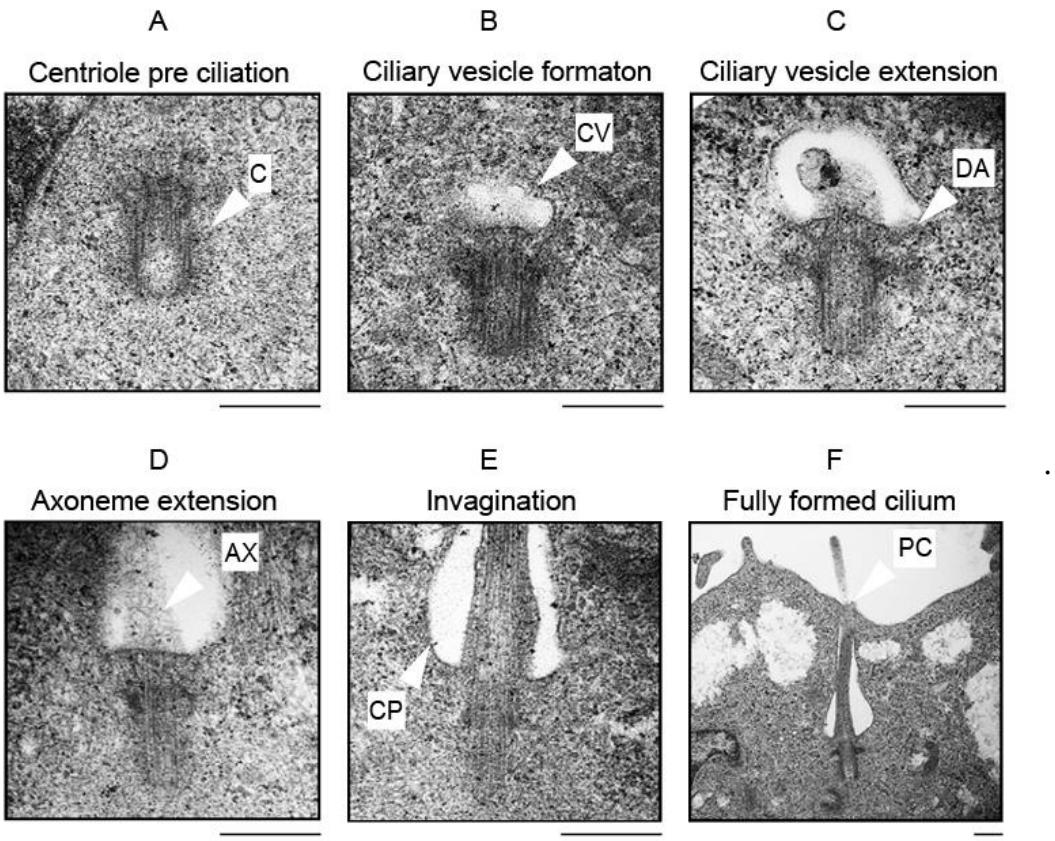

Figure 4.16. Stages of ciliation in serum starved wild-type RPE1 cells.
Transmission electron micrographs of centrioles/basal bodies at various stages during ciliogenesis. Images A-F were captured to illustrate the generation of a primary cilium. Abbreviations: C-centriole, CV-ciliary vesicle, DA-distal appendage, AX-axoneme, CP-ciliary pocket, PC-primary cilium. Scale bars -500nm.

To investigate the ultrastructure of Cep164-deficient centrosomes, we once again conducted TEM (Figure 4.17.A). We analysed centriole length and diameter (Figure 4.17.B) along with qualitative features such as the morphology of the triplets and appendages.

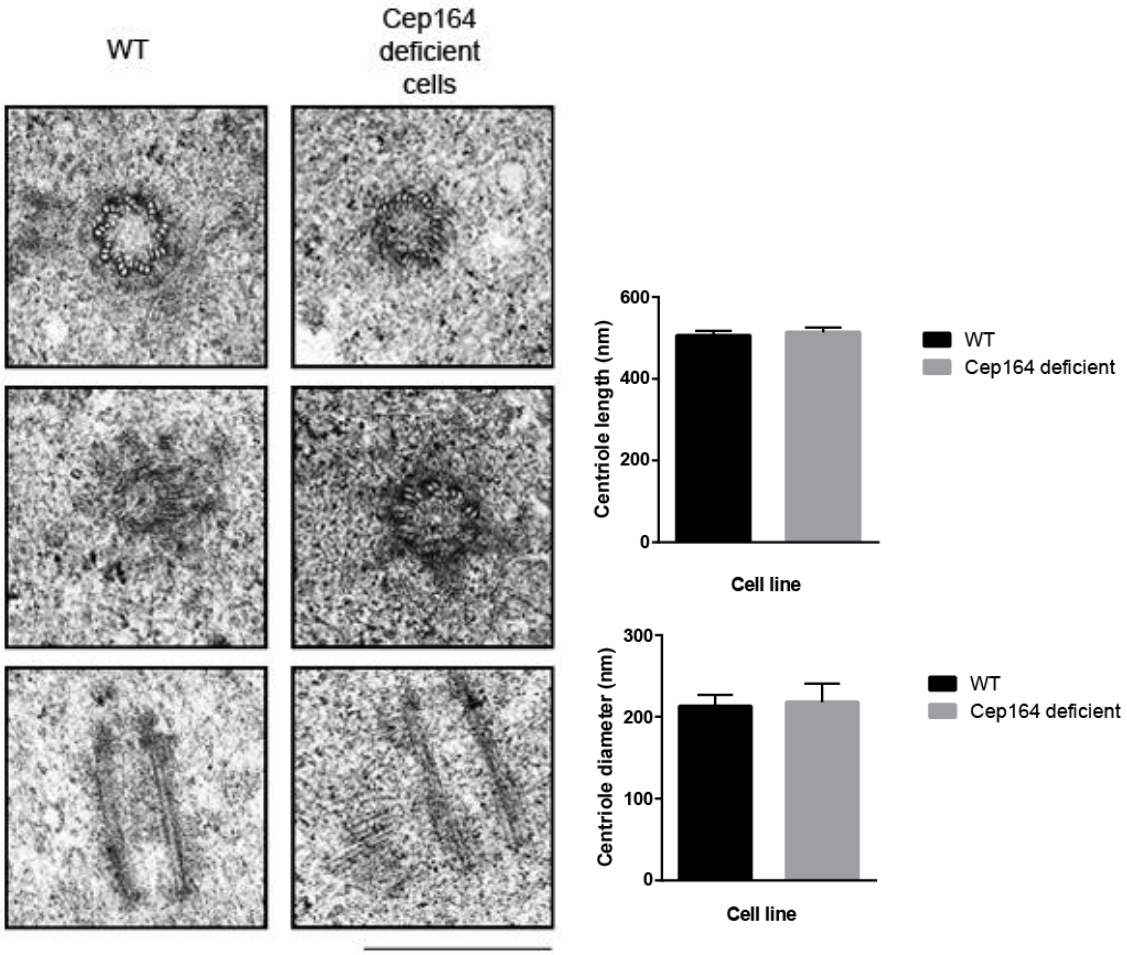

Figure 4.17. Cep164-deficient cells show normal centrosome morphology.
(A) Transmission electron microscopy of characteristic features of centrioles. Structures such as triplets, appendages and procentrioles are all evident. (B) Histogram displaying the average length and diameter of centrioles +SD. An unpaired t-test reveals no significant difference between the cell lines (P>0.01). N=5 for each cell line. Scale bar = 500nm

We observed no obvious ultra-structural anomalies in Cep164-deficient centrosomes. Centriole length and diameter were statistically similar while the morphology of the triplets and appendages were comparable. From these data, it is evident that the ciliation phenotype observed in these cells is not due to some structural change within the centriole. We wanted to investigate the exact stage of ciliogenesis at which Cep164-deficient cells were defective in during ciliation. A previous report using siRNA has demonstrated that Cep164 mediates the docking of vesicles to the mature centriole, an essential step for efficient ciliation (Schmidt et al., 2012). To assess if this was the case in Cep164-deficient cells, we serum starved them as previously and conducted TEM (Figure 4.18)

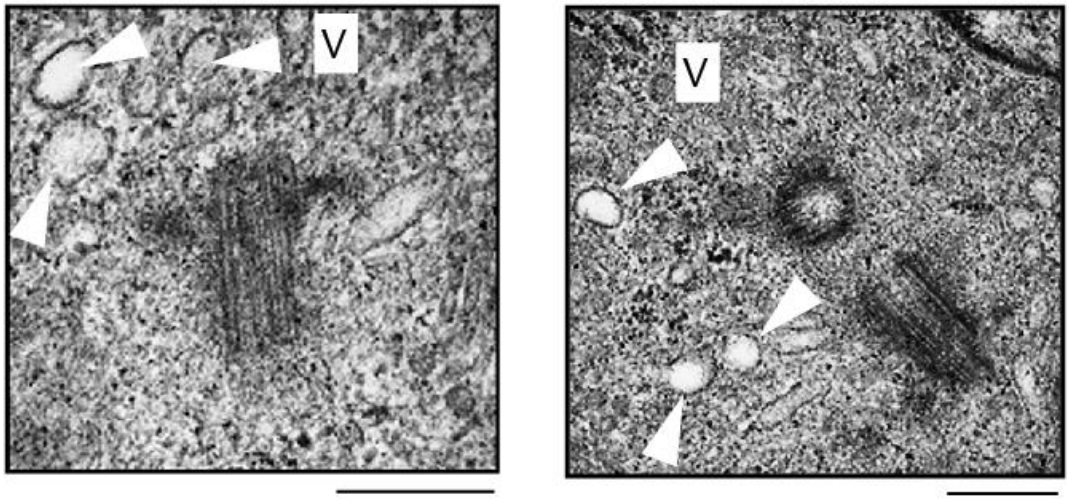

Figure 4.18. Cep164-deficient centrioles fail to dock vesicles

Electron micrographs of Cep164-deficient cells after serum starvation. Vesicles can be seen in the vicinity of the mature centriole but none are bound to it. V- vesicle. Scale bar = 500nm.

As expected no cilia were observed in serum starved Cep164-deficient cells under TEM. In agreement with previously reported data, early defects in cilium assembly appear to be the cause for lack of ciliation. We identified 16 vesicles that were in proximity to the centrioles (N=7 cells) but not bound (examples in Figure 4.18). This is the first evidence in a Cep164 knockout cell line of the stage of disruption in ciliogenesis. Further work, using siRNA mediated depletion of Cep164, has gone on to show that the recruitment of Tau tubulin kinase 2 by Cep164 triggers ciliogenesis (Cajanek and Nigg, 2014).

4.8 Cep164 deficient cells show a normal sensitivity to DNA damage.

Cep164 has been described to have a role in the DNA damage response. However, data presented in Chapter 3 did not find any sensitivity to DNA damage upon Cep164 depletion in the chicken model. As we were concerned about incomplete depletion masking the phenotype we disrupted *CEP164* in human RPE1 cells. As this cell line has been verified by Western blot, immunofluorescence and genomic sequencing we are confident no residual protein remains. The lack of ciliation, which is rescued upon re-expression of Cep164, also agrees with this viewpoint.

Centrosome duplication and the DNA replication are coupled through the cell cycle. However, genotoxic stress is known to uncouple these events leading to

centrosome over-amplification (Nigg and Stearns, 2011). As Cep164 is a centrosomal protein with a potential involvement in the DNA damage response, we investigated if its ablation increased the cells susceptibility to centrosome amplification after DNA damage (Figure 4.19).

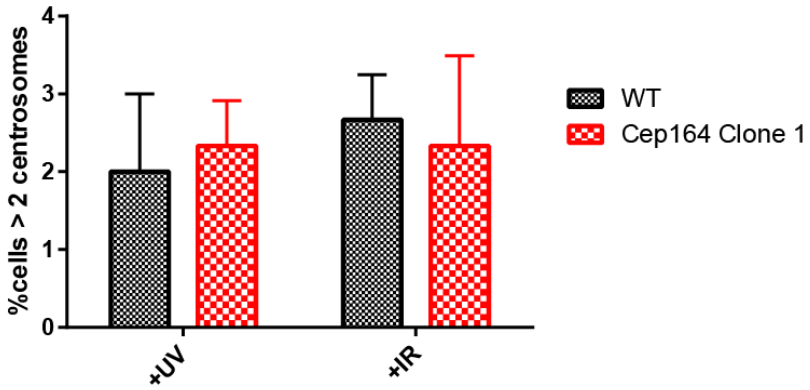

Figure 4.19. Cep164-deficient cells show comparable levels of centrosome amplification to WT after genotoxic stress.
Quantitation of cells with aberrant centrosome number in cells of the indicated genotype and after specified treatment. Briefly cells were treated with 10Gy gamma radiation or 10J/m^2 UV-C radiation and the number of centrosomes was determined by counting gamma-tubulin foci 72 hours later. Histogram shows mean of 3 separate experiments of 100 cells + SD.

There was no change in the ability or severity of centrosome amplification in Cep164-deficient cells after genotoxic stress. This is consistent with its role at the distal appendages in ciliation and not in the duplication of centrosomes. However, Cep164 has been reported to be involved in nucleotide excision repair and the lack of a response in the DT40 cell line was one of the reasons the model system was switched. The localisation of Cep164 to sites of DNA damage has been previously described (Pan and Lee, 2009). To investigate this, RPE1 cells were irradiated with UV light and using our novel monoclonal antibody, tracked Cep164 (Figure 4.20)

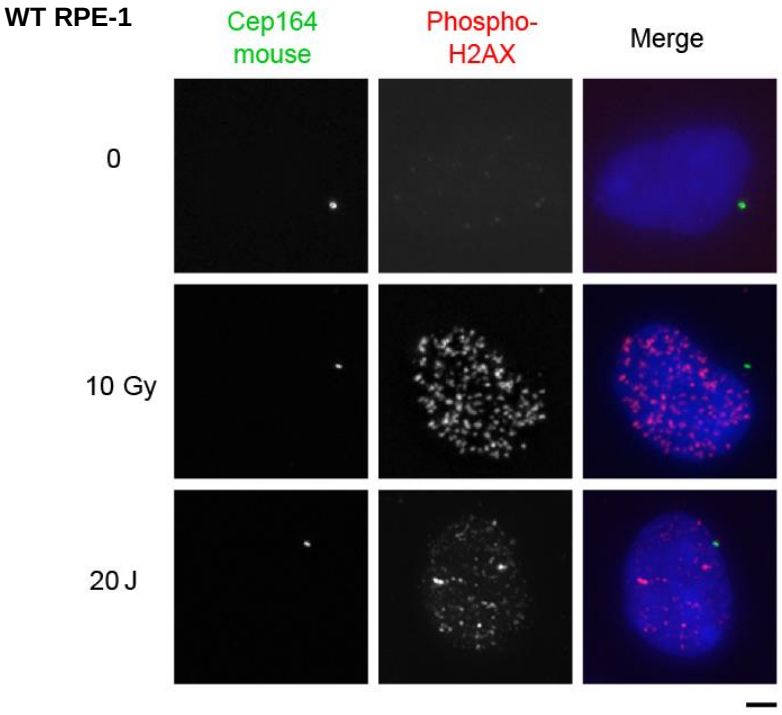

Figure 4.20. Cep164 shows no localisation to nuclear DNA damage.
WT cells were treated with 20J/m^2 UV or 10 Gy IR and fixed 15 mins later. No localisation of Cep164 (IF3G10) with γ-H2AX is visible. The centrosomal fraction of Cep164 appears unaffected. Scale bar-5μm.

We did not observe any localisation of Cep164 with DNA-damage induced γ-H2AX foci after UV or IR treatment. γ-H2AX is a known to localise to damaged DNA with increased levels verifying the cells have incurred stress. To further investigate the role (if any) of Cep164 in the NER pathway we performed a clonogenic survival assay on *CEP164* knockout cells. For this experiment we treated cells with UV-C light to induce the NER pathway and allowed colonies to form (described in Section 2.6.4.3) (Figure 4.21). We included a centrin2-deficient cell line in this experiment (Prosser & Morrison, 2015) as it has previously been shown that centrin2 is necessary for the effective nucleotide excision repair (Dantas et al., 2011; Prosser and Morrison, 2015).

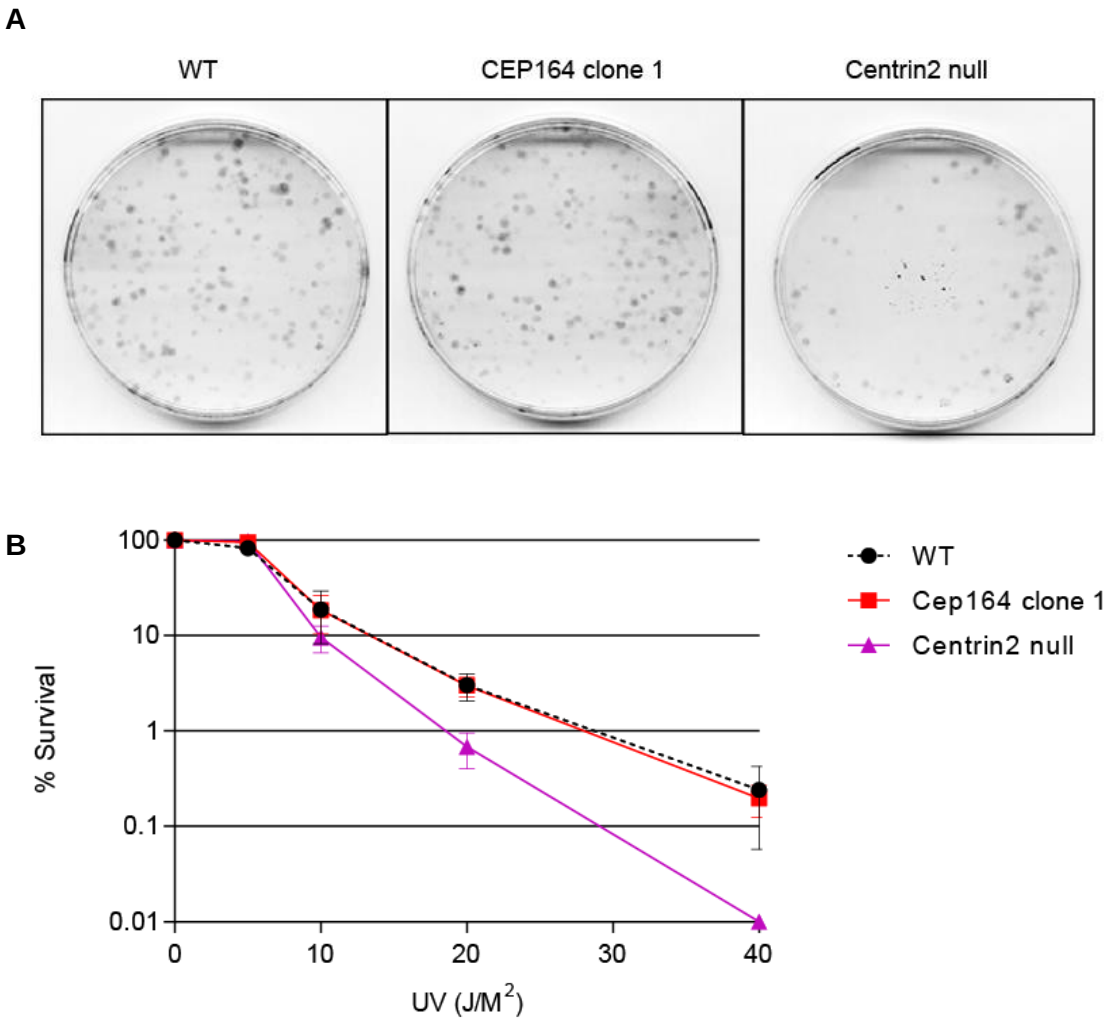

Figure 4.21. Cep164-deficient cells show normal sensitivity to UV while Centrin-2 deficient cells are hyper-sensitive.

(A) Clonogenic survival plates two weeks after UV treatment (20J/m^2) shows a clear difference between the genotypes. There are less colonies on the Centrin2 null plate compared to both the Cep164 clone 1 and WT plates (B) Clonogenic survival assay of cells of indicated genotype treated with varying doses of UV radiation. Data points show mean ± SD of the survival fractions in 3 separate experiments.

Here we have provided further evidence for the role of Centrin2 in the NER pathway, previously reported in DT40 cells (Dantas et al., 2011). However, using clonogenic survival assays, no sensitivity to UV is apparent in the absence of Cep164 . This is in contradiction with previously reported studies using siRNA (Pan and Lee, 2009; Sivasubramaniam et al., 2008). These results agree with the data presented in the DT40 system (Chapter 3). Thus from our studies and the evidence we have presented we have found that Cep164 is essential for ciliogenesis but dispensable for the repair of UV-induced DNA damage lesions.

Chapter 5. Discussion

Cep164 is a recently discovered protein, first described in 2003 and the first function attributed to it in 2007 (Andersen et al., 2003; Graser et al., 2007). The primary tool to study Cep164 functions to date has been siRNA-mediated knockdown. siRNA has provided some good insights into the roles of Cep164 but has some limitations such as the potential for residual protein and possible off-target effects (Jackson and Linsley, 2010). To perform a more robust study on the roles of Cep164, we decided to use a reverse genetic approach in vertebrates.

In the chicken DT40 model we used an auxin-inducible degron (AID) system to deplete the endogenous Cep164 protein (Nishimura et al., 2009). We also inserted a GFP tag at the gene locus to track Cep164 through fluorescence microscopy. By analysing the chicken genome, we were able to discern the locus and clone the putative *CEP164* gene. This protein turned out to be slightly smaller than expected, with a mass of 135kDa. However, comparing the homology between the chicken and human Cep164, we found that while the protein is not highly conserved at the primary sequence level, structural features such as a WW domain and coiled-coil regions are present in both. Following the cloning of chicken *CEP164*, we transiently overexpressed it in DT40 cells and confirmed its presence at the centrosome. At this stage of the project we did not possess an antibody to Cep164 that recognised the chicken protein, so this visualisation was important in confirming Cep164 as a centrosomal protein in chicken.

From a search of the EST database, cDNA clones from torso, testis and brain all contained the Cep164 sequence, indicating its expression was not tissue-specific. Due to the role of cilia in development and the requirement of Cep164 in ciliogenesis, this widespread expression is not surprising. While Cep164 expression is not tissue-specific, it has been reported to fluctuate during cell cycle stages, peaking in S phase (Graser et al., 2007).

With the successful integration of the AID-GFP tag we could achieve efficient and sustained depletion of the Cep164 protein 30 mins after auxin addition. This is comparable to a previous study using the AID system in DT40 cells to ablate CENP-H, which showed complete depletion after 45 minutes (Nishimura et al., 2009). After depletion of Cep164 we investigated the localisation of a number of centrosomal proteins using immunofluorescence microscopy. The proteins chosen

marked various features of the centrosome, including the centrioles, appendages, satellites and PCM. We found no observable difference in the recruitment of the proteins tested, indicating that Cep164 is not required for their localisation to the centrosome. However, the availability of antibodies that are functional in detecting chicken proteins is an obstacle when conducting immunofluorescence microscopy in DT40 cells. Ideally a complete characterisation of all known distal appendage proteins by super-resolution microscopy would be conducted. This could provide insight into any significant change in protein recruitment upon Cep164 depletion. Indeed, recent work has postulated a hierarchal assembly of distal appendage proteins (DAPs), in which Cep164 recruitment to DAs is dependent on SCLT1 (Tanos et al., 2013). However, this work did not examine if a direct interaction occurs between Cep164 and SCLT1 or if another protein acts between them, providing a point of interest for future studies.

In continuing to investigate any potential centrosome ultrastructural anomalies in Cep164-deficient chicken cells, we conducted transmission electron microscopy (TEM). From our analysis we concluded that there was no obvious defect to centriole structure as the microtubule triplets were intact and both the centriolar length and diameter was consistent with wild-type. As Cep164 is a distal appendage protein, we hypothesised that defects at these structures may be present in the absence of Cep164. However, even under TEM, we found the appendages are difficult to visualise in DT40 cells and no definite conclusion could be made regarding their integrity following Cep164-depletion. Recently, Cep164 has been shown to recruit TTBK2 to the mother centriole to promote ciliogenesis (Oda et al., 2014). Therefore it is possible that the role of Cep164 at the mother centriole is as a recruitment factor and does not actually contribute to the physical structure of the appendages.

There is a link between the centrosome and the DNA damage response. Proteins that localise to the centrosome partake in DDR activities and centrosome composition and number is directly affected by DNA damage. The G2-M arrest that permits centrosome amplification is partly mediated by ATM (Dodson et al., 2004). As Cep164 has been reported to be an interactor of ATM/ATR, we postulated that its absence could affect DNA-damage induced centrosome amplification (Sivasubramaniam et al., 2008). To investigate this, we treated cells with ionising irradiation and quantified the number of centrosomes 24hrs later. We found that the

depletion of Cep164 had no effect on the cell's ability to amplify centrosomes. In addition to an interaction with ATM/ATR, it has been also been reported that absence of Cep164 results in an increased S-phase, thus we were somewhat surprised that centrosome amplification was normal (Slaats et al., 2014).

To further explore the connection between the DNA damage response and Cep164, we conducted DDR assays that we have shown to be reliable in previous studies (Dantas et al., 2011). We tested the sensitivity of Cep164 depleted cells to both ionising radiation and UV light. A previous study demonstrated that knockdown of Cep164 in Hela cells results in hypersensitivity to UV-light (Pan and Lee, 2009). To investigate this in our chicken cells, we depleted Cep164 and carried out IR and UV clonogenic assays. To our surprise, we did not see any sensitivity to either UV or IR radiation. At this stage of the study we began to question the efficacy of the AID system. Although our western blot data showed a very clear depletion, this depletion was verified using a GFP antibody and not an antibody against Cep164. Therefore, there was a possibility that the cells were producing a splice-variant that did not contain the AID-GFP tag, making it non-depletable and masking any potential phenotype. There was no obvious and straightforward way to test this hypothesis. If we conducted an RT-PCR we would simply amplify part of the tagged transcript, regardless of primer design. We did consider raising an antibody to the chicken Cep164 protein, but decided against it to pursue other options. The main other option we are referring to was influenced by advancements in in CRISPR/Cas9 gene targeting technologies. Due to this we decided to switch model system to RPE-1 cells. By proceeding with our study in this human cell line, we could take advantage of a greater access to antibodies and also investigate ciliation, a process RPE-1 cells readily undergo and in which Cep164 has been shown to be involved (Graser et al., 2007).

A bioinformatically-generated list of CRISPR gRNA sequences for the human exome is available online (Mali et al., 2013). There are at least 21 sequences which can be used to target various exons on the *CEP164* locus. For our study we chose three sequences, one for each of exon 3,5 and 7. While the gRNAs for exon 3 and 5 were ineffective, we successfully disrupted the *CEP164* locus using the gRNA for exon 7, creating the first Cep164 null cell line. The underlying reason for the failure of gRNAs targeting exons 3 and 5 was not explored in this study, but one

could speculate the region targeted was inaccessible and thus resistant to the CRISPR/Cas9 system.

While we were conducting our study on Cep164, a project running concurrently in our lab was developing monoclonal antibodies to various centrosomal proteins. One of the antibodies developed was a mouse monoclonal to the N-terminus of the Cep164 protein (work by Dr. David Gaboriau). This antibody detected an antigen at the centrosome and was a useful reagent as it allowed us to confirm the loss of Cep164 in human cells. Likewise, the *CEP164* knockout helped confirm the specificity of the antibody.

With our knockout clones confirmed through immunofluorescence microscopy, Western blot and sequencing, we were confident we had nullified *CEP164*. As Cep164 is known to be required for efficient ciliogenesis we tested this phenomenon in our null cell line. Through immunofluorescence microscopy we confirmed the lack of cilia after serum starvation using three independent cilia markers. This was an important confirmation as it provided further evidence that no functional Cep164 protein remained in the cell (Graser et al., 2007) . Crucially, we also achieved the rescue of this phenotype upon re-expression of the Cep164 protein in null cells.

To further examine the stage of ciliation at which Cep164-deficient cells are hampered, we conducted TEM after serum starvation. From this we confirmed that the role of Cep164 in ciliation is in the binding of distal appendage vesicles to the mother centriole. Being one of the early stages of ciliogenesis, it would be interesting to investigate if Cep164 is also necessary for the maintenance of cilia after they have already formed. Rescuing our deficient cell line with an AID-tagged Cep164 could test this hypothesis, as Cep164 could be depleted after cilia have already formed and changes (if any) in ciliation monitored.

The reported localisation of Cep164 is somewhat inconsistent. While it is generally regarded as a centrosomal protein, some work has described it as nuclear (Pan and Lee, 2009; Sivasubramaniam et al., 2008). Our antibody detected an antigen exclusively at the centrosome, even after DNA damage. In addition to this, our endogenously tagged chicken Cep164 only showed signal at the centrosome. When we overexpressed either the chicken or human Cep164 in their respective cell lines, we also did not observe any nuclear signal, although some cytoplasmic protein was observed. These results were puzzling, as we at least expected a re-localisation

to UV-induced damage foci as has previously been established (Chaki et al., 2012; Pan and Lee, 2009; Sivasubramaniam et al., 2008). On further investigation it is evident that the reported nuclear localisation is detected with a specific antibody, Cep164-N11, common to studies reporting a DNA damage phenotype associate with Cep164 depletion (Chaki et al., 2012; Pan and Lee, 2009; Sivasubramaniam et al., 2008). The Cep164-N11 antibody used in these studies is a mouse monoclonal that was raised against the first 194 amino acids of the protein sequence. This is actually similar to the region of the Cep164 protein that we used as an antigen, which was from amino acid 6-296.

While the difference in localisation between antibodies raised questions about specificity, we decided to nonetheless investigate the DNA damage response in our Cep164-deficient cells. To do this, we subjected cells them to UV radiation and conducted clonogenic assays. We were surprised to see no sensitivity to this DNA damage stress, as it has been previously reported in Hela cells (Pan and Lee, 2009; Sivasubramaniam et al., 2008). However this result did agree with our previous results in the chicken model.

There are some experiments that could be conducted to further clarify the role of Cep164 in the DNA damage response. Obtaining the N11 antibody would be extremely beneficial to test its localisation in our Cep164-deficient RPE-1 cells. If the antibody still detects protein in Cep164-deficient cells it indicates that there is a potential cross-reactivity with some nuclear protein. Of course there is also possibility of a splice-variant escaping both targeting by our gRNA and detection by our antibody. This splice variant would also have to play no part in ciliation, so we feel this is highly unlikely.

Obtaining the exact siRNA used in experiments showing a DNA damage phenotype would also be useful. We could use it on our Cep164 deficient-cells and conduct clonogenic assays after DNA damage. This would allow us to test for off-target effects or if the DNA damage phenotype was specific to Hela cells. Incidentally the Cep164-N11 antibody was only used in Hela cells in published data, thus it would also be informative to test our monoclonol antibody in this cell line. It is conceivable that due to their cancerous nature, Cep164 has re-localised to the nucleus.

Chapter 6. Conclusion

We have generated null alleles of *CEP164* in human hTERT-RPE1 cells and a conditionally null clone in the chicken DT40 line. In both systems, we find that CEP164 deficiency has limited impact on proliferation, centriole integrity or the cellular ability to respond to DNA damage induced by IR or UV irradiation. We find that the loss of CEP164 does, however, entirely ablate primary ciliogenesis, consistent with a defect in docking of the primary ciliary vesicle to the mother centriole that was previously described in the absence of CEP164 (Cajanek and Nigg, 2014; Graser et al., 2007; Schmidt et al., 2012). While our data are thus consistent with published work on CEP164 as a key component in primary cilium formation, they do not provide support for a role for CEP164 in the DNA damage response. We did not see a proliferative decline, such as that described in IMCD cells after siRNA knockdown of CEP164 (Chaki et al., 2012) or an acceleration of cell cycle progression, as has been described after siRNA knockdown of CEP164 in RPE-FUCCI cells (Slaats et al., 2014). In our null lines, we observed no elevated sensitivity to IR or UV irradiation in the absence of CEP164, which contrasts with the phenotypes of UV sensitivity and loss of the G2-to-M checkpoint reported with siRNA knockdown of CEP164 in HeLa cells (Pan and Lee, 2009; Sivasubramaniam et al., 2008). These discrepancies have potential implications for the models of how *CEP164* mutations lead to disease.

There are clear technical differences in the approaches that we have used and those previously reported. An obvious possibility is that the gradual or partial depletion imposed by siRNA treatment may lead to cellular responses different to those seen with the loss of a protein, although our degron-mediated experiment would have been expected to address this. Another possibility is that off-target effects of the siRNA treatments used resulted in more marked phenotypes. While the proliferative decline and cell cycle defects in IMCD3 cells were rescued by transgenic expression of the human CEP164 (Chaki et al., 2012; Slaats et al., 2014), it is worth noting that rescues for the UV sensitivity and checkpoint defects seen in CEP164 knockdown cells were not performed (Pan and Lee, 2009; Sivasubramaniam et al., 2008), so that the specificity of these RNAi phenotypes cannot be assessed.

We have not seen any significant nuclear localisation of CEP164 during the normal cell cycle or after DNA damage in 1 chicken and 3 human cell lines, using 3 different antibodies and multiple, differently-tagged versions of transgenically-expressed CEP164. Similarly to published results (Schmidt et al., 2012), our experiments have detected only cytosolic or centrosomal signals, in contrast to the predominantly nuclear signals reported with those antibodies generated in the original study that implicated CEP164 in the DDR (Sivasubramaniam et al., 2008). Controls for the specificity of the nuclear immunofluorescence signals after CEP164 knockdown or depletion have not been detailed (Pan and Lee, 2009; Sivasubramaniam et al., 2008). Tagging experiments and several antibodies used in a recently-published study showed predominantly cytosolic or centrosomal CEP164 signals, although these authors also described nuclear CEP164 foci using the previously-published CEP164 reagents (Chaki et al., 2012). The absence of a nuclear localisation of CEP164 is consistent with the normal responses to induced DNA damage that we have observed. We have performed our DNA damage sensitivity and localisation analyses in cell lines from different tissues. Thus, while we cannot exclude the possibility that CEP164 contributes to the DDR in certain cell types, this does not appear to be a general activity of the protein.

Taken together, our results confirm that Cep164 is essential for ciliation, where it mediates the docking of distal appendage vesicles to the mother centriole. However, reverse genetic analysis of Cep164 in both chicken and human cells have shown it to be dispensable for the DNA damage response after both IR and UV irradiation.

References

Agircan, F.G., and E. Schiebel. 2014. Sensors at centrosomes reveal determinants of local separase activity. *PLoS Genet*. 10:e1004672.

Allen, R.D. 1969. The morphogenesis of basal bodies and accessory structures of the cortex of the ciliated protozoan Tetrahymena pyriformis. *J Cell Biol*. 40:716-33.

Andersen, J.S., C.J. Wilkinson, T. Mayor, P. Mortensen, E.A. Nigg, and M. Mann. 2003. Proteomic characterization of the human centrosome by protein correlation profiling. *Nature*. 426:570-4.

Anderson, R.G. 1972. The three-dimensional structure of the basal body from the rhesus monkey oviduct. *J Cell Biol*. 54:246-65.

Antonczak, A.K., L.I. Mullee, Y. Wang, D. Comartin, T. Inoue, L. Pelletier, and C.G. Morrison. 2015. Opposing effects of pericentrin and microcephalin on the pericentriolar material regulate CHK1 activation in the DNA damage response. *Oncogene*.

Arakawa, H., D. Lodygin, and J.M. Buerstedde. 2001. Mutant loxP vectors for selectable marker recycle and conditional knock-outs. *BMC Biotechnol*. 1:7.

Araki, M., C. Masutani, M. Takemura, A. Uchida, K. Sugasawa, J. Kondoh, Y. Ohkuma, and F. Hanaoka. 2001. Centrosome protein centrin 2/caltractin 1 is part of the xeroderma pigmentosum group C complex that initiates global genome nucleotide excision repair. *J Biol Chem*. 276:18665-72.

Arquint, C., K.F. Sonnen, Y.D. Stierhof, and E.A. Nigg. 2012. Cell-cycle-regulated expression of STIL controls centriole number in human cells. *J Cell Sci*. 125:1342-52.

Augustin, A., C. Spenlehauer, H. Dumond, J. Menissier-De Murcia, M. Piel, A.C. Schmit, F. Apiou, J.L. Vonesch, M. Kock, M. Bornens, and G. De Murcia. 2003. PARP-3 localizes preferentially to the daughter centriole and interferes with the G1/S cell cycle progression. *J Cell Sci*. 116:1551-62.

Avasthi, P., and W.F. Marshall. 2012. Stages of ciliogenesis and regulation of ciliary length. *Differentiation*. 83:S30-42.

Azimzadeh, J., P. Hergert, A. Delouvee, U. Euteneuer, E. Formstecher, A. Khodjakov, and M. Bornens. 2009. hPOC5 is a centrin-binding protein required for assembly of full-length centrioles. *J Cell Biol*. 185:101-14.

Azimzadeh, J., M.L. Wong, D.M. Downhour, A. Sanchez Alvarado, and W.F. Marshall. 2012. Centrosome loss in the evolution of planarians. *Science*. 335:461-3.

Bahe, S., Y.D. Stierhof, C.J. Wilkinson, F. Leiss, and E.A. Nigg. 2005. Rootletin forms centriole-associated filaments and functions in centrosome cohesion. *J Cell Biol*. 171:27-33.

Bailly, E., M. Doree, P. Nurse, and M. Bornens. 1989. p34cdc2 is located in both nucleus and cytoplasm; part is centrosomally associated at G2/M and enters vesicles at anaphase. *Embo j*. 8:3985-95.

Balczon, R., L. Bao, W.E. Zimmer, K. Brown, R.P. Zinkowski, and B.R. Brinkley. 1995. Dissociation of centrosome replication events from cycles of DNA synthesis and mitotic division in hydroxyurea-arrested Chinese hamster ovary cells. *J Cell Biol*. 130:105-15.

Barnes, B.G. 1961. Ciliated secretory cells in the pars distalis of the mouse hypophysis. *J Ultrastruct Res*. 5:453-67.

Bartek, J., and J. Lukas. 2007. DNA damage checkpoints: from initiation to recovery or adaptation. *Curr Opin Cell Biol*. 19:238-45.

Basto, R., J. Lau, T. Vinogradova, A. Gardiol, C.G. Woods, A. Khodjakov, and J.W. Raff. 2006. Flies without centrioles. *Cell*. 125:1375-86.

Bernardes de Jesus, B.M., M. Bjoras, F. Coin, and J.M. Egly. 2008. Dissection of the molecular defects caused by pathogenic mutations in the DNA repair factor XPC. *Mol Cell Biol*. 28:7225-35.

Bernstein, K.A., and R. Rothstein. 2009. At loose ends: resecting a double-strand break. *Cell*. 137:807-10.

Betschinger, J., and J.A. Knoblich. 2004. Dare to be different: asymmetric cell division in Drosophila, C. elegans and vertebrates. *Curr Biol*. 14:R674-85.

Bird, A.W., and A.A. Hyman. 2008. Building a spindle of the correct length in human cells requires the interaction between TPX2 and Aurora A. *J Cell Biol*. 182:289-300.

Bobinnec, Y., A. Khodjakov, L.M. Mir, C.L. Rieder, B. Edde, and M. Bornens. 1998. Centriole disassembly in vivo and its effect on centrosome structure and function in vertebrate cells. *J Cell Biol*. 143:1575-89.

Bohr, V.A., C.A. Smith, D.S. Okumoto, and P.C. Hanawalt. 1985. DNA repair in an active gene: removal of pyrimidine dimers from the DHFR gene of CHO cells is much more efficient than in the genome overall. *Cell*. 40:359-69.

Borel, F., O.D. Lohez, F.B. Lacroix, and R.L. Margolis. 2002. Multiple centrosomes arise from tetraploidy checkpoint failure and mitotic centrosome clusters in p53 and RB pocket protein-compromised cells. *Proc Natl Acad Sci U S A*. 99:9819-24.

Bornens, M. 2002. Centrosome composition and microtubule anchoring mechanisms. *Curr Opin Cell Biol*. 14:25-34.

Brown, J.A., E. Bourke, C. Liptrot, P. Dockery, and C.G. Morrison. 2010. MCPH1/BRIT1 limits ionizing radiation-induced centrosome amplification. *Oncogene*. 29:5537-44.

Brown, W.R., S.J. Hubbard, C. Tickle, and S.A. Wilson. 2003. The chicken as a model for large-scale analysis of vertebrate gene function. *Nat Rev Genet*. 4:87-98.

Buerstedde, J.M., and S. Takeda. 1991. Increased ratio of targeted to random integration after transfection of chicken B cell lines. *Cell*. 67:179-88.

Bunz, F., A. Dutriaux, C. Lengauer, T. Waldman, S. Zhou, J.P. Brown, J.M. Sedivy, K.W. Kinzler, and B. Vogelstein. 1998. Requirement for p53 and p21 to sustain G2 arrest after DNA damage. *Science*. 282:1497-501.

Cajanek, L., and E.A. Nigg. 2014. Cep164 triggers ciliogenesis by recruiting Tau tubulin kinase 2 to the mother centriole. *Proc Natl Acad Sci U S A*. 111:E2841-50.

Carvalho-Santos, Z., J. Azimzadeh, J.B. Pereira-Leal, and M. Bettencourt-Dias. 2011. Evolution: Tracing the origins of centrioles, cilia, and flagella. *J Cell Biol*. 194:165-75.

Chaki, M., R. Airik, A.K. Ghosh, R.H. Giles, R. Chen, G.G. Slaats, H. Wang, T.W. Hurd, W. Zhou, A. Cluckey, H.Y. Gee, G. Ramaswami, C.J. Hong, B.A. Hamilton, I. Cervenka, R.S. Ganji, V. Bryja, H.H. Arts, J. van Reeuwijk, M.M. Oud, S.J. Letteboer, R. Roepman, H. Husson, O. Ibraghimov-Beskrovnaya, T. Yasunaga, G. Walz, L. Eley, J.A. Sayer, B. Schermer, M.C. Liebau, T. Benzing, S. Le Corre, I. Drummond, S. Janssen, S.J. Allen, S. Natarajan, J.F. O'Toole, M. Attanasio, S. Saunier, C. Antignac, R.K. Koenekoop, H. Ren, I. Lopez, A. Nayir, C. Stoetzel, H. Dollfus, R. Massoudi, J.G. Gleeson, S.P. Andreoli, D.G. Doherty, A. Lindstrad, C. Golzio, N. Katsanis, L. Pape, E.B. Abboud, A.A. Al-Rajhi, R.A. Lewis, H. Omran, E.Y. Lee, S. Wang, J.M. Sekiguchi, R. Saunders, C.A. Johnson, E. Garner, K. Vanselow, J.S. Andersen, J. Shlomai, G. Nurnberg, P. Nurnberg, S. Levy, A. Smogorzewska, E.A. Otto, and F. Hildebrandt. 2012. Exome capture reveals ZNF423 and CEP164 mutations, linking renal ciliopathies to DNA damage response signaling. *Cell*. 150:533-48.

Chestukhin, A., C. Pfeffer, S. Milligan, J.A. DeCaprio, and D. Pellman. 2003. Processing, localization, and requirement of human separase for normal anaphase progression. *Proc Natl Acad Sci U S A*. 100:4574-9.

Ciccia, A., and S.J. Elledge. 2010. The DNA damage response: making it safe to play with knives. *Mol Cell*. 40:179-204.

Cizmecioglu, O., M. Arnold, R. Bahtz, F. Settele, L. Ehret, U. Haselmann-Weiss, C. Antony, and I. Hoffmann. 2010. Cep152 acts as a scaffold for recruitment of Plk4 and CPAP to the centrosome. *J Cell Biol*. 191:731-9.

Cong, L., F.A. Ran, D. Cox, S. Lin, R. Barretto, N. Habib, P.D. Hsu, X. Wu, W. Jiang, L.A. Marraffini, and F. Zhang. 2013. Multiplex genome engineering using CRISPR/Cas systems. *Science*. 339:819-23.

Corbit, K.C., A.E. Shyer, W.E. Dowdle, J. Gaulden, V. Singla, M.H. Chen, P.T. Chuang, and J.F. Reiter. 2008. Kif3a constrains beta-catenin-dependent Wnt signalling through dual ciliary and non-ciliary mechanisms. *Nat Cell Biol*. 10:70-6.

Cottee, M.A., N. Muschalik, Y.L. Wong, C.M. Johnson, S. Johnson, A. Andreeva, K. Oegema, S.M. Lea, J.W. Raff, and M. van Breugel. 2013. Crystal structures of the CPAP/STIL complex reveal its role in centriole assembly and human microcephaly. *Elife*. 2:e01071.

Craig, A., M. Scott, L. Burch, G. Smith, K. Ball, and T. Hupp. 2003. Allosteric effects mediate CHK2 phosphorylation of the p53 transactivation domain. *EMBO Rep*. 4:787-92.

Cunha-Ferreira, I., A. Rodrigues-Martins, I. Bento, M. Riparbelli, W. Zhang, E. Laue, G. Callaini, D.M. Glover, and M. Bettencourt-Dias. 2009. The SCF/Slimb ubiquitin ligase limits centrosome amplification through degradation of SAK/PLK4. *Curr Biol*. 19:43-9.

Dammermann, A. 2002. Assembly of centrosomal proteins and microtubule organization depends on PCM-1. *The Journal of Cell Biology*. 159:255-266.

Dantas, T.J., Y. Wang, P. Lalor, P. Dockery, and C.G. Morrison. 2011. Defective nucleotide excision repair with normal centrosome structures and functions in the absence of all vertebrate centrins. *J Cell Biol*. 193:307-18.

De Brabander, M., G. Geuens, R. Nuydens, R. Willebrords, and J. De Mey. 1982. Microtubule stability and assembly in living cells: the influence of metabolic inhibitors, taxol and pH. *Cold Spring Harb Symp Quant Biol*. 46 Pt 1:227-40.

de Laat, W.L., N.G. Jaspers, and J.H. Hoeijmakers. 1999. Molecular mechanism of nucleotide excision repair. *Genes Dev*. 13:768-85.

Debec, A., W. Sullivan, and M. Bettencourt-Dias. 2010. Centrioles: active players or passengers during mitosis? *Cell Mol Life Sci*. 67:2173-94.

Delattre, M., and P. Gonczy. 2004. The arithmetic of centrosome biogenesis. *J Cell Sci*. 117:1619-30.

Dingemans, K.P. 1969. The relation between cilia and mitoses in the mouse adenohypophysis. *J Cell Biol*. 43:361-7.

Dippell, R.V. 1968. The development of basal bodies in paramecium. *Proc Natl Acad Sci U S A*. 61:461-8.

Dodson, H., E. Bourke, L.J. Jeffers, P. Vagnarelli, E. Sonoda, S. Takeda, W.C. Earnshaw, A. Merdes, and C. Morrison. 2004. Centrosome amplification induced by DNA damage occurs during a prolonged G2 phase and involves ATM. *Embo j*. 23:3864-73.

Doxsey, S., D. McCollum, and W. Theurkauf. 2005. Centrosomes in cellular regulation. *Annu Rev Cell Dev Biol*. 21:411-34.

Duensing, A., Y. Liu, S.A. Perdreau, J. Kleylein-Sohn, E.A. Nigg, and S. Duensing. 2007. Centriole overduplication through the concurrent formation of multiple daughter centrioles at single maternal templates. *Oncogene*. 26:6280-8.

Dutertre, S., M. Cazales, M. Quaranta, C. Froment, V. Trabut, C. Dozier, G. Mirey, J.P. Bouche, N. Theis-Febvre, E. Schmitt, B. Monsarrat, C. Prigent, and B. Ducommun. 2004. Phosphorylation of CDC25B by Aurora-A at the centrosome contributes to the G2-M transition. *J Cell Sci*. 117:2523-31.

Echelard, Y., D.J. Epstein, B. St-Jacques, L. Shen, J. Mohler, J.A. McMahon, and A.P. McMahon. 1993. Sonic hedgehog, a member of a family of putative signaling molecules, is implicated in the regulation of CNS polarity. *Cell*. 75:1417-30.

Egly, J.M. 2001. The 14th Datta Lecture. TFIIH: from transcription to clinic. *FEBS Lett*. 498:124-8.

Etienne-Manneville, S. 2010. From signaling pathways to microtubule dynamics: the key players. *Curr Opin Cell Biol*. 22:104-11.

Eykelenboom, J.K., E.C. Harte, L. Canavan, A. Pastor-Peidro, I. Calvo-Asensio, M. Llorens-Agost, and N.F. Lowndes. 2013. ATR activates the S-M checkpoint during unperturbed growth to ensure sufficient replication prior to mitotic onset. *Cell Rep*. 5:1095-107.

Falck, J., J.H. Petrini, B.R. Williams, J. Lukas, and J. Bartek. 2002. The DNA damage-dependent intra-S phase checkpoint is regulated by parallel pathways. *Nat Genet*. 30:290-4.

Fellous, A., J. Francon, A.M. Lennon, and J. Nunez. 1977. Microtubule assembly in vitro. Purification of assembly-promoting factors. *Eur J Biochem*. 78:167-74.

Feng, S., B. Wu, J. Peranen, and W. Guo. 2015. Kinetic activation of Rab8 guanine nucleotide exchange factor Rabin8 by Rab11. *Methods Mol Biol*. 1298:99-106.

Fry, A.M., T. Mayor, P. Meraldi, Y.D. Stierhof, K. Tanaka, and E.A. Nigg. 1998a. C-Nap1, a novel centrosomal coiled-coil protein and candidate substrate of the cell cycle-regulated protein kinase Nek2. *J Cell Biol*. 141:1563-74.

Fry, A.M., P. Meraldi, and E.A. Nigg. 1998b. A centrosomal function for the human Nek2 protein kinase, a member of the NIMA family of cell cycle regulators. *Embo j*. 17:470-81.

Fu, J., and D.M. Glover. 2012. Structured illumination of the interface between centriole and peri-centriolar material. *Open Biol*. 2:120104.

Fukasawa, K. 2005. Centrosome amplification, chromosome instability and cancer development. *Cancer Lett*. 230:6-19.

Fukasawa, K. 2008. P53, cyclin-dependent kinase and abnormal amplification of centrosomes. *Biochim Biophys Acta*. 1786:15-23.

Fukasawa, K., T. Choi, R. Kuriyama, S. Rulong, and G.F. Vande Woude. 1996. Abnormal centrosome amplification in the absence of p53. *Science*. 271:1744-7.

Gerdes, J.M., E.E. Davis, and N. Katsanis. 2009. The vertebrate primary cilium in development, homeostasis, and disease. *Cell*. 137:32-45.

Gibbons, I.R., and A.V. Grimstone. 1960. On flagellar structure in certain flagellates. *J Biophys Biochem Cytol*. 7:697-716.

Goetz, S.C., K.F. Liem, Jr., and K.V. Anderson. 2012. The spinocerebellar ataxia-associated gene Tau tubulin kinase 2 controls the initiation of ciliogenesis. *Cell*. 151:847-58.

Golsteyn, R.M., K.E. Mundt, A.M. Fry, and E.A. Nigg. 1995. Cell cycle regulation of the activity and subcellular localization of Plk1, a human protein kinase implicated in mitotic spindle function. *J Cell Biol*. 129:1617-28.

Gonczy, P. 2012. Towards a molecular architecture of centriole assembly. *Nat Rev Mol Cell Biol*. 13:425-35.

Graser, S., Y.D. Stierhof, S.B. Lavoie, O.S. Gassner, S. Lamla, M. Le Clech, and E.A. Nigg. 2007. Cep164, a novel centriole appendage protein required for primary cilium formation. *J Cell Biol*. 179:321-30.

Guarguaglini, G., P.I. Duncan, Y.D. Stierhof, T. Holmstrom, S. Duensing, and E.A. Nigg. 2005. The forkhead-associated domain protein Cep170 interacts with Polo-like kinase 1 and serves as a marker for mature centrioles. *Mol Biol Cell*. 16:1095-107.

Guderian, G., J. Westendorf, A. Uldschmid, and E.A. Nigg. 2010. Plk4 trans-autophosphorylation regulates centriole number by controlling betaTrCP-mediated degradation. *J Cell Sci*. 123:2163-9.

Guichard, P., D. Chretien, S. Marco, and A.M. Tassin. 2010. Procentriole assembly revealed by cryo-electron tomography. *EMBO J*. 29:1565-72.

Habedanck, R., Y.D. Stierhof, C.J. Wilkinson, and E.A. Nigg. 2005. The Polo kinase Plk4 functions in centriole duplication. *Nat Cell Biol*. 7:1140-6.

Haren, L., M.H. Remy, I. Bazin, I. Callebaut, M. Wright, and A. Merdes. 2006. NEDD1-dependent recruitment of the gamma-tubulin ring complex to the centrosome is necessary for centriole duplication and spindle assembly. *J Cell Biol*. 172:505-15.

Hauf, S., I.C. Waizenegger, and J.M. Peters. 2001. Cohesin cleavage by separase required for anaphase and cytokinesis in human cells. *Science*. 293:1320-3.

Heyer, W.D., K.T. Ehmsen, and J. Liu. 2010. Regulation of homologous recombination in eukaryotes. *Annu Rev Genet*. 44:113-39.

Hinchcliffe, E.H., C. Li, E.A. Thompson, J.L. Maller, and G. Sluder. 1999. Requirement of Cdk2-cyclin E activity for repeated centrosome reproduction in Xenopus egg extracts. *Science*. 283:851-4.

Hiraki, M., Y. Nakazawa, R. Kamiya, and M. Hirono. 2007. Bld10p constitutes the cartwheel-spoke tip and stabilizes the 9-fold symmetry of the centriole. *Curr Biol*. 17:1778-83.

Hirono, M. 2014. Cartwheel assembly. *Philos Trans R Soc Lond B Biol Sci*. 369.

Hochegger, H., D. Dejsuphong, E. Sonoda, A. Saberi, E. Rajendra, J. Kirk, T. Hunt, and S. Takeda. 2007. An essential role for Cdk1 in S phase control is revealed via chemical genetics in vertebrate cells. *J Cell Biol*. 178:257-68.

Hochegger, H., S. Takeda, and T. Hunt. 2008. Cyclin-dependent kinases and cell-cycle transitions: does one fit all? *Nat Rev Mol Cell Biol*. 9:910-6.

Holland, A.J., and D.W. Cleveland. 2009. Boveri revisited: chromosomal instability, aneuploidy and tumorigenesis. *Nat Rev Mol Cell Biol*. 10:478-87.

Holland, A.J., W. Lan, S. Niessen, H. Hoover, and D.W. Cleveland. 2010. Polo-like kinase 4 kinase activity limits centrosome overduplication by autoregulating its own stability. *J Cell Biol*. 188:191-8.

Huangfu, D., A. Liu, A.S. Rakeman, N.S. Murcia, L. Niswander, and K.V. Anderson. 2003. Hedgehog signalling in the mouse requires intraflagellar transport proteins. *Nature*. 426:83-7.

Hung, L.Y., C.J. Tang, and T.K. Tang. 2000. Protein 4.1 R-135 interacts with a novel centrosomal protein (CPAP) which is associated with the gamma-tubulin complex. *Mol Cell Biol*. 20:7813-25.

International Chicken Genome Sequencing, C. 2004. Sequence and comparative analysis of the chicken genome provide unique perspectives on vertebrate evolution. *Nature*. 432:695-716.

Ishikawa, H., A. Kubo, S. Tsukita, and S. Tsukita. 2005. Odf2-deficient mother centrioles lack distal/subdistal appendages and the ability to generate primary cilia. *Nat Cell Biol*. 7:517-24.

Jackman, M., C. Lindon, E.A. Nigg, and J. Pines. 2003. Active cyclin B1-Cdk1 first appears on centrosomes in prophase. *Nat Cell Biol*. 5:143-8.

Jackson, A.L., and P.S. Linsley. 2010. Recognizing and avoiding siRNA off-target effects for target identification and therapeutic application. *Nat Rev Drug Discov*. 9:57-67.

Jackson, S.P. 2002. Sensing and repairing DNA double-strand breaks. *Carcinogenesis*. 23:687-96.

Jackson, S.P., and D. Durocher. 2013. Regulation of DNA damage responses by ubiquitin and SUMO. *Mol Cell*. 49:795-807.

Jilani, Y., S. Lu, H. Lei, L.M. Karnitz, and A. Chadli. 2015. UNC45A localizes to centrosomes and regulates cancer cell proliferation through ChK1 activation. *Cancer Lett*. 357:114-20.

Jones, M.L., S.L. Murden, D. Bem, S.J. Mundell, P. Gissen, M.E. Daly, S.P. Watson, A.D. Mumford, and U.G.s. group. 2012. Rapid genetic diagnosis of heritable platelet function disorders with next-generation sequencing: proof-of-principle with Hermansky-Pudlak syndrome. *J Thromb Haemost*. 10:306-9.

Kalab, P., and R. Heald. 2008. The RanGTP gradient - a GPS for the mitotic spindle. *J Cell Sci*. 121:1577-86.

Kanai, M., M. Uchida, S. Hanai, N. Uematsu, K. Uchida, and M. Miwa. 2000. Poly(ADP-ribose) polymerase localizes to the centrosomes and chromosomes. *Biochem Biophys Res Commun*. 278:385-9.

Katsura, M., T. Tsuruga, O. Date, T. Yoshihara, M. Ishida, Y. Tomoda, M. Okajima, M. Takaku, H. Kurumizaka, A. Kinomura, H.K. Mishima, and K. Miyagawa. 2009. The ATR-Chk1 pathway plays a role in the generation of centrosome aberrations induced by Rad51C dysfunction. *Nucleic Acids Res*. 37:3959-68.

Keller, L.C., S. Geimer, E. Romijn, J. Yates, 3rd, I. Zamora, and W.F. Marshall. 2009. Molecular architecture of the centriole proteome: the conserved WD40 domain protein POC1 is required for centriole duplication and length control. *Mol Biol Cell*. 20:1150-66.

Kervestin, S., and A. Jacobson. 2012. NMD: a multifaceted response to premature translational termination. *Nat Rev Mol Cell Biol*. 13:700-12.

Kim, K., S. Lee, J. Chang, and K. Rhee. 2008. A novel function of CEP135 as a platform protein of C-NAP1 for its centriolar localization. *Exp Cell Res*. 314:3692-700.

Kim, S., K. Lee, J.H. Choi, N. Ringstad, and B.D. Dynlacht. 2015. Nek2 activation of Kif24 ensures cilium disassembly during the cell cycle. *Nat Commun*. 6:8087.

Kim, S.T., B. Xu, and M.B. Kastan. 2002. Involvement of the cohesin protein, Smc1, in Atm-dependent and independent responses to DNA damage. *Genes Dev*. 16:560-70.

Kitagawa, D., I. Vakonakis, N. Olieric, M. Hilbert, D. Keller, V. Olieric, M. Bortfeld, M.C. Erat, I. Fluckiger, P. Gonczy, and M.O. Steinmetz. 2011. Structural basis of the 9-fold symmetry of centrioles. *Cell*. 144:364-75.

Kleylein-Sohn, J., J. Westendorf, M. Le Clech, R. Habedanck, Y.D. Stierhof, and E.A. Nigg. 2007. Plk4-induced centriole biogenesis in human cells. *Dev Cell*. 13:190-202.

Klotz, C., M.C. Dabauvalle, M. Paintrand, T. Weber, M. Bornens, and E. Karsenti. 1990. Parthenogenesis in Xenopus eggs requires centrosomal integrity. *J Cell Biol*. 110:405-15.

Knodler, A., S. Feng, J. Zhang, X. Zhang, A. Das, J. Peranen, and W. Guo. 2010. Coordination of Rab8 and Rab11 in primary ciliogenesis. *Proc Natl Acad Sci U S A*. 107:6346-51.

Kochanski, R.S., and G.G. Borisy. 1990. Mode of centriole duplication and distribution. *J Cell Biol*. 110:1599-605.

Kohlmaier, G., J. Loncarek, X. Meng, B.F. McEwen, M.M. Mogensen, A. Spektor, B.D. Dynlacht, A. Khodjakov, and P. Gonczy. 2009. Overly long centrioles and defective cell division upon excess of the SAS-4-related protein CPAP. *Curr Biol*. 19:1012-8.

Koledova, Z., A. Kramer, L.R. Kafkova, and V. Divoky. 2010. Cell-cycle regulation in embryonic stem cells: centrosomal decisions on self-renewal. *Stem Cells Dev*. 19:1663-78.

Kollman, J.M., A. Merdes, L. Mourey, and D.A. Agard. 2011. Microtubule nucleation by gamma-tubulin complexes. *Nat Rev Mol Cell Biol*. 12:709-21.

Kong, D., V. Farmer, A. Shukla, J. James, R. Gruskin, S. Kiriyama, and J. Loncarek. 2014. Centriole maturation requires regulated Plk1 activity during two consecutive cell cycles. *J Cell Biol*. 206:855-65.

Kozminski, K.G., K.A. Johnson, P. Forscher, and J.L. Rosenbaum. 1993. A motility in the eukaryotic flagellum unrelated to flagellar beating. *Proc Natl Acad Sci U S A*. 90:5519-23.

Kramer, A., N. Mailand, C. Lukas, R.G. Syljuasen, C.J. Wilkinson, E.A. Nigg, J. Bartek, and J. Lukas. 2004. Centrosome-associated Chk1 prevents premature activation of cyclin-B-Cdk1 kinase. *Nat Cell Biol*. 6:884-91.

Kumagai, A., and W.G. Dunphy. 1999. Binding of 14-3-3 proteins and nuclear export control the intracellular localization of the mitotic inducer Cdc25. *Genes Dev*. 13:1067-72.

Lacey, K.R., P.K. Jackson, and T. Stearns. 1999. Cyclin-dependent kinase control of centrosome duplication. *Proc Natl Acad Sci U S A*. 96:2817-22.

Lawo, S., M. Hasegan, G.D. Gupta, and L. Pelletier. 2012. Subdiffraction imaging of centrosomes reveals higher-order organizational features of pericentriolar material. *Nat Cell Biol*. 14:1148-58.

Lee, K., and K. Rhee. 2012. Separase-dependent cleavage of pericentrin B is necessary and sufficient for centriole disengagement during mitosis. *Cell Cycle*. 11:2476-85.

Lee, K.H., Y. Johmura, L.R. Yu, J.E. Park, Y. Gao, J.K. Bang, M. Zhou, T.D. Veenstra, B. Yeon Kim, and K.S. Lee. 2012. Identification of a novel Wnt5a-CK1varepsilon-Dvl2-Plk1-mediated primary cilia disassembly pathway. *EMBO J*. 31:3104-17.

Lenart, P., M. Petronczki, M. Steegmaier, B. Di Fiore, J.J. Lipp, M. Hoffmann, W.J. Rettig, N. Kraut, and J.M. Peters. 2007. The small-molecule inhibitor BI 2536 reveals novel insights into mitotic roles of polo-like kinase 1. *Curr Biol*. 17:304-15.

Li, J., M. Tan, L. Li, D. Pamarthy, T.S. Lawrence, and Y. Sun. 2005. SAK, a new polo-like kinase, is transcriptionally repressed by p53 and induces apoptosis upon RNAi silencing. *Neoplasia*. 7:312-23.

Li, S., J.J. Fernandez, W.F. Marshall, and D.A. Agard. 2012. Three-dimensional structure of basal body triplet revealed by electron cryo-tomography. *EMBO J*. 31:552-62.

Lin, S.Y., R. Rai, K. Li, Z.X. Xu, and S.J. Elledge. 2005. BRIT1/MCPH1 is a DNA damage responsive protein that regulates the Brca1-Chk1 pathway, implicating checkpoint dysfunction in microcephaly. *Proc Natl Acad Sci U S A*. 102:15105-9.

Lin, Y.N., C.T. Wu, Y.C. Lin, W.B. Hsu, C.J. Tang, C.W. Chang, and T.K. Tang. 2013. CEP120 interacts with CPAP and positively regulates centriole elongation. *J Cell Biol*. 202:211-9.

Loffler, H., T. Bochtler, B. Fritz, B. Tews, A.D. Ho, J. Lukas, J. Bartek, and A. Kramer. 2007. DNA damage-induced accumulation of centrosomal Chk1 contributes to its checkpoint function. *Cell Cycle*. 6:2541-8.

Loncarek, J., P. Hergert, V. Magidson, and A. Khodjakov. 2008. Control of daughter centriole formation by the pericentriolar material. *Nat Cell Biol*. 10:322-8.

Lu, Q., C. Insinna, C. Ott, J. Stauffer, P.A. Pintado, J. Rahajeng, U. Baxa, V. Walia, A. Cuenca, Y.S. Hwang, I.O. Daar, S. Lopes, J. Lippincott-Schwartz, P.K. Jackson, S. Caplan, and C.J. Westlake. 2015. Early steps in primary cilium assembly require EHD1/EHD3-dependent ciliary vesicle formation. *Nat Cell Biol*. 17:531.

Lukas, J., C. Lukas, and J. Bartek. 2011. More than just a focus: The chromatin response to DNA damage and its role in genome integrity maintenance. *Nat Cell Biol*. 13:1161-9.

Mahaney, B.L., K. Meek, and S.P. Lees-Miller. 2009. Repair of ionizing radiation-induced DNA double-strand breaks by non-homologous end-joining. *Biochem J*. 417:639-50.

Mali, P., L. Yang, K.M. Esvelt, J. Aach, M. Guell, J.E. DiCarlo, J.E. Norville, and G.M. Church. 2013. RNA-guided human genome engineering via Cas9. *Science*. 339:823-6.

Malumbres, M., and M. Barbacid. 2009. Cell cycle, CDKs and cancer: a changing paradigm. *Nat Rev Cancer*. 9:153-66.

Marshall, W.F., and J.L. Rosenbaum. 2001. Intraflagellar transport balances continuous turnover of outer doublet microtubules: implications for flagellar length control. *J Cell Biol*. 155:405-14.

Masui, Y., and C.L. Markert. 1971. Cytoplasmic control of nuclear behavior during meiotic maturation of frog oocytes. *J Exp Zool*. 177:129-45.

Matsumoto, Y., K. Hayashi, and E. Nishida. 1999. Cyclin-dependent kinase 2 (Cdk2) is required for centrosome duplication in mammalian cells. *Curr Biol*. 9:429-32.

Matsuo, K., K. Ohsumi, M. Iwabuchi, T. Kawamata, Y. Ono, and M. Takahashi. 2012. Kendrin is a novel substrate for separase involved in the licensing of centriole duplication. *Curr Biol*. 22:915-21.

Matsuyama, M., H. Goto, K. Kasahara, Y. Kawakami, M. Nakanishi, T. Kiyono, N. Goshima, and M. Inagaki. 2011. Nuclear Chk1 prevents premature mitotic entry. *J Cell Sci*. 124:2113-9.

Mayor, T., Y.D. Stierhof, K. Tanaka, A.M. Fry, and E.A. Nigg. 2000. The centrosomal protein C-Nap1 is required for cell cycle-regulated centrosome cohesion. *J Cell Biol*. 151:837-46.

Mazia, D., P.J. Harris, and T. Bibring. 1960. The Multiplicity of the Mitotic Centers and the Time-Course of Their Duplication and Separation. *J Biophys Biochem Cytol*. 7:1-20.

Meek, K., V. Dang, and S.P. Lees-Miller. 2008. DNA-PK: the means to justify the ends? *Adv Immunol*. 99:33-58.

Mellon, I., G. Spivak, and P.C. Hanawalt. 1987. Selective removal of transcription-blocking DNA damage from the transcribed strand of the mammalian DHFR gene. *Cell*. 51:241-9.

Mennella, V., D.A. Agard, B. Huang, and L. Pelletier. 2014. Amorphous no more: subdiffraction view of the pericentriolar material architecture. *Trends Cell Biol*. 24:188-97.

Meraldi, P., R. Honda, and E.A. Nigg. 2002. Aurora-A overexpression reveals tetraploidization as a major route to centrosome amplification in p53-/- cells. *Embo j*. 21:483-92.

Mogensen, M.M., A. Malik, M. Piel, V. Bouckson-Castaing, and M. Bornens. 2000. Microtubule minus-end anchorage at centrosomal and non-centrosomal sites: the role of ninein. *J Cell Sci*. 113 (Pt 17):3013-23.

Moritz, M., M.B. Braunfeld, V. Guenebaut, J. Heuser, and D.A. Agard. 2000. Structure of the gamma-tubulin ring complex: a template for microtubule nucleation. *Nat Cell Biol*. 2:365-70.

Nachury, M.V., A.V. Loktev, Q. Zhang, C.J. Westlake, J. Peranen, A. Merdes, D.C. Slusarski, R.H. Scheller, J.F. Bazan, V.C. Sheffield, and P.K. Jackson. 2007. A core complex of BBS proteins cooperates with the GTPase Rab8 to promote ciliary membrane biogenesis. *Cell*. 129:1201-13.

Nakamura, A., H. Arai, and N. Fujita. 2009. Centrosomal Aki1 and cohesin function in separase-regulated centriole disengagement. *J Cell Biol*. 187:607-14.

Nigg, E.A. 2007. Centrosome duplication: of rules and licenses. *Trends Cell Biol*. 17:215-21.

Nigg, E.A., and J.W. Raff. 2009. Centrioles, centrosomes, and cilia in health and disease. *Cell*. 139:663-78.

Nigg, E.A., and T. Stearns. 2011. The centrosome cycle: Centriole biogenesis, duplication and inherent asymmetries. *Nat Cell Biol*. 13:1154-60.

Nishimura, K., T. Fukagawa, H. Takisawa, T. Kakimoto, and M. Kanemaki. 2009. An auxin-based degron system for the rapid depletion of proteins in nonplant cells. *Nat Methods*. 6:917-22.

Nyberg, K.A., R.J. Michelson, C.W. Putnam, and T.A. Weinert. 2002. Toward maintaining the genome: DNA damage and replication checkpoints. *Annu Rev Genet*. 36:617-56.

Oakley, C.E., and B.R. Oakley. 1989. Identification of gamma-tubulin, a new member of the tubulin superfamily encoded by mipA gene of Aspergillus nidulans. *Nature*. 338:662-4.

Oda, T., S. Chiba, T. Nagai, and K. Mizuno. 2014. Binding to Cep164, but not EB1, is essential for centriolar localization of TTBK2 and its function in ciliogenesis. *Genes Cells*. 19:927-40.

Oegema, K., C. Wiese, O.C. Martin, R.A. Milligan, A. Iwamatsu, T.J. Mitchison, and Y. Zheng. 1999. Characterization of two related Drosophila gamma-tubulin complexes that differ in their ability to nucleate microtubules. *J Cell Biol*. 144:721-33.

Ohta, T., R. Essner, J.H. Ryu, R.E. Palazzo, Y. Uetake, and R. Kuriyama. 2002. Characterization of Cep135, a novel coiled-coil centrosomal protein involved in microtubule organization in mammalian cells. *J Cell Biol*. 156:87-99.

Oricchio, E., C. Saladino, S. Iacovelli, S. Soddu, and E. Cundari. 2006. ATM is activated by default in mitosis, localizes at centrosomes and monitors mitotic spindle integrity. *Cell Cycle*. 5:88-92.

Paintrand, M., M. Moudjou, H. Delacroix, and M. Bornens. 1992. Centrosome organization and centriole architecture: their sensitivity to divalent cations. *J Struct Biol*. 108:107-28.

Palazzo, R.E., J.M. Vogel, B.J. Schnackenberg, D.R. Hull, and X. Wu. 2000. Centrosome maturation. *Curr Top Dev Biol*. 49:449-70.

Pan, Y.R., and E.Y. Lee. 2009. UV-dependent interaction between Cep164 and XPA mediates localization of Cep164 at sites of DNA damage and UV sensitivity. *Cell Cycle*. 8:655-64.

Paoletti, A., M. Moudjou, M. Paintrand, J.L. Salisbury, and M. Bornens. 1996. Most of centrin in animal cells is not centrosome-associated and centrosomal centrin is confined to the distal lumen of centrioles. *J Cell Sci*. 109 (Pt 13):3089-102.

Pazour, G.J., N. Agrin, J. Leszyk, and G.B. Witman. 2005. Proteomic analysis of a eukaryotic cilium. *J Cell Biol*. 170:103-13.

Pedersen, L.B., and J.L. Rosenbaum. 2008. Intraflagellar transport (IFT) role in ciliary assembly, resorption and signalling. *Curr Top Dev Biol*. 85:23-61.

Pedersen, L.B., I.R. Veland, J.M. Schroder, and S.T. Christensen. 2008. Assembly of primary cilia. *Dev Dyn*. 237:1993-2006.

Pelletier, L., E. O'Toole, A. Schwager, A.A. Hyman, and T. Muller-Reichert. 2006. Centriole assembly in Caenorhabditis elegans. *Nature*. 444:619-23.

Pelletier, L., N. Ozlu, E. Hannak, C. Cowan, B. Habermann, M. Ruer, T. Muller-Reichert, and A.A. Hyman. 2004. The Caenorhabditis elegans centrosomal protein SPD-2 is required for both pericentriolar material recruitment and centriole duplication. *Curr Biol*. 14:863-73.

Peng, C.Y., P.R. Graves, R.S. Thoma, Z. Wu, A.S. Shaw, and H. Piwnica-Worms. 1997. Mitotic and G2 checkpoint control: regulation of 14-3-3 protein binding by phosphorylation of Cdc25C on serine-216. *Science*. 277:1501-5.

Peranen, J., P. Auvinen, H. Virta, R. Wepf, and K. Simons. 1996. Rab8 promotes polarized membrane transport through reorganization of actin and microtubules in fibroblasts. *J Cell Biol*. 135:153-67.

Peters, J.M. 2006. The anaphase promoting complex/cyclosome: a machine designed to destroy. *Nat Rev Mol Cell Biol*. 7:644-56.

Picard, A., E. Karsenti, M.C. Dabauvalle, and M. Doree. 1987. Release of mature starfish oocytes from interphase arrest by microinjection of human centrosomes. *Nature*. 327:170-2.

Piel, M., P. Meyer, A. Khodjakov, C.L. Rieder, and M. Bornens. 2000. The respective contributions of the mother and daughter centrioles to centrosome activity and behavior in vertebrate cells. *J Cell Biol*. 149:317-30.

Polo, S.E., and S.P. Jackson. 2011. Dynamics of DNA damage response proteins at DNA breaks: a focus on protein modifications. *Genes Dev*. 25:409-33.

Prosser, S.L., and C.G. Morrison. 2015. Centrin2 regulates CP110 removal in primary cilium formation. *J Cell Biol*. 208:693-701.

Pugacheva, E.N., S.A. Jablonski, T.R. Hartman, E.P. Henske, and E.A. Golemis. 2007. HEF1-dependent Aurora A activation induces disassembly of the primary cilium. *Cell*. 129:1351-63.

Puklowski, A., Y. Homsi, D. Keller, M. May, S. Chauhan, U. Kossatz, V. Grunwald, S. Kubicka, A. Pich, M.P. Manns, I. Hoffmann, P. Gonczy, and N.P. Malek. 2011. The SCF-FBXW5 E3-ubiquitin ligase is regulated by PLK4 and targets HsSAS-6 to control centrosome duplication. *Nat Cell Biol*. 13:1004-9.

Rath, A., M. Glibowicka, V.G. Nadeau, G. Chen, and C.M. Deber. 2009. Detergent binding explains anomalous SDS-PAGE migration of membrane proteins. *Proc Natl Acad Sci U S A*. 106:1760-5.

Robbins, E., G. Jentzsch, and A. Micali. 1968. The centriole cycle in synchronized HeLa cells. *J Cell Biol*. 36:329-39.

Rohaly, G., J. Chemnitz, S. Dehde, A.M. Nunez, J. Heukeshoven, W. Deppert, and I. Dornreiter. 2005. A novel human p53 isoform is an essential element of the ATR-intra-S phase checkpoint. *Cell*. 122:21-32.

Salah, Z., A. Alian, and R.I. Aqeilan. 2012. WW domain-containing proteins: retrospectives and the future. *Front Biosci (Landmark Ed)*. 17:331-48.

Sancar, A., L.A. Lindsey-Boltz, K. Unsal-Kacmaz, and S. Linn. 2004. Molecular mechanisms of mammalian DNA repair and the DNA damage checkpoints. *Annu Rev Biochem*. 73:39-85.

Santamaria, A., B. Wang, S. Elowe, R. Malik, F. Zhang, M. Bauer, A. Schmidt, H.H. Sillje, R. Korner, and E.A. Nigg. 2011. The Plk1-dependent phosphoproteome of the early mitotic spindle. *Mol Cell Proteomics*. 10:M110 004457.

Sato, C., R. Kuriyama, and K. Nishizawa. 1983. Microtubule-organizing centers abnormal in number, structure, and nucleating activity in x-irradiated mammalian cells. *J Cell Biol*. 96:776-82.

Sato, K., E. Sundaramoorthy, E. Rajendra, H. Hattori, A.D. Jeyasekharan, N. Ayoub, R. Schiess, R. Aebersold, H. Nishikawa, A.S. Sedukhina, H. Wada, T. Ohta, and A.R. Venkitaraman. 2012. A DNA-damage selective role for BRCA1 E3 ligase in claspin ubiquitylation, CHK1 activation, and DNA repair. *Curr Biol*. 22:1659-66.

Sato, N., K. Mizumoto, M. Nakamura, and M. Tanaka. 2000. Radiation-induced centrosome overduplication and multiple mitotic spindles in human tumor cells. *Exp Cell Res*. 255:321-6.

Schmidt, K.N., S. Kuhns, A. Neuner, B. Hub, H. Zentgraf, and G. Pereira. 2012. Cep164 mediates vesicular docking to the mother centriole during early steps of ciliogenesis. *J Cell Biol*. 199:1083-101.

Schneider, L., C.A. Clement, S.C. Teilmann, G.J. Pazour, E.K. Hoffmann, P. Satir, and S.T. Christensen. 2005. PDGFRalphaalpha signaling is regulated through the primary cilium in fibroblasts. *Curr Biol*. 15:1861-6.

Schockel, L., M. Mockel, B. Mayer, D. Boos, and O. Stemmann. 2011. Cleavage of cohesin rings coordinates the separation of centrioles and chromatids. *Nat Cell Biol*. 13:966-72.

Schon, O., A. Friedler, M. Bycroft, S.M. Freund, and A.R. Fersht. 2002. Molecular mechanism of the interaction between MDM2 and p53. *J Mol Biol*. 323:491-501.

Schultz, J., R.R. Copley, T. Doerks, C.P. Ponting, and P. Bork. 2000. SMART: a web-based tool for the study of genetically mobile domains. *Nucleic Acids Res*. 28:231-4.

Selby, C.P., and A. Sancar. 1993. Molecular mechanism of transcription-repair coupling. *Science*. 260:53-8.

Shimada, M., and K. Komatsu. 2009. Emerging connection between centrosome and DNA repair machinery. *J Radiat Res*. 50:295-301.

Sillibourne, J.E., I. Hurbain, T. Grand-Perret, B. Goud, P. Tran, and M. Bornens. 2013. Primary ciliogenesis requires the distal appendage component Cep123. *Biol Open*. 2:535-45.

Sillibourne, J.E., F. Tack, N. Vloemans, A. Boeckx, S. Thambirajah, P. Bonnet, F.C. Ramaekers, M. Bornens, and T. Grand-Perret. 2010. Autophosphorylation of polo-like kinase 4 and its role in centriole duplication. *Mol Biol Cell*. 21:547-61.

Singla, V., M. Romaguera-Ros, J.M. Garcia-Verdugo, and J.F. Reiter. 2010. Ofd1, a human disease gene, regulates the length and distal structure of centrioles. *Dev Cell*. 18:410-24.

Sir, J.H., M. Putz, O. Daly, C.G. Morrison, M. Dunning, J.V. Kilmartin, and F. Gergely. 2013. Loss of centrioles causes chromosomal instability in vertebrate somatic cells. *J Cell Biol*. 203:747-56.

Sivasubramaniam, S., X. Sun, Y.R. Pan, S. Wang, and E.Y. Lee. 2008. Cep164 is a mediator protein required for the maintenance of genomic stability through modulation of MDC1, RPA, and CHK1. *Genes Dev*. 22:587-600.

Slaats, G.G., A.K. Ghosh, L.L. Falke, S. Le Corre, I.A. Shaltiel, G. van de Hoek, T.D. Klasson, M.F. Stokman, I. Logister, M.C. Verhaar, R. Goldschmeding, T.Q. Nguyen, I.A. Drummond, F. Hildebrandt, and R.H. Giles. 2014. Nephronophthisis-associated CEP164 regulates cell cycle progression, apoptosis and epithelial-to-mesenchymal transition. *PLoS Genet*. 10:e1004594.

Slansky, J.E., and P.J. Farnham. 1996. Introduction to the E2F family: protein structure and gene regulation. *Curr Top Microbiol Immunol*. 208:1-30.

Sluder, G. 2014. One to only two: a short history of the centrosome and its duplication. *Philos Trans R Soc Lond B Biol Sci*. 369.

Sluder, G., and J.J. Nordberg. 2004. The good, the bad and the ugly: the practical consequences of centrosome amplification. *Curr Opin Cell Biol*. 16:49-54.

Sonnen, K.F., A.M. Gabryjonczyk, E. Anselm, Y.D. Stierhof, and E.A. Nigg. 2013. Human Cep192 and Cep152 cooperate in Plk4 recruitment and centriole duplication. *J Cell Sci*. 126:3223-33.

Sonnen, K.F., L. Schermelleh, H. Leonhardt, and E.A. Nigg. 2012. 3D-structured illumination microscopy provides novel insight into architecture of human centrosomes. *Biol Open*. 1:965-76.

Sorokin, S. 1962. Centrioles and the formation of rudimentary cilia by fibroblasts and smooth muscle cells. *J Cell Biol*. 15:363-77.

Sorokin, S.P. 1968. Reconstructions of centriole formation and ciliogenesis in mammalian lungs. *J Cell Sci*. 3:207-30.

Spalluto, C., D.I. Wilson, and T. Hearn. 2012. Nek2 localises to the distal portion of the mother centriole/basal body and is required for timely cilium disassembly at the G2/M transition. *Eur J Cell Biol*. 91:675-86.

Spektor, A., W.Y. Tsang, D. Khoo, and B.D. Dynlacht. 2007. Cep97 and CP110 suppress a cilia assembly program. *Cell*. 130:678-90.

Steere, N., M. Wagner, S. Beishir, E. Smith, L. Breslin, C.G. Morrison, H. Hochegger, and R. Kuriyama. 2011. Centrosome amplification in CHO and DT40 cells by inactivation of cyclin-dependent kinases. *Cytoskeleton (Hoboken)*. 68:446-58.

Stevens, N.R., H. Roque, and J.W. Raff. 2010. DSas-6 and Ana2 coassemble into tubules to promote centriole duplication and engagement. *Dev Cell*. 19:913-9.

Strnad, P., and P. Gonczy. 2008. Mechanisms of procentriole formation. *Trends Cell Biol*. 18:389-96.

Strnad, P., S. Leidel, T. Vinogradova, U. Euteneuer, A. Khodjakov, and P. Gonczy. 2007. Regulated HsSAS-6 levels ensure formation of a single procentriole per centriole during the centrosome duplication cycle. *Dev Cell*. 13:203-13.

Sugasawa, K. 2010. Regulation of damage recognition in mammalian global genomic nucleotide excision repair. *Mutat Res*. 685:29-37.

Sugasawa, K., J.M. Ng, C. Masutani, S. Iwai, P.J. van der Spek, A.P. Eker, F. Hanaoka, D. Bootsma, and J.H. Hoeijmakers. 1998. Xeroderma pigmentosum group C protein complex is the initiator of global genome nucleotide excision repair. *Mol Cell*. 2:223-32.

Takata, M., M.S. Sasaki, E. Sonoda, C. Morrison, M. Hashimoto, H. Utsumi, Y. Yamaguchi-Iwai, A. Shinohara, and S. Takeda. 1998. Homologous recombination and non-homologous end-joining pathways of DNA double-strand break repair have overlapping roles in the maintenance of chromosomal integrity in vertebrate cells. *Embo j*. 17:5497-508.

Tamura, K., F.U. Battistuzzi, P. Billing-Ross, O. Murillo, A. Filipski, and S. Kumar. 2012. Estimating divergence times in large molecular phylogenies. *Proc Natl Acad Sci U S A*. 109:19333-8.

Tamura, K., G. Stecher, D. Peterson, A. Filipski, and S. Kumar. 2013. MEGA6: Molecular Evolutionary Genetics Analysis version 6.0. *Mol Biol Evol*. 30:2725-9.

Tanos, B.E., H.J. Yang, R. Soni, W.J. Wang, F.P. Macaluso, J.M. Asara, and M.F. Tsou. 2013. Centriole distal appendages promote membrane docking, leading to cilia initiation. *Genes Dev*. 27:163-8.

Taschner, M., S. Bhogaraju, and E. Lorentzen. 2012. Architecture and function of IFT complex proteins in ciliogenesis. *Differentiation*. 83:S12-22.

Thein, K.H., J. Kleylein-Sohn, E.A. Nigg, and U. Gruneberg. 2007. Astrin is required for the maintenance of sister chromatid cohesion and centrosome integrity. *J Cell Biol*. 178:345-54.

Tibelius, A., J. Marhold, H. Zentgraf, C.E. Heilig, H. Neitzel, B. Ducommun, A. Rauch, A.D. Ho, J. Bartek, and A. Kramer. 2009. Microcephalin and pericentrin regulate mitotic entry via centrosome-associated Chk1. *J Cell Biol*. 185:1149-57.

Tsang, W.Y., and B.D. Dynlacht. 2008. sSgo1, a guardian of centriole cohesion. *Dev Cell*. 14:320-2.

Tsou, M.F., and T. Stearns. 2006. Mechanism limiting centrosome duplication to once per cell cycle. *Nature*. 442:947-51.

Tsou, M.F., W.J. Wang, K.A. George, K. Uryu, T. Stearns, and P.V. Jallepalli. 2009. Polo kinase and separase regulate the mitotic licensing of centriole duplication in human cells. *Dev Cell*. 17:344-54.

Uhlmann, F., F. Lottspeich, and K. Nasmyth. 1999. Sister-chromatid separation at anaphase onset is promoted by cleavage of the cohesin subunit Scc1. *Nature*. 400:37-42.

van Breugel, M., M. Hirono, A. Andreeva, H.A. Yanagisawa, S. Yamaguchi, Y. Nakazawa, N. Morgner, M. Petrovich, I.O. Ebong, C.V. Robinson, C.M. Johnson, D. Veprintsev, and B. Zuber. 2011. Structures of SAS-6 suggest its organization in centrioles. *Science*. 331:1196-9.

Veleri, S., S.H. Manjunath, R.N. Fariss, H. May-Simera, M. Brooks, T.A. Foskett, C. Gao, T.A. Longo, P. Liu, K. Nagashima, R.A. Rachel, T. Li, L. Dong, and A. Swaroop. 2014. Ciliopathy-associated gene Cc2d2a promotes assembly of subdistal appendages on the mother centriole during cilia biogenesis. *Nat Commun*. 5:4207.

Vorobjev, I.A., and S. Chentsov Yu. 1982. Centrioles in the cell cycle. I. Epithelial cells. *J Cell Biol*. 93:938-49.

Walker, R.A., E.T. O'Brien, N.K. Pryer, M.F. Soboeiro, W.A. Voter, H.P. Erickson, and E.D. Salmon. 1988. Dynamic instability of individual microtubules analyzed by video light microscopy: rate constants and transition frequencies. *J Cell Biol*. 107:1437-48.

Wang, W.J., R.K. Soni, K. Uryu, and M.F. Tsou. 2011. The conversion of centrioles to centrosomes: essential coupling of duplication with segregation. *J Cell Biol*. 193:727-39.

Wang, X., Y. Yang, Q. Duan, N. Jiang, Y. Huang, Z. Darzynkiewicz, and W. Dai. 2008. sSgo1, a major splice variant of Sgo1, functions in centriole cohesion where it is regulated by Plk1. *Dev Cell*. 14:331-41.

Wei, Q., Q. Xu, Y. Zhang, Y. Li, Q. Zhang, Z. Hu, P.C. Harris, V.E. Torres, K. Ling, and J. Hu. 2013. Transition fibre protein FBF1 is required for the ciliary entry of assembled intraflagellar transport complexes. *Nat Commun*. 4:2750.

West, S.C. 2003. Molecular views of recombination proteins and their control. *Nat Rev Mol Cell Biol*. 4:435-45.

Westlake, C.J., L.M. Baye, M.V. Nachury, K.J. Wright, K.E. Ervin, L. Phu, C. Chalouni, J.S. Beck, D.S. Kirkpatrick, D.C. Slusarski, V.C. Sheffield, R.H. Scheller, and P.K. Jackson. 2011. Primary cilia membrane assembly is initiated by Rab11 and transport protein particle II (TRAPPII) complex-dependent trafficking of Rabin8 to the centrosome. *Proc Natl Acad Sci U S A*. 108:2759-64.

Winding, P., and M.W. Berchtold. 2001. The chicken B cell line DT40: a novel tool for gene disruption experiments. *J Immunol Methods*. 249:1-16.

Wong, Y.L., J.V. Anzola, R.L. Davis, M. Yoon, A. Motamedi, A. Kroll, C.P. Seo, J.E. Hsia, S.K. Kim, J.W. Mitchell, B.J. Mitchell, A. Desai, T.C. Gahman, A.K. Shiau, and K. Oegema. 2015. Cell biology. Reversible centriole depletion with an inhibitor of Polo-like kinase 4. *Science*. 348:1155-60.

Wood, R.D. 1996. DNA repair in eukaryotes. *Annu Rev Biochem*. 65:135-67.

Woodruff, J.B., O. Wueseke, V. Viscardi, J. Mahamid, S.D. Ochoa, J. Bunkenborg, P.O. Widlund, A. Pozniakovsky, E. Zanin, S. Bahmanyar, A. Zinke, S.H. Hong, M. Decker, W. Baumeister, J.S. Andersen, K. Oegema, and A.A. Hyman. 2015. Centrosomes. Regulated assembly of a supramolecular centrosome scaffold in vitro. *Science*. 348:808-12.

Xu, X., Z. Weaver, S.P. Linke, C. Li, J. Gotay, X.W. Wang, C.C. Harris, T. Ried, and C.X. Deng. 1999. Centrosome amplification and a defective G2-M cell cycle checkpoint induce genetic instability in BRCA1 exon 11 isoform-deficient cells. *Mol Cell*. 3:389-95.

Yamazoe, M., E. Sonoda, H. Hochegger, and S. Takeda. 2004. Reverse genetic studies of the DNA damage response in the chicken B lymphocyte line DT40. *DNA Repair (Amst)*. 3:1175-85.

Yang, J., M. Adamian, and T. Li. 2006. Rootletin interacts with C-Nap1 and may function as a physical linker between the pair of centrioles/basal bodies in cells. *Mol Biol Cell*. 17:1033-40.

Yazdi, P.T., Y. Wang, S. Zhao, N. Patel, E.Y. Lee, and J. Qin. 2002. SMC1 is a downstream effector in the ATM/NBS1 branch of the human S-phase checkpoint. *Genes Dev*. 16:571-82.

Ye, X., H. Zeng, G. Ning, J.F. Reiter, and A. Liu. 2014. C2cd3 is critical for centriolar distal appendage assembly and ciliary vesicle docking in mammals. *Proc Natl Acad Sci U S A*. 111:2164-9.

Yue, Z., A. Carvalho, Z. Xu, X. Yuan, S. Cardinale, S. Ribeiro, F. Lai, H. Ogawa, E. Gudmundsdottir, R. Gassmann, C.G. Morrison, S. Ruchaud, and W.C. Earnshaw.

2008. Deconstructing Survivin: comprehensive genetic analysis of Survivin function by conditional knockout in a vertebrate cell line. *J Cell Biol*. 183:279-96.

Zachos, G., M.D. Rainey, and D.A. Gillespie. 2003. Chk1-deficient tumour cells are viable but exhibit multiple checkpoint and survival defects. *EMBO J*. 22:713-23.

Zhang, S., P. Hemmerich, and F. Grosse. 2007. Centrosomal localization of DNA damage checkpoint proteins. *J Cell Biochem*. 101:451-65.

Zheng, Y., M.L. Wong, B. Alberts, and T. Mitchison. 1995. Nucleation of microtubule assembly by a gamma-tubulin-containing ring complex. *Nature*. 378:578-83.

Zhou, B.B., and S.J. Elledge. 2000. The DNA damage response: putting checkpoints in perspective. *Nature*. 408:433-9.

Scientific communications

Publications and Presentations

Peer-reviewed publications:

- Daly OM, Gaboriau D, Karakaya K, King S, Dantas TJ, Lalor P, Dockery P, Krämer A, Morrison CG: **Gene-targeted CEP164-deficient cells show a ciliation defect with intact DNA repair capacity.** J Cell Sci. 2016 Mar 10. pii: jcs.186221.
- Sir JH, Pütz M, Daly O, Morrison CG, Dunning M, Kilmartin JV, Gergely F: **Loss of centrioles causes chromosomal instability in vertebrate somatic cells**. J Cell Biol. 2013 Dec 9;203(5):747-56. doi: 10.1083/jcb.
- Baffet AD, Martin CA, Scarfone I, Daly OM, David A, Tibelius A, Lattao R, Hussain MS, Woodruff JB: **Meeting report - building a centrosome**. J Cell Sci. 2013 Aug 1;126(Pt 15):3259-62. doi: 10.1242/jcs.136721
- Dantas TG**,** Daly OM, Conroy PC, Tomas M, Wang Y, Lalor P, Dockery P, Ferrando-May E & Morrison CG: **Calcium-binding capacity of centrin2 is required for linear POC5 assembly but not for nucleotide excision repair**. PLOS ONE 2013 Jul 2;8(7):e68487. doi: 10.1371/journal.pone.0068487
- Dantas TG, Daly OM, Morrison CG: **Such small hands: the roles of centrins/caltractins in the centriole and in genome maintenance**. Cell Mol Life Sci. 2012 Sep;69(18):2979-97. doi: 10.1007/s00018-012-0961-1. Review

---

Poster presentations:

- American Society for Cell Biology annual meeting, New Orleans, USA, December 14-18, 2013: Daly OM and Morrison CG. **Reverse Genetic Analysis of Cep164 in vertebrate cells.**
- The Company of Biologists "Building a Centrosome" meeting. Sussex, UK: Daly OM, Dantas TJ and Morrison CG**. Reverse Genetic Analysis of Cep164 in vertebrate cells.**